

Nanochitin and Nanochitosan: Chitin Nanostructure Engineering with Multiscale Properties for Biomedical and Environmental Applications

Suyoung Lee, Lam Tan Hao, Jeyoung Park,* Dongyeop X. Oh,* and Dong Soo Hwang*

Nanochitin and nanochitosan (with random-copolymer-based multiscale architectures of glucosamine and *N*-acetylglucosamine units) have recently attracted immense attention for the development of green, sustainable, and advanced functional materials. Nanochitin and nanochitosan are multiscale materials from small oligomers, rod-shaped nanocrystals, longer nanofibers, to hierarchical assemblies of nanofibers. Various physical properties of chitin and chitosan depend on their molecular- and nanostructures; translational research has utilized them for a wide range of applications (biomedical, industrial, environmental, and so on). Instead of reviewing the entire extensive literature on chitin and chitosan, here, recent developments in multiscale-dependent material properties and their applications are highlighted; immune, medical, reinforcing, adhesive, green electrochemical materials, biological scaffolds, and sustainable food packaging are discussed considering the size, shape, and assembly of chitin nanostructures. In summary, new perspectives for the development of sustainable advanced functional materials based on nanochitin and nanochitosan by understanding and engineering their multiscale properties are described.

1. Introduction

Chitin is one of the most abundant biopolymers with cellulose, being produced ≈ 100 billion tons annually on the earth.^[1] Chitin and cellulose share many similarities, such as insolubility in water and common organic solvents, biodegradability, and forming hierarchical nanofibrous multiscale materials.^[2–6] Chitosan, the most important derivative of chitin, is produced commercially through the deacetylation of chitin.^[1] Although the chemical structures of chitin and chitosan are very similar to that of cellulose, they have additional unique properties, such as greater chemical accessibility, antibacterial properties, and immune activities. Therefore, studies to develop chitin and chitosan as new advanced materials have tremendously progressed in many countries recently.^[7–10]

Although chitin and chitosan have numerous potential applications in various research fields more than cellulose, they have fewer practical applications than


cellulose and its derivatives. One explanation for this phenomenon is that cellulose is produced in immobile plants, while chitosan and chitin are mainly produced in moving invertebrate animals (such as insects and crustaceans); therefore, a lack of a usable material supply limits applications of chitin. However, the differing physicochemical and biological properties of chitin and chitosan reported in the literature could be a more valid reason for their fewer practical applications than cellulose and its derivatives. Furthermore, reports of their physicochemical and biological properties are often mutually exclusive; some reports indicate anti-inflammation, whereas others indicate proinflammation properties, some reports indicate the presence, and other the absence, of adhesive properties. To utilize chitin and chitosan as eco-friendly advanced materials, it is vital to understand the reason for these mutually exclusive properties. This review has been written to resolve this issue.

The issue of experimental conflict is more likely to arise from insufficient information about how chitin and chitosan behave at different scales. The usage of polyethylene (PE, with the chemical formula $(C_2H_4)_n$, one of the most ubiquitous synthetic polymers, varies as n (and the molecular weight) increases, from fuel, wax, and commodity plastics, to high-performance

S. Lee, J. Park, D. S. Hwang
Division of Environmental Science and Engineering
Department of Chemical Engineering
Pohang University of Science and Technology (POSTECH)
77 Cheongam-ro, Pohang 37673, Republic of Korea
E-mail: jypark@kriect.re.kr; dshwang@postech.ac.kr

L. T. Hao, J. Park, D. X. Oh
Research Center for Bio-Based Chemistry
Korea Research Institute of Chemical Technology (KRICT)
Ulsan 44429, Republic of Korea
E-mail: dongyeop@kriect.re.kr

L. T. Hao, J. Park, D. X. Oh
Advanced Materials and Chemical Engineering
University of Science and Technology (UST)
Daejeon 34113, Republic of Korea

 The ORCID identification number(s) for the author(s) of this article can be found under <https://doi.org/10.1002/adma.202203325>.

© 2022 The Authors. Advanced Materials published by Wiley-VCH GmbH. This is an open access article under the terms of the Creative Commons Attribution-NonCommercial License, which permits use, distribution and reproduction in any medium, provided the original work is properly cited and is not used for commercial purposes.

DOI: 10.1002/adma.202203325

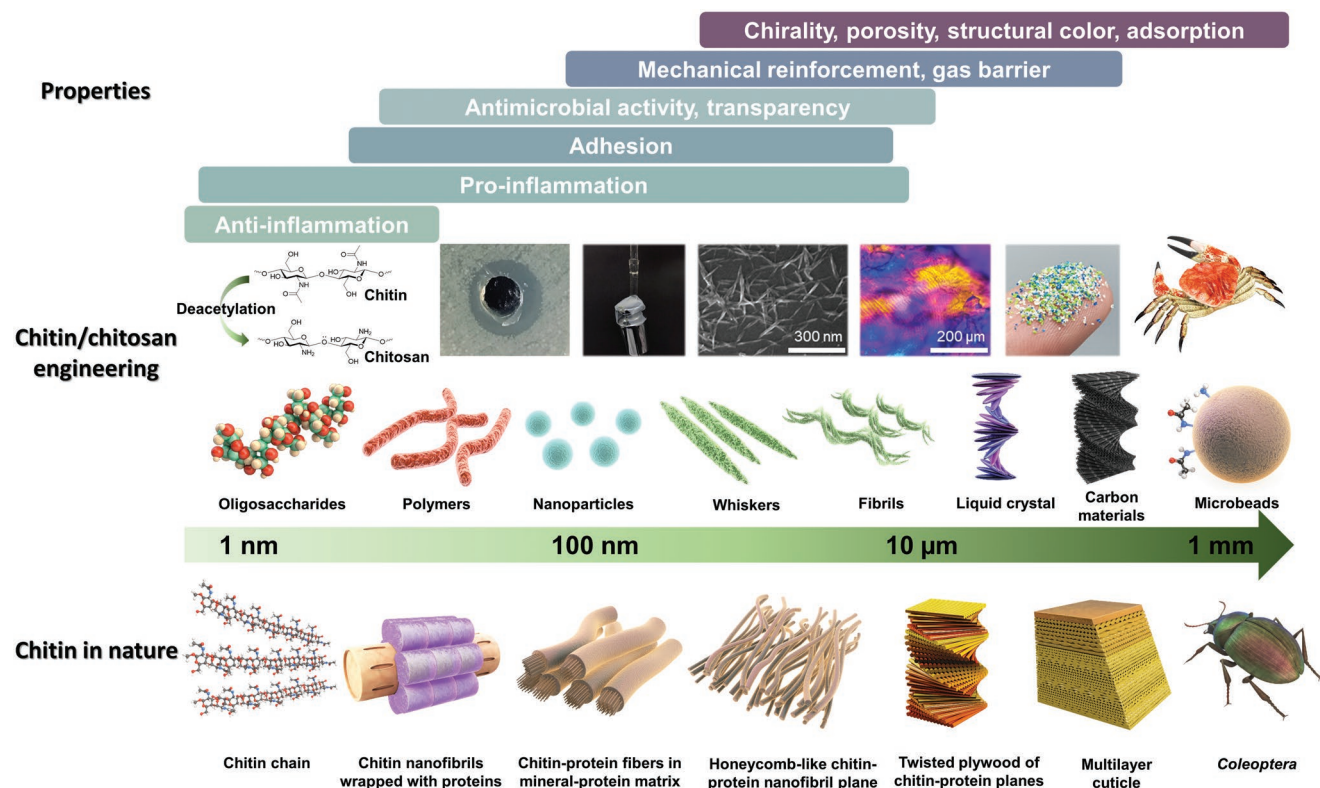


Figure 1. Effects of multiscale hierarchy on the engineering strategy and the derived scale-dependent physicochemical and biological properties of chitin and chitosan.

engineering plastics. Similarly, the physicochemical properties of chitin and chitosan depend on their molecular weight, and vary from the molecular scale to the nano- and micro-scales (Figure 1). Therefore, unlike the existing review papers on chitin and chitosan, this paper reviews the characteristics of chitin and chitosan and the latest research results from the perspective of multiscale-dependent material properties. This review aims to provide an in-depth understanding of the scale-dependent characteristics of chitin and chitosan, to enable their effective use by researchers and end users as biofunctional and sustainable materials.

1.1. Overview of Chitin and Chitosan

Chitin and chitosan are linear copolymers of randomly distributed $\beta(1\rightarrow4)$ -linked *N*-acetyl-D-glucosamine (GlcNAc) and D-glucosamine (GlcN),^[2] defined by three structural parameters: 1) degree of acetylation (D_A : the molar fraction of GlcNAc residues), 2) pattern of acetylation (P_A : the sequence of GlcN and GlcNAc residues (random or block) along the polymer chain), and 3) molecular weight (MW).^[11] Although there is no accepted distinction between chitin and chitosan, the polymer is usually labeled chitin when the D_A value is greater than 0.5; otherwise, chitosan.^[12] The MWs of chitin and chitosan depend on the source, and the MW of chitin is much higher than that of chitosan.^[13,14] A variability in structural parameters results in a broad spectrum of physicochemical properties, imparting functional versatility for different applications.

The most distinguishing feature between chitin and chitosan is their solubility. Chitin is insoluble in water and common organic solvents due to strong hydrogen bonding between its acetamide (NHCOCH_3) and hydroxy (OH) groups. Only few solvents and solvent systems are capable of dissolving chitin, such as hot concentrated aqueous solutions of thiocyanate, calcium halide, or mineral acids, irritant organic solvents (e.g., hexafluoroisopropanol alcohol, trichloroacetic acids, and formic acid), and some ionic liquids.^[2] From green chemistry and economic perspectives, the processing of chitin in these extreme and expensive solvents can limit the industrial production and commercialization of chitin-based products. Chitosan, on the other hand, is readily soluble in dilute acidic aqueous media at $\text{pH} < 6$, because its amino groups (NH_2) are significantly protonated at low pH values (the NH_3^+ group has a $\text{p}K_a$ of 6.0–6.5).^[2,15,16] Generally, the aqueous solubility of chitosan increases on increasing acidity, decreasing D_A , more random P_A , and decreasing MW.^[15,17] Although the chemical versatility of the NH_2 group over the OH group enables various functionalizations that tune the properties of chitin and chitosan, it necessitates a tight control of the substitution degree and the use of a protecting group for selectivity.

1.2. Chitin in Nature

Chitin is a primary component of the exoskeletons of arthropods including crustaceans and insects, cell walls of fungi, and beaks and gladii of mollusks.^[2,18–22] Similar to most biological constructs, chitin is complexed with other substances and

exhibits different crystalline allomorphs. Chitin is mostly complexed with protein, which can be hardened through calcification in crustaceans,^[23] and cross-linking with polyphenols in insects.^[21] In fungi, chitin is complexed with other polysaccharides.^[24] The structure of chitin and its association with other substances is finely controlled through biosynthesis and assembly, resulting in an infinite number of structural differences across chitin-producing species.^[25] This leads to structural-functional diversities, such as exceptional mechanical properties in the mantis shrimp's dactyl club,^[26] mechanical gradients in the squid's beaks,^[22] and structural colors in many butterflies' and beetle species' wings.^[27,28]

The crustacean exoskeleton is an example of the self-assembly of chitin into a hierarchical structure. Native chitin is a semicrystalline 1D fibril material consisting of crystalline (microfibers or rod-like entities) and amorphous regions. The fibrils are stabilized through intra- and intermolecular hydrogen bonds, van der Waals forces, hydrophobic interactions, and electrostatic attraction. The chitin crystal is composed of a longitudinal assembly of 18–25 chains into a fibril (2–5 nm thick) wrapped by proteins. The chitin-protein complexes coalesce into bundles of 10–20 nm thickness, and the bundles form horizontal and parallel planes which are stacked helicoidally (with a gradual direction change from one plane to the next by a continuous rotation). This is known as the plywood, Bouligand, chiral nematic, or cholesteric structure (Figure 2).^[29]

Chitin exists in three crystal allomorphs (α , β , and γ) with different packing and relative directions of adjacent chains. The most thermodynamically stable and abundant allomorph is α -chitin, composed of an antiparallel arrangement of chains, which is mainly found in crustaceans, insect cuticles, and

fungi.^[2,30–33] The less-abundant β -chitin, formed through a parallel arrangement of chains, is mostly found in squid pens, the peritrophic matrix of insects, tubeworms, and marine diatoms.^[2,25,30,34] Both allomorphs contain interchain C–O \cdots HN hydrogen bonds, forming strong intraplane hydrogen bonding, and each chain contains O-3' \cdots H-O-5' intrachain hydrogen bonds.^[30] α -chitin has interplane hydrogen bonds involving the C6'-OH group,^[32] whereas no interplane hydrogen bonding occurs in β -chitin.^[34] Thus, the β form is more flexible and chemically reactive than the α form. The γ form is naturally rare and it comprises alternating parallel-/antiparallel-aligned chains.^[2]

2. Biological and Physical Properties of Chitin and Chitosan at the Molecular-, Nano-, and Higher Scales

The applications of polyethylene, the most commonly used polymer material, are influenced by its phase, crystal structure, and mechanical properties, which depend on its MW. Similarly, the physical properties and biological activities of chitin also depend on its MW. Many properties of chitin and chitosan (such as water solubility, adhesion, and immune response) do not always remain mutually exclusive on the arrangement according to MW, as described in this section. In this section, four types of chitin and chitosan (classified according to MW) are discussed in the following order: oligosaccharide (oligomer <0 kDa) < low molecular weight (LMW; 10–100 kDa) < medium molecular weight (MMW; 100–300 kDa) < high molecular weight (HMW >300 kDa).

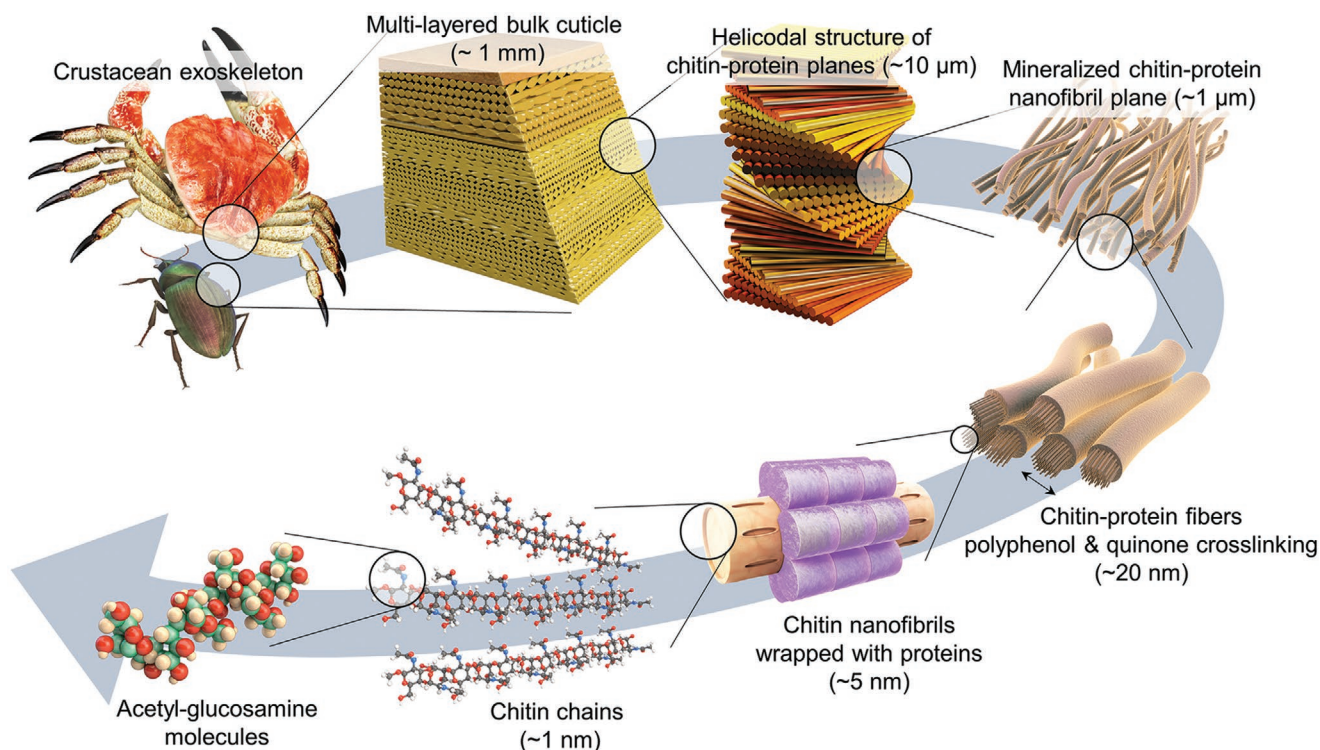


Figure 2. Multiscale structures of chitin in nature.

2.1. Properties of Chitin and Chitosan at the Molecular Level

2.1.1. Persistent Length-Dependent Properties

In polymers, the persistent length causes a rapid change in the physical properties of the polymer chain. Rigidity is quantified as the total persistence length (L_t), which represents the sum of intrinsic (L_p) and electrostatic (L_e) persistence lengths.^[35] Chain formation is determined by L_p and contour length (L_c); $L_t/L_c \geq 1$ indicates rod formation, and $L_t/L_c < 1$ indicates that the chain forms a random coil (Figure 3a).^[36] The L_p of chitin ($D_A = 0$) is ≈ 9 nm;^[37] thus, it exhibits rod-like behavior at oligomer size, with different physicochemical and biological properties than HMW chitosan, which has thread-like behavior. Therefore, oligomer-size chitin is water-soluble, regardless of the buffer pH, while chitin with a chain length higher than its persistent length is insoluble or partially soluble in aqueous solutions, depending on the buffer pH.

2.1.2. Adhesion, Cohesion, and Solubility in Aqueous Solutions

Chain stiffness influences the rheological behavior and formation of inter-/intra-chain hydrogen bond networks that form multimers, and the adhesion properties of chitin vary with persistent length. The surface forces apparatus (SFA), a widely

used technique for measuring intermolecular forces in biological and polymeric systems with precise force (approximately nanonewtons) and distance resolutions (≈ 0.1 nm), has been used to test the molecular interaction of chitin molecules with different MWs and D_A .^[38,39] The interaction forces of 150 kDa chitin with low D_A and 5 kDa chitin with low D_A have been measured at various pH values (3.0, 6.5, and 8.5).^[40] At pH 3.0, LMW chitin with low D_A ($L_t \approx 10.2$ nm) and $L_c \approx 15.6$ nm) shows rigid rod-like behavior with similar values. On the other hand, HMW chitosan exhibits Gaussian-chain properties with improved chain flexibility and mobility than the LMW chitosan, with $L_c \approx 343.2$ nm $\gg L_t$. The adhesion of LMW chitosan (5 kDa, $W_{ad} \approx 3.6$ mJ m⁻²) was $\approx 40\%$ lower than that of HMW chitosan (≈ 150 kDa, $W_{ad} \approx 7.3$ mJ m⁻²) to mica, whereas the cohesion of the LMW chitosan film ($W_{co} \approx 0.22$ mJ m⁻²) was 10 times lower than that of the HMW chitosan film ($W_{co} \approx 8.5$ mJ m⁻²) at pH 3.0 (Figure 3b–g). This could be due to the high valence and flexibility of the HMW chitosan. The HMW chitosan has a longer L_c than L_p , which facilitates stronger electrostatic interactions and more hydrogen bonds, whereas short-chain LMW chitosan, with a longer persistence length than contour length, is highly stiff and compactly packed on oppositely charged surfaces. Thus, the overcharged LMW chitosan-coated films repel each other in a symmetric mode, reducing cohesiveness greatly; in an asymmetric mode, the overcharged LMW chitosan films exhibit attraction, with a slightly smaller

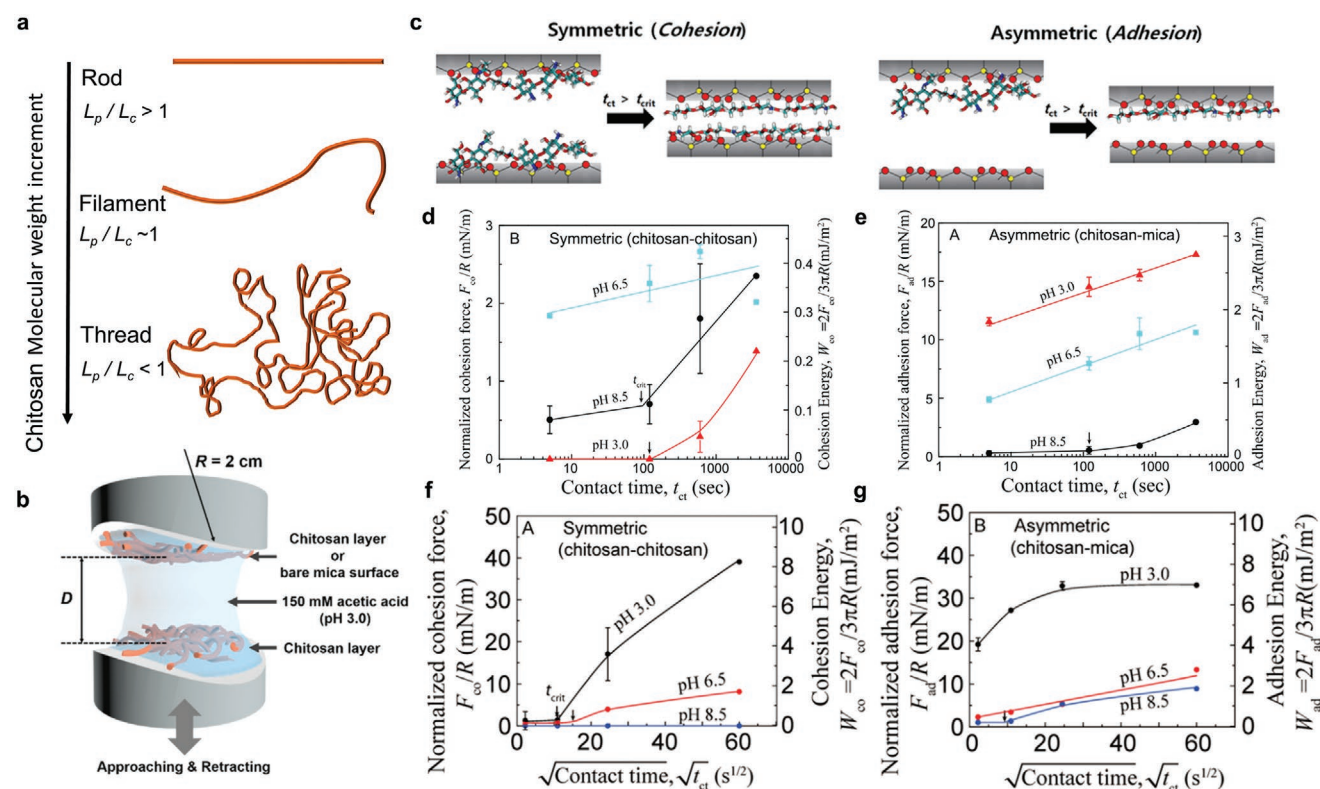


Figure 3. a) Chain formation according to the MW of chitin and chitosan. Schematic diagrams of the SFA experiment. b) The interaction force measurement between chitosan coated mica surface by buffer treatment (with different pH) between chitosan coated mica surface. b) Adapted with permission.^[41] Copyright 2021, Elsevier. c) Cohesion and adhesion mechanism of chitosan film. Adapted with permission.^[38] Copyright 2013, American Chemical Society. d,e) Normalized force–contact time curve of chitosan (5 kDa chitosan): d) adhesion and e) cohesion. d,e) Adapted with permission.^[40] Copyright 2015, Elsevier. f,g) 150 kDa chitosan: f) adhesion and g) cohesion. f,g) Reproduced with permission.^[38] Copyright 2013, American Chemical Society.

magnitude than the HMW case. Therefore, LMW chitosan is soluble in biological pH ranges due to their low self-interaction, but HMW chitosan is only soluble in acidic pH.

In addition to MW, the cohesion and adhesion have been measured with SFA, to determine the effect of D_A on chitosan interactions. The cohesion of LMW chitosan to the mica surface increases, whereas the adhesion of LMW chitosan (≈ 5 kDa, D_A : 11%, 61%, 98%) reduces on increasing the D_A .^[41] LMW chitosan molecular interactions are mainly mediated by electrostatic interactions due to the various ratios of positively charged amine groups, which depend on D_A . On increasing D_A , both the adhesion and cohesion forces in HMW chitosan (≈ 135 kDa, D_A : 18%, 29%, 50%) decrease; chain flexibility and mobility, which decrease as D_A increases, have a significant impact on the interaction of HMW chitosan due to the long chain length of HMW chitosan. Thus, LMW chitosan interaction mainly depends on the chitosan chain charge, which becomes less positive on increasing D_A , whereas HMW chitosan exhibits strong cohesion and adhesion due to its chain flexibility, which decreases as D_A increases.

2.1.3. Immune-Modulating Activities

Although there are numerous publications reporting the immune activities of chitin and chitosan, their results are conflicting and diverse, varying with the origin of the chitin (from crustaceans, insects, and fungi), impurities (endotoxin contamination, protein, and mineral), D_A , and MW.^[42–46] Inadequate explanations for the opposite immune effects of glucosamine derivatives (chitin, chitosan) make biomaterial application challenging. Among the different parameters that affect immune responses, MW has been selected in this review paper to analyze chitosan immunological activities. The degradation of chitin and chitosan, which induces immune stimulation, causes the disappearance of the immune-stimulating activity of the existing chitin and chitosan.^[47–49] Upon treating macrophages with intermediate-size chitin fragments (40–70 μm), tumor necrosis factor- α (TNF- α) is secreted, whereas small-size chitin fragments (<40 μm mostly 2–10 μm) induce the release of TNF- α and Interleukin (IL)-10.^[46] The treatment of mice with chitin through intranasal administration induces an accumulation of innate effector cells. Interestingly, messenger RNA (mRNA) and protein levels of acidic mammalian chitinase (AMCase, a mammalian chitinase that can degrade chitin) that are expressed at an early stage of chitin infection due to the accumulation of innate effector cells return to the basal level on day 9. Additionally, chitin-induced eosinophil and basophil accumulations are inhibited in AMCase-treated chitin or AMCase-overexpressed mice.^[47] More specifically, on the degradation of chitin and chitosan to hexamer, the secretion of inflammatory cytokines decreases, and the chitin and chitosan oligomers induce macrophage activation, unlike large chitosan polymers, by acting as positive feedback for chitotriosidase secretion.^[48,50] Thus, when chitin is first introduced, it induces innate immune-cell activation, but it is subsequently degraded into small fragments by chitin/chitosan degradation enzymes, which negatively regulate innate cells.

The recognition between immune cell receptors and ligands is critical for the initiation of immune signaling and responses.^[51,52] Chitin, a component of fungal cell walls and bacterial peptidoglycans, is a well-known pathogen-associated molecular pattern (PAMP) recognized by pattern recognition receptors (PRRs) in immune cells.^[53–55] Chitin and chitosan immune-activity mediating PRRs have been studied with C-type lectin receptors (dectin-1 and mannose receptor; MR) and toll-like receptors (TLRs; TLR2 and TLR4).^[46,56–58] PRRs and ligands bind via noncovalent interaction forces (such as electrostatic, hydrophobic, hydrogen bonding, and van der Waals forces) at specific binding sites.^[52,59] It has been reported that β -1,3-glucan, the ligand of dectin-1, weakly binds with the 6-mer, but exhibits strong binding with chitins longer than 25-mer.^[60] Therefore, chitin and chitosan exhibit different receptor dependencies toward the same receptor depending on the MW.^[46,55–57] Intermediate-size (40–70 μm) and small-size (<40 μm mostly 2–10 μm) chitin fragments induce different receptor-mediated pathways. The TLR2, dectin-1, and nuclear-factor- κB (NF- κB)-dependent pathways are mediated in the presence of the intermediate-size fraction, whereas the small-size fraction stimulates the TLR2-dependent and -independent, and dectin-1-dependent pathways, which involve MR and spleen tyrosine kinase.^[46] It has also been reported that for the TLR2-mediated immune activity of oligomeric chitin, a minimum size (6-mer) chitin is required to activate the immune responses by TLR2, while larger chitins (10- to 15-mer) exhibit the highest expression of proinflammatory cytokines. Although 5-mer chitin can bind to TLR2, it is too short to act as a bridge to form a TLR dimer to initiate signaling (Figure 4).^[49] A study compared the naïve T cell differentiation immune responses and interaction forces between chitosans (1 and 15 kDa) and PRRs. Chitosan oligomers induce regulatory T cell (Treg) differentiation of naïve T cells, whereas LMW chitosan does not. After the PRRs (TLR2, TLR4, dectin-1, and MR) are blocked, the chitosan oligomer induces the Treg differentiation. The involvement of dectin-1 is predominant, with some MR, whereas TLR4 is only marginally involved and TLR2 is not involved. Subsequently, differences in the interaction forces with receptors according to the MW of chitosan have been measured through SFA, and the results are correlated with those of the receptor-blocking experiment.^[61] Thus, each receptor requires the appropriate ligand binding strength to activate an immune response. This might be affected by the chain length and rigidity of chitin and chitosan, which vary with the MW.

2.1.4. Effect of MW on Immune Stimulation (HMW to Oligomer)

Immunostimulating activity is exhibited by chitins and chitosans with various MW values (ranging from HMWs to oligomers), and the signaling pathways or cytokine productions that induce inflammation are summarized in Table 1.^[46,47,50,56,57,62–70] Oligomers and LMWs significantly induce proinflammatory responses in RAW 264.7 cells. On degrading HMW chitosan (300 kDa) and treating it with different MWs of chitosan, the smaller chitosans (71 and 3.3 kDa, and the oligosaccharide mixture) increase nitric oxide (NO), inducible nitric oxide synthase (iNOS), TNF- α , and IL-6 production, and activate the NF- κB ,

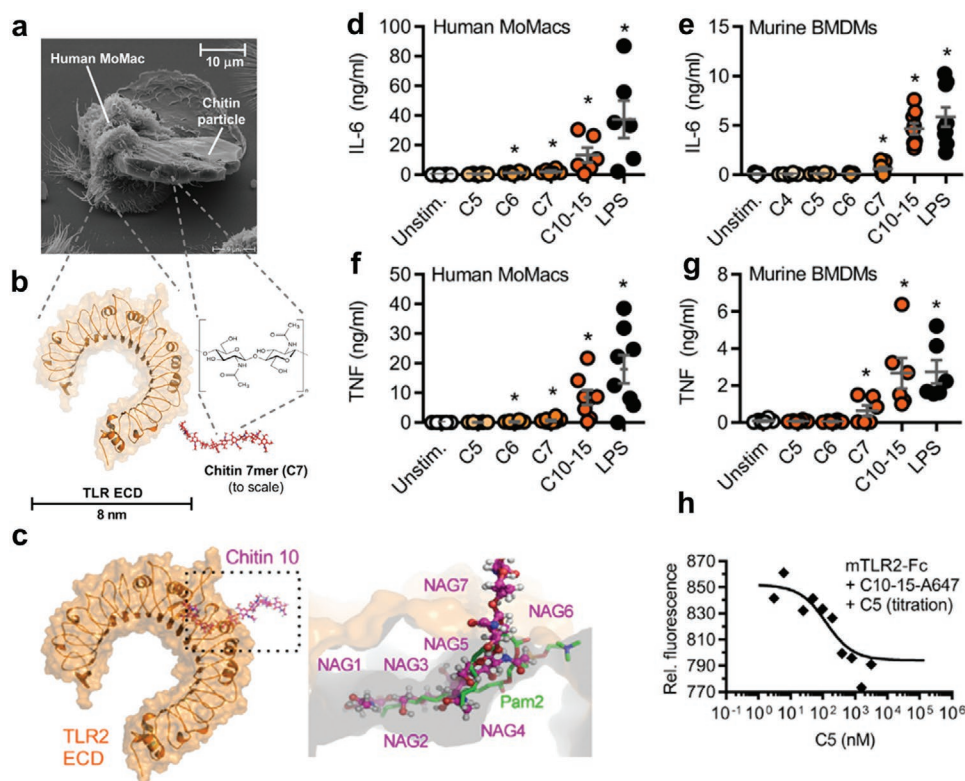


Figure 4. TLR2 binding and immune activity according to chitin size. a) Electron microscopy image of human-monocyte-derived macrophages (MDMs) engulfing a chitin particle. b) Size comparison of a typical ectodomain of TLR2 and a heptamer of chitin. c) Binding of a chitin 10-mer (magenta) and the TLR2 (orange) Pam2 (green) in a lipopeptide binding pocket. Cytokine level (ng mL^{-1}) of IL-6 in d) human MDMs, and e) murine mouse bone-marrow-derived macrophages (BMDMs). Cytokine level (mg mL^{-1}) of TNF- α in f) human MDMs, and g) murine mouse BMDMs. h) Binding measurement of Alexa647-labeled chitin 10–15-mer and mTLR2–Fc protein with chitin 5-mer titration. a–h) Adapted with permission.^[49] Copyright 2018, The Authors, published by John Wiley and Sons.

whereas larger chitosans (300, 156, and 72 kDa) inhibit the immune responses. Chitosans (small and large) bind to TLR4 and activate or inhibit the mitogen-activated protein kinase (MAPK) pathway to induce or suppress the secretion of proinflammation molecules.^[62] Oligomer (3 kDa) and LMW (50 kDa) chitosans exhibit similar mRNA levels of TNF- α and iNOS, whereas chitosan oligomers significantly increase the production of proinflammatory cytokines.^[63] The immunostimulatory activity of chitosans (3 and 50 kDa) in macrophages is mediated by NF- κ B, activator protein-1 (AP-1), MAPK, and phosphoinositide 3-kinase (PI3K)/Akt signaling pathways. Moreover, oligomer chitosans regulate immune activity through NF- κ B and the AP-1 signaling pathway.^[64] The 1.87 kDa chitosan also activates proinflammation; immune stimulation increases the phosphorylation of c-Jun N-terminal kinase (JNK), ERK, and p38 (which are related to the MAPK signaling pathway), increasing the phosphorylated-Akt levels and the phosphorylation of 3-phosphoinositide-dependent protein kinase-1 and p85 (which are related to the PI3K/Akt signaling pathways).^[65]

2.1.5. Immune Suppression of the Chitin and Chitosan Oligomers

Immunosuppression activities of chitin and chitosan are mainly exhibited in the oligomer range (1–10 kDa). In vitro and in vivo

experiments indicate that chitosan oligomers suppress the NF- κ B and MAPK pathways and activate the AMP-activated protein kinase (AMPK) pathway, inhibiting the secretion of cytokines and chemokines, and inducing proinflammation (Table 2).^[61,71–83] Chitosan can attenuate the inflammatory responses induced by lipopolysaccharide (LPS); chitosan oligomers (2- to 7-mer, $200 \mu\text{g mL}^{-1}$) suppress LPS-induced inflammation mediated by TLR4/NF- κ B signaling pathway in porcine intestinal columnar epithelial cells, and the mRNA levels of IL-6, IL-8, and nuclear p65 expression are inhibited.^[71] In LPS-induced RAW 264.7 cells, chitosan oligomers inhibit proinflammatory cytokines' (NO, TNF- α , IL-1 β , and IL-6) secretion, and prostaglandin E₂ (PGE₂) production. Additionally, it inhibits iNOS and cyclooxygenase-2 (COX-2) for NO and PGE₂ production, and downregulates the NF- κ B signaling pathway.^[72–74] The application of chitosan oligomers (0.4–1.2 kDa) to LPS-stimulated THP-1 cells decreases the secretion of TNF- α , IL-1 β , and IL-6 secretion, and activates AMPK in T84 cells.^[75] Allergic asthma is attributed to tissue infiltration with T helper 2 (Th2) cells, basophils, neutrophils, eosinophils, and mast cells, expressing IL-4, IL-5, and IL-13 cytokines.^[78] In basophilic leukemia cell line (RBL-2H3) mast cells, chitosan oligomers (1–5 kDa) reduce the calcium ionophore A23187-stimulated RBL-2H3 cell-induced histamine and β -hexosaminidase release, and intracellular Ca²⁺ levels. Furthermore, chitosan oligomers inhibit the phosphorylation

Table 1. The proinflammatory activities of chitin and chitosan depending on MW.

Chitosan	D_A [%]	Endotoxin	Cells or animal models	Immune activity	Ref.
300 kDa	5	Nondetected	RAW 264.7 cell	Larger chitosans (300, 156, 72 kDa) significantly inhibit immune stimulation by inhibiting NF- κ B activation. Smaller chitosans (7.1 and 3.3 kDa, <3.3 kDa) induce immune stimulation by activating NF- κ B and JNK signaling proteins.	[62]
156 kDa	13				
72 kDa	16				
7.1 kDa	17				
3.3 kDa	18				
<3.3 kDa	–				
50 kDa	–	<0.5 EU mL ⁻¹	RAW 264.7 cell	Both chitosans induce TNF- α , IL-6, IFN- γ , NO, and iNOS production. The 3 kDa chitosan exhibits a stronger immune response than the 50 kDa chitosan.	[63]
3 kDa	–				
50 kDa	–	<0.5 EU mL ⁻¹	RAW 264.7 cell	Both chitosans enhance COX-2 and IL-10 mRNA levels, and induce immune stimulation via NF- κ B and AP-1 pathways. The 3 kDa chitosan exhibits a stronger immune response than the 50 kDa chitosan.	[64]
3 kDa	–				
β -chitosan, 2.1 kDa	14	Nondetected	RAW 264.7 cell	α -chitosan exhibits better immunostimulatory effects than β -chitosan, and activates macrophages through the MAPK and PI3K/Akt signaling pathways.	[65]
α -chitosan, 1.8 kDa					
Chitin fragments	–	Nondetected	Peritoneal macrophage	Chitins of the 40–70 μ m fraction activate TLR2 and MyD88 by the IL-17A/IL-17AR pathway and induce acute inflammation in the lung.	[56]
100 μ m			BMDMs		
70–100 μ m			WT Mice		
40–70 μ m					
3–8-mer	0	–	RAW 264.7 cell	Chitosan increases NO and TNF- α production, and iNOS mRNA levels by activating TLR4 on macrophages.	[57]
600–800 kDa	15–25	–	Saos-2 (osteosarcoma cells)	Both chitosans reduce cell-line proliferation and viability to 90%. MW does not influence antitumor activity.	[66]
100–300 kDa			MCF-7 (human breast cancer cells)		
			HeLa (human epithelial cervical cancer cells)		
17.7 kDa,	14	–	Sarcoma 180 tumor cells in mice	17.7 and 10.1 kDa chitosan inhibit tumor-cell growth. The hexamer (1.57 kDa) exhibits the lowest antitumor activity.	[67]
10.1 kDa,	28.5				
1.57 kDa	42.1				
2- to 9-mer	46	–	HepG2 (liver-cancer cells) on a dynamic tumor-vessel microsystem	The proliferation and migration of HepG2 cells is considerably suppressed by partially acetylated chitosan, which decreases the production of pseudopod in liver-tumor cells.	[68]
Chitin with AMCase	–	–	BALB/c mice, C57BL/6 mice SPAM transgenic mice	Chitin accumulates allergy-induced innate immune cells. AMCase treatment inhibits the accumulation of immune cells.	[47]
Chitin fragments	–	Nondetected	Bone-marrow-derived dendritic cells (BMDCs)	40–70 μ m chitin fractions stimulate TNF- α , mediated by pathways that involve TLR2, dectin-1, and NF- κ B. <40 μ m chitin fractions induce TNF- α and IL-10, mediated by TLR2-dependent, -independent, and dectin-1-dependent pathways.	[46]
40–70 μ m					
<40 μ m					
3- to 10-mer	<15	–	RAW 264.7 cell	Chitosan stimulates TNF- α and IL-1 β production. Macrophage lectin receptor mediates internalization of chitosan.	[69]
Chitin/chitosan fragments	93/24	Endotoxin removal with NaOH	BMDMs	<20 μ m chitosan fractions induce IL-1 β release, the >100 μ m fractions induce very low amounts of release, while chitosan hexamers do not stimulate IL-1 β . Chitosan activates the NOD-like receptor pyrin domain-containing protein 3 (NLRP3) inflammasome in a phagocytosis-dependent manner, while chitin does not.	[50]
>100 μ m					
20–100 μ m					
<20 μ m hexamer					
Chitosan salt	–	100 EU g ⁻¹	BMDCs	Chitosan salts are engaged on the cyclic GMP-AMP synthase – stimulator of interferon genes (cGAS–STING) pathway and promote DC maturation by inducing type I IFN, and enhance Th1 response.	[70]

of MEK/ERK and p38 kinase involved in the MAPK pathway, thereby reducing proinflammatory cytokines' expression in allergy-stimulated RBL-2H3 mast cells.^[79,80]

In vitro experiments confirm that chitosan oligomers exhibit immune-suppression activity by inhibiting the signaling pathways and secretion of cytokines that induce inflammation. In vivo

Table 2. The anti-inflammatory activity of chitosan depends on MW.

Chitosan	D_A [%]	Endotoxin	Cells or animal models	Immune activity	Ref.
(≤ 10 kDa)	5–10	–	LPS-induced RAW 264.7 cell	Chitosan attenuates LPS-induced TNF- α , IL-6, and NO secretion.	[72]
5–10 kDa	10 and 50	–	LPS-induced RAW 264.7 cell	5–10 kDa chitosan inhibits LPS-stimulated TNF- α , IL-6, iNOS, COX-2, PGE2 expression. Lower DA chitosan exhibits a better anti-inflammatory effect.	[73]
1–5 kDa <1 kDa	–	–	LPS-induced RAW 264.7 cell	Both chitosans inhibit LPS-induced PGE2, NO, iNOS, COX-2 expression. 10–20 kDa chitosans decrease IL-1 β expression in a dose-dependent manner. No skin primary irritation reaction occurred in 32 volunteers.	[74]
10–20 kDa 1–3 kDa	–	–	LPS-induced RAW 264.7 cell Female human skin	Both chitosans inhibit LPS-induced PGE2, NO, iNOS, COX-2 expression. 10–20 kDa chitosans decrease IL-1 β expression in a dose-dependent manner. No skin primary irritation reaction occurred in 32 volunteers.	[74]
0.4–1.2 kDa (2–6-mer)	15	–	Vitamin D3-stimulated human THP-1 cell Colonic epithelial T84 cell	Chitosan reduces LPS-induced cytokines in differentiated THP-1 cells and activates AMPK in T84 cells.	[75]
15 kDa 1 kDa	15 2.6	0.6 EU mL ⁻¹ 0.14 EU mL ⁻¹	Naïve T cell (Dextran sulfate sodium) DSS-induced colitis mice	1 kDa chitosan induces Treg differentiation and alleviates colitis symptoms, but not the 15 kDa chitosan.	[61]
2- to 8-mer	0	–	DSS-induced colitis mice	Chitosan inhibits inflammation in the colonic mucosa by suppressing the activity of NF- κ B, myeloperoxidase, and COX-2, and reduces proinflammatory cytokines in serum levels.	[81]
<1 kDa (3- to 5-mer)	0	–	Basophilic leukemia RBL-2H3 cells Asthma model mice	Chitosan inhibits cytokine production and granulation in RBL-2H3 cells. In the oral administration of chitosan in asthma model animals, TNF- α , IL-4, IL-5, and IL-13 secretion in the lung tissue and bronchoalveolar lavage fluid are reduced.	[80]
5 kDa	10	–	Rabbit and human synoviocytes Osteoarthritis rabbit model	Chitosan inhibits synovial inflammation by AMPK activation.	[83]
2- to 6-mer	<5	–	Human umbilical vein endothelial cells (HUVECs)	Chitosan reduces LPS-induced the expression of IL-6 via the p38 MAPK and ERK1/2 pathways.	[76]
2- to 6-mer	<5	Endotoxin-free	LPS-induced HUVECs	Chitosan inhibits the production of IL-8 in LPS-induced HUVECs by blocking NF- κ B and AP-1 activation and p38 MAPK and phosphokinase Akt phosphorylation.	[77]
5–10 kDa 3–5 kDa 1–3 kDa	–	–	Calcium ionophore A23187 plus phorbol 12-myristate 13-acetate (PMA)-stimulated RBL-2H3 (basophilic leukemia) cells	1–3 kDa chitosan exhibits the strongest anti-inflammation effect. Chitosan attenuates the release of histamine and β -hexosaminidase, intracellular Ca ²⁺ elevation, and reduces mRNA and protein levels of proinflammatory cytokines by inhibiting MEK/ERK.	[79]
5–10 kDa	<10	–	Colonic epithelial T84 cell DSS-induced colitis mice Acetic-acid-induced colitis mice	Chitosan inhibits NF- κ B activation and TNF- α and IL-6 production in inflammatory bowel disease (IBD) mice, and epithelial barrier integrity loss in T84 cells.	[82]

experiments have been conducted to confirm the utility of chitosan oligomers as a potential therapy for autoimmune diseases. Studies have been conducted to confirm the therapeutic efficacy of the oral administration of chitosan oligomers to a dextran sulfate sodium (DSS)-induced colitis mouse model. On pretreatment with 1 kDa chitosan oligomers and 15 kDa LMW chitosan via oral administration, 1 kDa chitosan oligomers alleviate the typical symptoms of colitis, while 15 kDa LMW chitosan does not.^[61] TNF- α and IL-6 levels in colonic tissue are reduced and the symptoms of inflammation are alleviated on chitosan oligomer (5–10 kDa) pretreatment at 10–20 mg kg⁻¹ day⁻¹; intestinal inflammation is alleviated when chitosan oligomer is pretreated to a DSS-induced colitis model. In T84 cells, chitosan oligomers reduce NF- κ B activation and proinflammatory cytokine production, preventing TNF- α and H₂O₂-induced apoptosis. Thus, chitosan oligomer has preventive and therapeutic effects on IBD through the NF- κ B signaling inhibition and intestinal epithelial cell apoptosis.^[82]

However, there are studies reporting proinflammatory activities of chitosan with a degree of polymerization near 1 kDa.

Chitosan oligomers significantly increase NO and TNF- α production, and mRNA levels in macrophages.^[57,58,69] Thus, MW is an important parameter that affects the immune activity of chitin and chitosan, with certain limitations. In-depth studies are required on MW and other parameters (such as D_A , remaining endotoxin, and solubility) that can affect immune activity to understand the opposing immune activity of chitosan.

2.1.6. Antimicrobial Properties

Numerous studies have investigated the antimicrobial properties of chitosan against fungi and bacteria. Although the exact mechanism of action has not been elucidated, it is known that the interaction between the negatively charged component at the cell surface and the positively charged chitosan plays an important role. This interaction disrupts the cell membrane and alters the membrane-wall permeability causing intracellular electrolyte leakage, and chitosan passes through the

cell membrane and kills the cells by inhibiting DNA/RNA or protein synthesis.^[84,85] The antimicrobial action of chitosan is affected by various factors, such as MW, D_A , pH, chemical modification.^[86–88] The amount of positively charged residues is crucial for interacting against the membrane components; thus, lower D_A and pH yield a high antibacterial efficacy.^[88,89] However, as explained in Section 2.1.2, the MW influences the chain rigidity and solubility of chitosan. Since HMW chitosan forms stronger electrostatic interactions, 150 kDa chitosan has stronger adhesion and cohesion than the 5 kDa chitosan oligomer.^[38,40] Considering the effects of these factors, this paper focuses on the efficacy of MW.

Gram-positive bacteria have a thick peptidoglycan layer (with a variable thickness of 20–80 nm) on the cell wall covering the cell membrane, with no extra layer.^[54] The main antibacterial mechanism of gram-positive bacteria is electrostatic interaction with anionic teichoic acids in peptidoglycan, which disrupts the cells.^[90] The high amount of positive charge residues in chitosan forms several electrostatic interactions; therefore, a higher MW yields a better antibacterial efficacy. The 1815 and 366 kDa chitosan films show significant antibacterial activity against *Listeria innocua*.^[91] In addition, the 263, 199, and 141 kDa chitosan films^[92] and 300–3.3 kDa chitosan also exhibited better antibacterial activity with increasing MW against *Staphylococcus aureus*.^[88] The high MW of chitosan is also effective against other gram-positive bacteria, such as *S. aureus*, *Bacillus cereus*, *Enterococcus faecalis*, and *Micrococcus luteus* (135–42.5 kDa chitosan),^[89] and *Clostridium paraputrificum*, *Clostridium beijerinckii*, *Roseburia intestinalis*, and *Faecalibacterium prausnitzii* (60–2 kDa chitosan).^[93] However, the 2 and 3 kDa chitosan oligomers exhibit a very poor antibacterial activity.

By contrast, gram-negative bacteria have a thin peptidoglycan layer (7–8 nm thick) with an outer membrane (extra layer) composed of lipids.^[54] Further, gram-negative bacteria are mainly influenced by electrostatic interactions with lipopolysaccharides on the outer membrane.^[94] Interestingly, chitosan can pass through the cell membrane and interfere with DNA/RNA synthesis.^[95] The 1815 and 366 kDa chitosan films were tested against *Escherichia coli* growth, where 1815 kDa chitosan did not inhibit *E. coli* growth at all, whereas 366 kDa showed antibacterial activity. However, when the antibacterial activity was measured under the same conditions, the effect was marginal as compared to that with gram-positive bacteria.^[91] When 300–3.3 kDa chitosans were tested against *E. coli*, they exhibited a higher antibacterial activity in the higher MW range (300, 156, 72.1 kDa) than chitosan in the lower MW range (29.2, 7.7, and 3 kDa).^[88] However, the antibacterial activity against *E. coli*, *Pseudomonas aeruginosa*, *Klebsiella pneumoniae*, and *Salmonella typhi* increases by decreasing the MW range (135–42.5 kDa).^[89] Further, when chitosans with the MW range of 60–2 kDa were tested against *Bacteroides thetaiotaomicron* and *Bacteroides vulgatus*, the antibacterial effect increased as the MW increased.^[93] Although there are differences because of the bacterial strains, the antibacterial effect of MMW or LMW chitosan was better than that of HMW chitosan or chitosan oligomer on gram-negative bacteria. It is more difficult for HMW chitosan to penetrate the cell wall and cell membrane, but it interacts with the extracellular components, thereby altering the cell permeability and exhibiting antibacterial action.^[87] On the other hand,

LMW chitosan not only acts on the cell membrane, but also penetrates the cells to inhibit DNA/RNA and protein synthesis, thereby affecting mitochondrial functions.^[85,96]

The antifungal effects of chitosan depend on the fungal strains used. Fungal growth decreases on increasing MW for *Fusarium oxysporum*, and on decreasing D_A for *Alternaria solani*, whereas no MW or D_A dependence is observed for *Aspergillus niger*.^[89] The antifungal effect of chitosan has been investigated with three different MW values (247, 140, and 75 kDa) on *Candida* spp. The effect on growth depends on the fungal strain. An effect of MW on the antifungal activity of chitosan has been observed in *Candida tropicalis* and *Candida parapsilosis*, with the highest MW sample showing the highest activity. On the other hand, no correlation with chitosan MW is observed in its activity toward *Candida albicans*.^[97] On treatment of *Candida* spp with LMW and chitosan oligomers (6–20 kDa), chitosan exhibits antifungal activity in all the tested *Candida* spp, with higher antifungal activity for higher MW species; chitosans with smaller MW values (0.73–2.09 kDa) only show antifungal activity against *Cervalescotei*. *C. albicans*, with low sensitivity toward chitosan oligomers, exhibits the lowest antifungal effect among all the *Candida* spp.^[98]

2.2. Properties of Nanochitin

2.2.1. Nanoparticles, Nanowhiskers, and Nanofibers

Nanochitin (or chitin nanomaterials) includes high-aspect ratio chitin nanofibers (ChNFs), low-aspect ratio chitin nanowhiskers (or nanocrystals, ChNWs), and chitin nanospheres (or nanoparticles, NPs). Owing to its linear nature, nanowhiskers and nanofibers are more common polymer architectures of chitin.

Nanochitin is more extensively studied than nanochitosan, as the latter does not exhibit essential properties required for various applications. Although the deacetylation of nanochitin yields chitosan nanofibers^[99] and chitosan nanowhiskers,^[100] they are insoluble under acidic aqueous conditions because the deacetylation occurs only on the nanochitin surface. This review classifies these nanomaterials as the deacetylated variations of ChNFs and ChNWs (d-ChNFs, and d-ChNWs, respectively). Although some studies report the synthesis of chitosan nanofibers through bottom-up electrospinning of chitosan solutions,^[101–104] the products are obtained as nanofiber nonwoven mats, not as individual nanofibers. Chitosan NPs are another nanostructure of chitosan that can only be prepared through bottom-up synthesis techniques. The size of chitosan NPs can range up to 1 μm , and they are mostly applied in biomedical fields.^[7] This section focuses on the properties of 1D nanochitin produced via different top-down production routes and surface modifications.

2.2.2. Synthesis of 1D Nanochitin

To synthesize nanochitin, bulk chitin is first extracted from biomass. Because of the universality of the extraction process, the biomass source is the main factor determining the quality of the extracted chitin.^[18,23,105,106] The extracted chitin never has

a D_A of 1.0 because of some inevitable deacetylation during extraction.^[105]

There are two complementary routes, top-down and bottom-up, to produce nanochitin. In the top-down approach, bulk chitin is broken down into materials of desirable nanosize. In the bottom-up approach, bulk chitin is dissolved into individual molecules, which assemble into organized nanostructures.^[7,12,101,103,107] The bottom-up approach requires the use of harsh solvents/solvent systems and alters the crystal structure of nanochitin,^[108–110] whereas the top-down approach preserves the native crystal structure and rod-like morphology of nanochitin. Therefore, 1D nanochitin is predominantly produced via the top-down approach.

The top-down production of nanochitin can be broadly classified into chemical processes (acid hydrolysis, oxidation, and deep eutectic solvent (DES) solvolysis), and mechanical disintegration (Figure 5a and Table 3).^[100,111–143] The chemical methods are based on removing the disordered domains and defect regions from chitin, resulting in low-aspect-ratio nanowhiskers. The diameter (5–80 nm range) of ChNWs is controlled by varying the reaction parameters, whereas its length (from 50 nm to several micrometers) largely depends on the chitin origin.^[105,107] Additionally, chemical reagents simultaneously modify the ChNW surface. Inorganic acids partially deacetylate the ChNW surface, and sulfuric acid (H_2SO_4) also partially esterifies primary hydroxy ($C6'-OH$) groups to sulfate-half-ester groups (OSO_3H). Organic acids, oxidizers, and DES produce ChNW with aldehyde, carboxylate, and/or carboxylic acid ester groups. The most widely used chemical method employs boiling dilute HCl to hydrolyze bulk chitin to ChNWs. Compared with the chemical routes, mechanical disintegration breaks interfibrillar hydrogen bonds and longitudinally separates bulk chitin into high-aspect-ratio nanofibers (3–100 nm wide and several micrometers long). Because mechanical treatment consumes a large amount of energy,^[144] it is usually coupled with mild chemical treatments (such as deacetylation and oxidation), which introduce repulsive surfaces on chitin, promoting the disintegration into more refined nanofibers.

2.2.3. Post-Surface-Modification of Nanochitin

Post-surface-modification can tune the physicochemical properties and comprehensive performance of nanochitin. The modification is confined to chemically accessible regions on the nanochitin surface, the density of which decreases with increasing crystal size.^[145] Post-surface-modification of nanochitin can occur to amino groups (N-functionalization), hydroxy groups (O-functionalization), acetamide, and other functional groups introduced during the nanochitin production (Figure 5b). The hydrophilicity, relative chemical reactivity between functional groups, and the extent of modification are important factors to be considered during modification.

Most studies aim to decrease the hydrophilicity of nanochitin through long-chain alkyl, phenyl, or polymer grafting reactions.^[146–151] These reactions are usually conducted in nonaqueous conditions because water is a competing nucleophile to the hydroxy and amino groups of chitin. However, the intrinsic hydrophilicity of chitin makes it challenging to

remove the adsorbed water layer on its surface or disperse nanochitin in organic media.^[152,153] Despite these challenges, attempts to modify nanochitin surface have been conducted in aqueous conditions for safety and sustainability reasons. Surface reactions of chitin in water include (but are not limited to) deacetylation,^[100,154] N-sulfonation,^[155] chlorination,^[156] lactam formation,^[157,158] imine formation,^[146] amidation,^[159] and guanylation,^[160] which impart diverse and interesting properties to nanochitin.

Although the amino groups of nanochitin are highly reactive, modifying other functional groups is more strategically advantageous owing to the potential drawbacks of N-modification, such as reduced network bonding and biological activities. This requires N-protection/deprotection, which is costly and complicated. Considering O-modification, $C3'-OH$ is less accessible than $C6'-OH$ due to the steric hindrance and intrachain hydrogen bonding;^[1,30,161] thus, $C3'-OH$ modification requires harsh conditions, which can affect the crystallinity or MW of nanochitin.

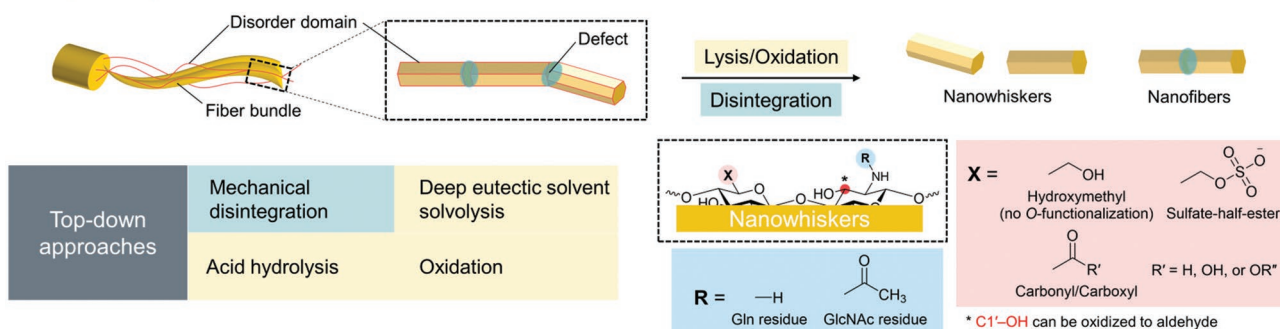
It is also important to control the extent of surface modification to maintain the intrinsic properties of nanochitin. Nanochitin crystals are maintained through intermolecular bonding; therefore, an excessive degree of modification can disrupt the bonding network, severely alter the crystal structure, reduce the MW, and ultimately degrade the performance of nanochitin.

2.2.4. Properties of 1D Nanochitin

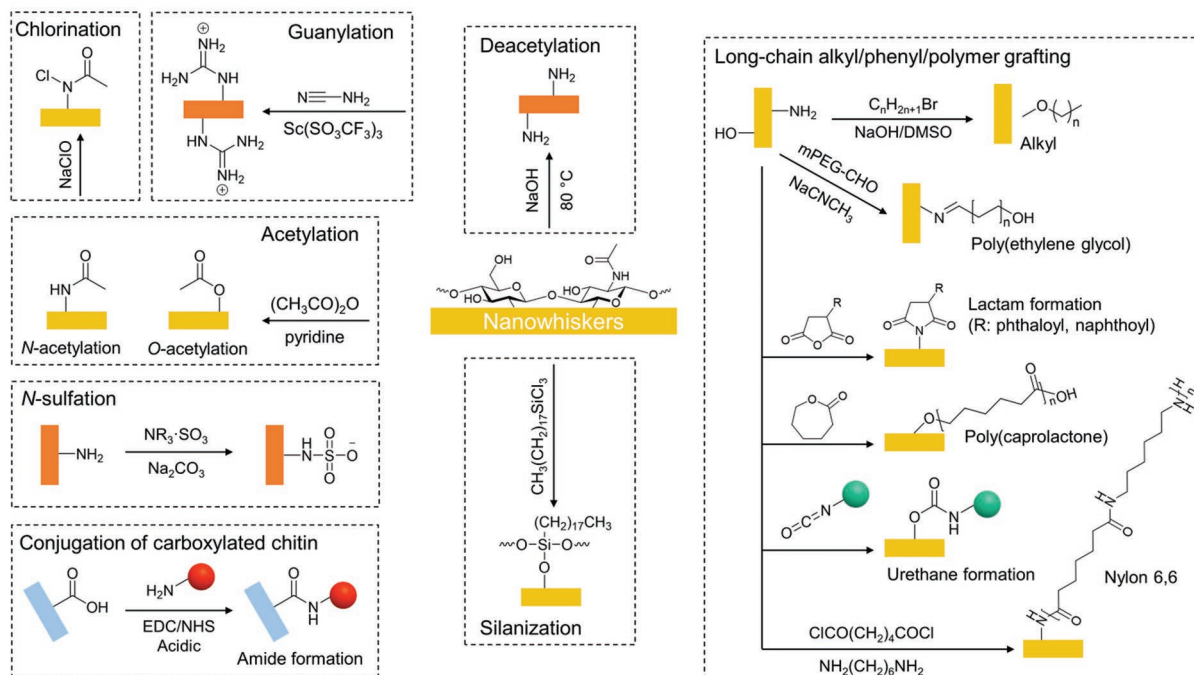
Various properties of nanochitin are governed by its dimensions. Like nanocellulose, the ultimate tensile strength (UTS) of nanochitin exponentially increases when the size decreases from the macroscale to the nanoscale according to the relation $\sigma \sim 1/\sqrt{D}$, where σ is the UTS, and D is the diameter (width) of the fiber.^[162] The UTS increases from ≈ 71 –237 MPa for α -ChNF-based macrofibers (≈ 100 –300 μm wide)^[163–165] to 1.6 GPa for an individual α -ChNF (37 nm wide).^[166] In addition, the UTS of α -ChNF films made from 6 nm wide nanofibers is ≈ 200 –250 MPa, 2–2.5-fold greater than those made from 19 nm wide nanofibers (100 MPa).^[167] In addition to the width, the length of nanochitin also remarkably affects its UTS; longer nanofibers align more readily and pack more tightly, resulting in better entanglement and interfibrillar cohesion transfers than shorter nanowhiskers. Casted films of α -ChNF exhibit an UTS of >100 MPa,^[167–170] whereas those of ChNWs fall below 50 MPa.^[170]

The mechanical properties of nanochitin are also affected by other factors including crystallinity and surface chemistry, although the relationships are not straightforward. For example, a computational model suggests that the mechanical properties of the α -chitin crystal are superior to those of the β -chitin crystal,^[171] but experimental data show otherwise. β -ChNF films have an UTS of 277 MPa, 1.7 times higher than that of α -ChNF films (156.5 MPa).^[172,173] An individual β -ChNF (UTS of 3.0 GPa) is nearly 2 times stronger than an individual α -ChNF (UTS of 1.6 GPa),^[166] probably because the aspect ratio of a β -ChNF is usually much higher than that of an α -ChNF. In addition, because the acetamide group contributes to the hydrogen bonding network in the nanochitin crystalline structure, ChNFs

a. Top-down production and functionalization



b. Post surface modification



c. Target properties



Figure 5. Chitin at the nanoscale. a) Schematic top-down production of nanochitin through chemical and physical routes into individual nanocrystals or nanofibers, accompanied with surface changes (summarized in Table 3). b) Overview of the chemical reactions enabling the post-surface-functionalization of nanochitin showing the functionalization of amino and hydroxy, acetamide, and other functional groups. The red and green circles represent functional groups or attached polymer chains that can tune the properties of nanochitin. c) Target properties of ChNWs: c1) a scanning electron microscopic (SEM) image showing the needle-like morphology of ChNWs; c2) a colloidally stable 1 wt% aqueous ChNW suspension at pH 4.0; c3) an X-ray diffraction pattern of highly crystalline α -ChNWs. c1) Adapted with permission.^[160] Copyright 2021, American Chemical Society.

Table 3. Top-down production routes for nanochitin and resulting properties.

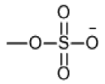
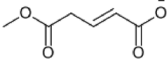
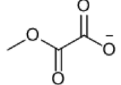
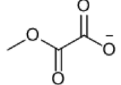
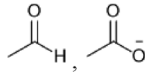
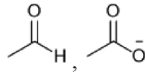
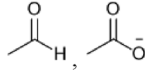
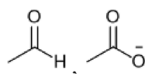
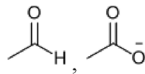
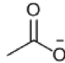
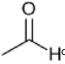
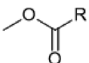
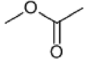
Production route	Reagents/methods	Chitin crystal allomorph and source	C6'-OH modification	Colloidal stability	Average size [nm]		Crystallinity index [%]	Yield [%]	Refs. ^{a)}
					Width	Length			
Inorganic acid hydrolysis	HCl	α -Chitin (crab shells)	Unmodified	Stable in acidic water	6–50	100–500	NR (highly crystalline)	<60	[111,112–114]
		α -Chitin (shrimp shells)	Unmodified	Stable in acidic water	15–30	150–250	87	NR ^{b)}	[100]
		β -Chitin (Riftia tubes)	Unmodified	Stable in acidic water	\approx 18	500 nm–10 μ m	NR	NR	[115]
		β -Chitin (squid pen)	Unmodified	Stable in acidic water	10	50–300	NR	NR	[116]
	H ₂ SO ₄	α -Chitin (crab shells)		Relatively stable in water	8.0	Nano to micro	86–93	80–83	[117]
Organic acid hydrolysis	Maleic acid	α -Chitin (shrimp shells)		Sterically stable in water	Nano	Nano	72–82	1.6–10	[118]
		α -Chitin (shrimp shells)		Electronically/sterically stable in water	12.5–13.0	600–1100	>80	81	[119]
	Oxalic acid	α -Chitin (shrimp shells)		Electronically/sterically stable in water	12.5–13.0	600–1100	>80	81	[119]
Oxidation	(2,2,6,6-Tetramethylpiperidin-1-yl)oxyl radical (TEMPO)/NaClO/NaBr	α -Chitin (crab shells)		Stable in acidic and alkaline water	7–20	50–500	93	NR	[120]
		α -Chitin (shrimp shells)		Stable in acidic and alkaline water	15–30	150–250	73–85	NR	[100]
		β -Chitin (tube worm)		Stable in water	20–50	Several micrometers	\approx 60–65	16–70 ^{c)}	[121]
	TEMPO/NaClO ₂ /NaClO	α -Chitin		Stable in acidic and alkaline water	5–15	200–600	\approx 92–95	>80 ^{c)}	[122,123]
	TEMPO/laccase/O ₂	α -Chitin		Stable in water	24	480	\approx 92–93	43–65	[124]
	Ammonium persulfate	α -Chitin (crab shells)		Relatively stable in water	15	400–500	79–94	38	[125,126]
	Potassium periodate	α -Chitin (shrimp shells, crab shells)		Relatively stable in water	12	220–250	97	40–50	[127]
Deep eutectic solvent solvolysis	Choline chloride (ChCl) as a proton acceptor and various organic acids as proton donors	α -Chitin (crab shells)		Sterically stable in water	29–83	165–844	85–92	78–88	[128]
	ChCl as a proton acceptor and <i>p</i> -toluenesulfonic acid as proton donors	α -Chitin	Unmodified	Electrostatically stable in aqueous acids	12–44	206–399	NR	NR	[129]

Table 3. Continued.

Production route	Reagents/methods	Chitin crystal allomorph and source	C6'-OH modification	Colloidal stability	Average size [nm]		Crystallinity index [%]	Yield [%]	Refs. ^{a)}	
					Width	Length				
	ChCl as a proton acceptor and ZnCl ₂ as a proton donor in acetic acid/anhydride	α -Chitin (shrimp shells)		Sterically stable in water, some aggregates	20–80	100–700	85–89	Up to 62%	[130]	
Mechanical disintegration	Magnetic stirring	Partly deacetylated α -chitin	Unmodified	Electrostatically stable in aqueous acids	6.2	250	57	85–90	[131]	
	Blending		Unmodified	NR	10–20	Several micrometers	NR	NR	[132–134]	
	Ultrasonication	α -Chitin (crab and shrimp shells) β -Chitin (squid pen)	Unmodified	NR	NR	30–120				[135]
	High-pressure homogenization		α -Chitin	Unmodified	NR	80–100, some aggregates	Several micrometers	85	NR	[137,138]
	Stone milling		Partly deacetylated α -chitin	Unmodified	Electrostatically stable in aqueous acids	3–30		44	NR	[139,140]
Grinding and high-pressure water-jet shearing		α -chitin	Unmodified	NR	Nano		86–89	NR	[141]	

^{a)}References cited are studies with different production routes or chitin sources, or studies on optimizing the production process; ^{b)}NR, not reported; ^{c)}Yield of insoluble fractions; ^{d)}The modification occurs at C1'-OH.

are calculated to be stiffer and stronger than d-ChNFs.^[174,175] However, experimental data show that an appropriate deacetylation degree can improve the mechanical properties of d-ChNFs because charged amino groups promote the fibrillation of d-ChNFs into more refined filaments.^[173] Overall, dimension predominantly controls the mechanical properties of nanochitin. High-aspect-ratio ChNFs exhibit a higher mechanical performance and require a lower percolation threshold in nanocomposites^[176] than low-aspect-ratio ChNWs. When nanochitin becomes wider, or it is longer than the critical length (usually >1 μ m), its cohesion strength decreases because multiple defects arise due to interchain misalignment, resulting in reduced interfibrillar interactions and entanglements.

Beyond the mechanical properties, other frequently considered properties of nanochitin include transparency and colloidal behavior. Dilute suspensions and thin films of nanochitin are generally transparent because nanochitin has a diameter less than one-tenth of the visible wavelength. Although the size–transparency relationship for 1D nanochitin has not been well established, thinner and shorter nanochitin with a monodisperse size is generally more transparent.^[100,177,178] The transparency is also controlled by other factors, such as nanochitin concentration, pH, and ionic strength of a suspension, or nanochitin alignment, thickness, and roughness of a film.

As a rod-like particle, the colloidal behavior of nanochitin suspensions can be described by two factors, aspect ratio

multiplied by concentration (Onsager's theory), and surface potential (Derjaguin–Landau–Verwey–Overbeek (DLVO) theory).^[179,180] The Onsager's theory indicates that for a monodisperse system, high-aspect-ratio ChNFs require a lower critical concentration for phase separation and gelation than low-aspect-ratio ChNWs, and are more promising as a rheological modifier. According to the DLVO theory, nanochitin is generally colloidally stable in acidic aqueous environments at a low concentration because of the electrostatic repulsion of protonated amino groups on the crystal surface. Destabilization occurs when the amino groups are deprotonated at neutral or basic pH, or in organic solvents. Additionally, electrolyte addition over a critical concentration screens the surface charge of the colloids and reduces the interparticle repulsion, and aggregation of nanochitin occurs when interparticle forces become attractive. Nanochitin can be stabilized in neutral and basic pH conditions by introducing a functional group that ionizes under these conditions, such as through sulfation, guanlylation, or oxidation (Table 3). In high-ionic-strength aqueous solutions or organic solvents, nanochitin can be made dispersible by introducing long alkyl/polymer chains that induce interparticle steric repulsion.^[117–127,146,160,181]

Overall, three target properties established for cellulose nanocrystals (CNCs)^[182] can be used to evaluate the quality of nanochitin: nanosize, colloidal stability, and crystallinity. Ideal nanochitin has at least 1D in the nanoscale (Figure 5c1).

The nanochitin size and aspect ratio are determined using scanning/transmission electron microscopy (SEM/TEM) or atomic force microscopy.^[105,160,183,184] The colloidal stability of charged nanochitin can be inferred by zeta-potential measurements;^[100,183] aqueous suspensions with a zeta value greater than +30 mV are considered highly stable (Figure 5c2).^[185] The crystallinity index and crystal allomorphs of nanochitin are typically determined using X-ray diffraction, and can be used to evaluate the production route (Figure 5c3).

2.3. Hierarchically Assembled Structures of Chitin

2.3.1. Assembly of Nanochitin

An isotropic suspension of HCl-hydrolyzed ChNWs can spontaneously separate to form a coexisting anisotropic left-handed chiral nematic (cholesteric) phase above a critical nanowhisker concentration (Figure 6a).^[111,112,186] The chiral nematic phase

can be visualized as fingerprint patterns using polarized optical microscopy (POM) (Figure 6b), or as ordered domains using TEM (Figure 6c). It consists of parallel aligned ChNW planes; the planes are stacked on one another and rotate about a central perpendicular axis, forming a structure resembling the plywood structure of chitin in nature. The length of the cholesteric pitch (p) is twice the ridge-to-ridge distance of the fingerprint pattern.^[186] Unlike iridescent chiral nematic CNC films,^[3] ChNWs form transparent films without iridescence (loss of chiral nematic twisting) after water evaporation, although a layered structure of ChNW is observed (Figure 6d).^[187] The chirality arising during the self-assembly is assumed to be a result of a twist in the structure of the ChNWs and CNCs (Figure 6e).^[111,188–190]

The Onsager's theory, which suggests the critical concentration for isotropic–chiral nematic transition depending on the aspect ratio of nanochitin, is only valid for a monodisperse system (Section 2.2.4). Nanochitin is usually polydisperse (Table 3). Its phase transition is better described through the

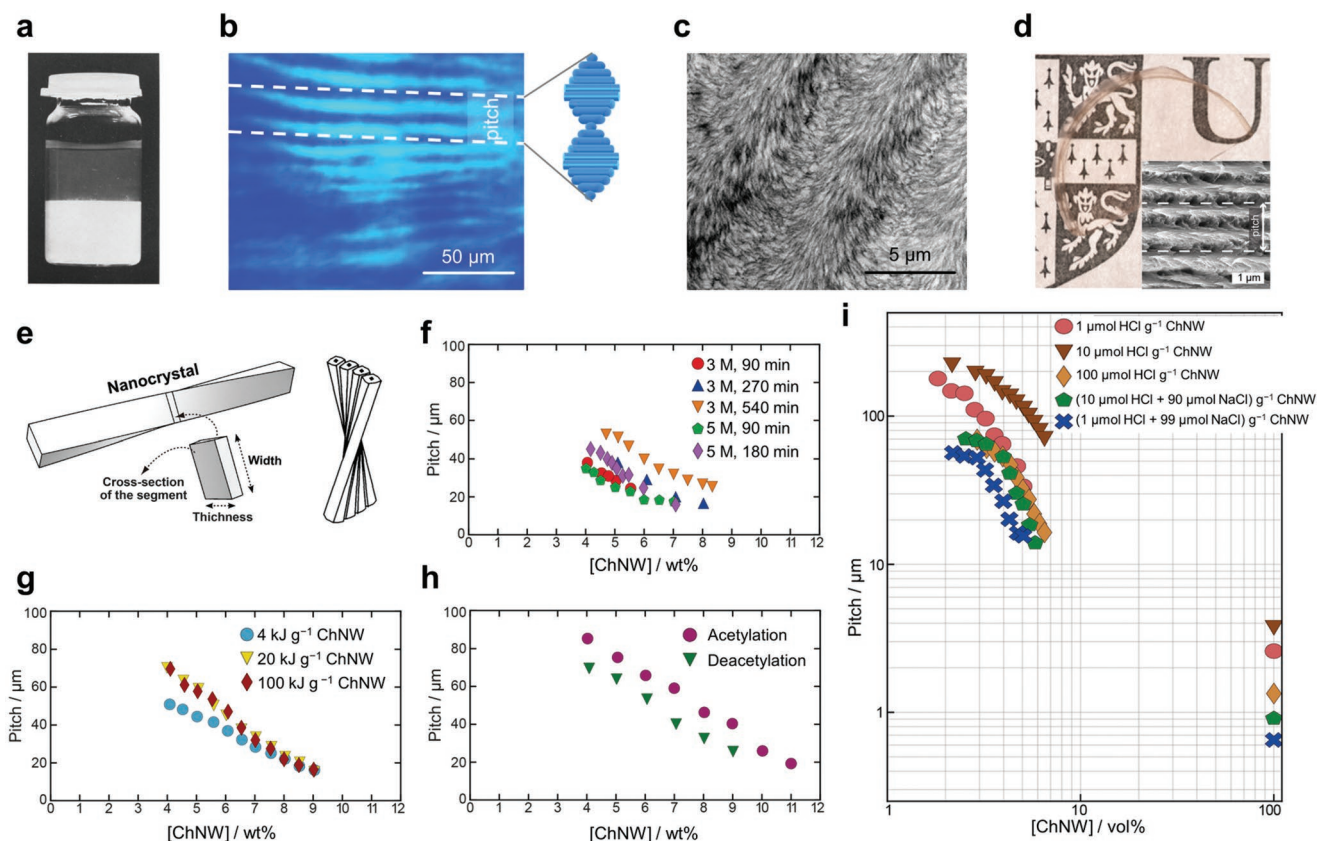


Figure 6. The liquid-crystal behavior of aqueous nanochitin suspensions. a) Phase separation of aqueous suspensions of HCl-hydrolyzed ChNWs on standing. Reproduced with permission.^[111] Copyright 1993, Elsevier. b) The fingerprint pattern of the nanochitin chiral nematic phase observed using POM, showing the pitch-height measurement. c) TEM image of nanochitin chiral nematic structure. b) Adapted under the terms of the CC-BY Creative Commons Attribution 4.0 International license (<https://creativecommons.org/licenses/by/4.0/>).^[153] Copyright 2016, The Authors, published by Springer Nature. c) Reproduced under the terms of the CC-BY Creative Commons Attribution 4.0 International license (<https://creativecommons.org/licenses/by/4.0/>).^[153] Copyright 2016, The Authors, published by Springer Nature. d) A transparent ChNW film, retaining its helicoidal nanoarchitecture (inset) upon water evaporation. Reproduced with permission.^[187] Copyright 2019, American Chemical Society. e) Illustration of the twisted structure of a single ChNW and the chiral nematic arrangement of four ChNWs in close contact. Left: Reproduced with permission.^[188] Copyright 2020, American Chemical Society; Right: Reproduced with permission.^[111] Copyright 1993, Elsevier. f–i) Factors controlling the self-assembly of aqueous ChNW suspensions, including hydrolysis conditions (HCl concentration in M and hydrolysis time in min) (f), tip sonication energy (g), acetylation state of the starting bulk chitin (h), and pH and ionic strengths of ChNW suspensions (i). f–i) Adapted with permission.^[187] Copyright 2019, American Chemical Society.

excluded volume of rods, where the critical concentration for phase separation and the volume fraction of the liquid crystal phase are both a function of $(L^2D)^n$; L and D are length and width of nanochitin, respectively, and n is an exponent.^[179,187] Although n is determined for CNCs, current literature data are not sufficient to produce the empirical value for nanochitin. However, some general observations for CNCs can be applied to nanochitin. For example, in a polydisperse system, nanofibers tend to form the chiral nematic phase, while nanowhiskers tend to remain in the isotropic phase.^[191,192]

The self-assembly of ChNWs also depends on its surface chemistry, charge density, and environmental factors such as pH and ionic strength.^[187,193] Generally, smaller ChNWs with greater charge density obtained from more extensive hydrolysis and higher-energy tip sonication require a higher critical concentration for phase separation. The resulting chiral nematic phases exhibit a higher pitch height (Figure 6f,g). Deacetylated chitin is more prone to hydrolysis due to the solubility of deacetylated portions in the acidic medium. It forms thinner and shorter nanowhiskers that self-assemble into chiral nematic structures with shorter pitches compared with highly acetylated chitin (Figure 6h). Ionic strength and pH produce opposite effects. Lowering the pH increases pitch height due to the repulsive forces between positively charged ChNW surfaces. At H^+ concentrations greater than a critical value, ionic strength becomes a predominant factor, forming shorter peak heights due to compression of the electrical double layer around the nanowhiskers (Figure 6i).^[187]

In addition to α -ChNWs, other studies have attempted to produce ordered structures of surface-modified nanochitin and the β form. N-sulfated-ChNWs form liquid crystals.^[155] Strong birefringence has been observed for aqueous suspensions of β -ChNFs,^[194] zwitterionic carboxylated ChNWs,^[195] and poly(ethylene glycol)-grafted-ChNWs,^[146] but a higher organization into the chiral nematic phase does not occur; more research is required to elucidate this phenomenon. The ordering of nanochitin has been also reported in conditions other than aqueous suspensions. Oh et al. disintegrated bulk α -chitin using calcium ion (Ca^{2+})-saturated methanol into ChNFs and obtained a nematic phase in isopropyl alcohol after solvent exchange.^[153] Additionally, well-dispersed ChNWs can be oriented into highly anisotropic nematic structures using fast water evaporation in a confined space,^[196] mechanical force,^[163] and magnetic fields.^[197,198] The nematic alignment of nanochitin can be used to fabricate strong anisotropic adhesives for dry surfaces^[196] and has immense potential for packaging applications.

2.3.2. Chitin-Derived Nitrogen-Doped Carbon Materials

The hierarchically assembled structures of chitin can be used to produce nitrogen-doped carbon materials.^[199] Chitin has a relatively higher carbonization efficiency than other natural polymers because it does not melt on heating. Most importantly, it can retain an ordered porous structure after extraction from the biomass. These features allow the direct preparation of self-N-doped porous carbon materials with homogeneously distributed nitrogen in the porous carbon matrix. The multivalency of nitrogen and carbon and their large electronegativity difference

enables diverse interactions, allowing various applications of N-doped carbon materials, from environmental management to electrochemistry.^[200]

At the micro-length-scale (Figure 1), the performance of N-doped carbon materials is mainly controlled by properties such as porosity (surface area), N-doping position, N-doping level, and bonding configuration.^[201,202] N-doped carbon materials are prepared from chitin or chitosan by thermal treatment, which involves pyrolysis at high temperatures (900 °C) in an inert-gas atmosphere, or hydrothermal treatment at milder temperatures (≈ 200 °C).^[203–206] Pyrolysis produces whole carbon materials with higher surface area and low N-doping levels, whereas hydrothermal treatment results in carbon-sheath/chitin-core materials with high N-doping levels.^[203,207]

3. Applications of Chitin and Chitosan Nanostructures with Multiscale Properties

3.1. Biomedical Applications

Chitin, chitosan, and nanochitins are positively charged polyelectrolyte substances extracted from natural sources; therefore, they are likely to be contaminated with harmful negatively charged endotoxins derived from gram-negative bacteria. Thus, endotoxin removal and investigations of the multiscale physical properties of nanochitin are vital before the biomedical use of these samples; otherwise, unreliable research results could necessitate the repetition of time-consuming animal experiments.

3.1.1. Sealants and Hemostatic Materials

In 1940, Mark G. M. Pryor (Cambridge University) identified that polyphenolic compounds cross-link the chitin structure of insect exoskeletons, and Norman de Bruyne (Royal Aircraft Establishment) invented phenol-/resorcinol-formaldehyde adhesives for use in aircraft construction by mimicking chitin compounds. After the success of this biomimetic adhesive, many researchers have used chitin and other related materials as adhesives. SFA experiments indicate that hydrogen bonding significantly influences the bonding strength of chitin and chitosan, which depends on the hydrogen-bond ratio of the amine and hydroxyl groups. MW, which can affect the hydrogen-bond ratio, also influences the bonding strength.^[40,41] Chitosan shows good adhesion to human blood and some chitosan-containing hemostatic materials have been approved by the United States Food and Drug Administration (U. Although chitosan has adhesive properties, it swells under wet conditions and loses its positive charge at physiological pH, drastically reducing its binding force.^[208] Therefore, the application of chitosan as a bioadhesive requires modifications to overcome these limitations. Many researchers have conjugated phenolic compounds (such as quinone, catechol, and gallol) with chitin and chitosan, mimicking the cross-linking and adhesion mechanisms of insect cuticles and underwater adhesives of marine fouling organisms (Figure 7a).^[209,210] Phenolic compounds increase adhesion under wet conditions by several chemical interactions, such

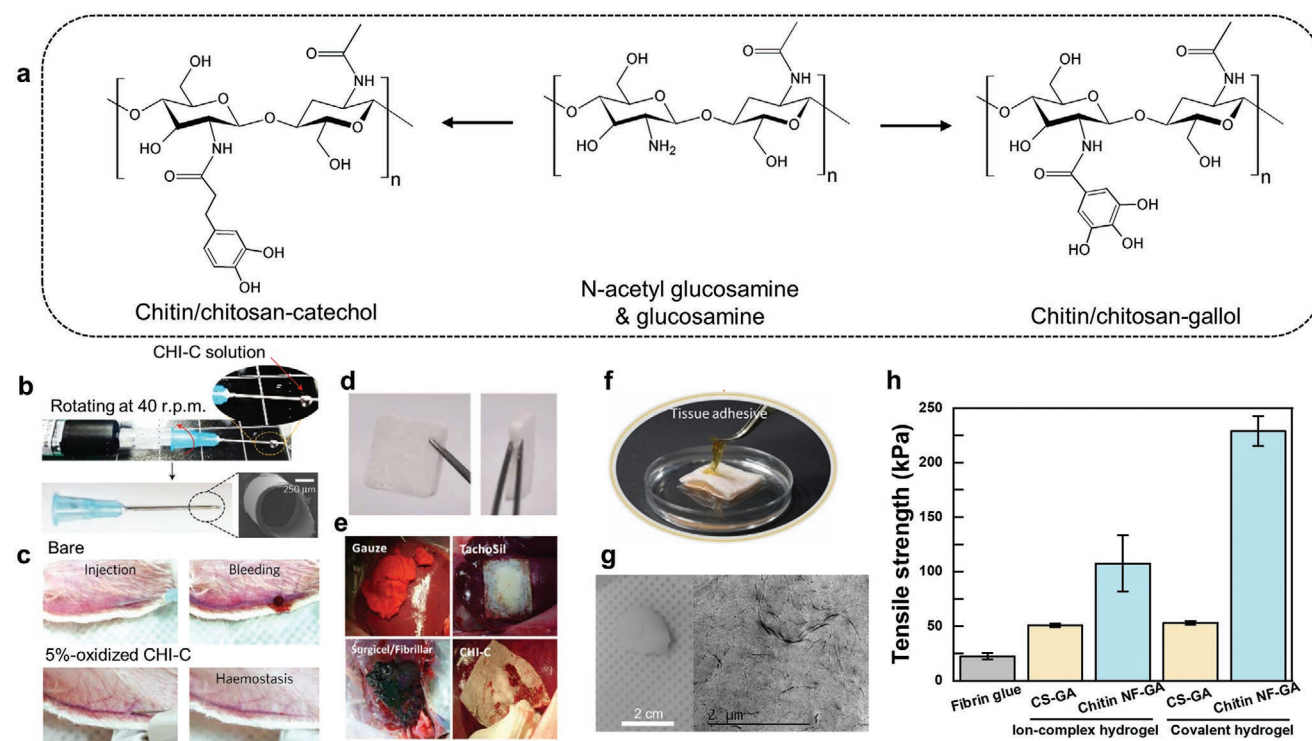


Figure 7. a) Chemical structures of chitosan modified with phenolic compounds, such as b–e) catechol and f–h) gallol. b) Photographs of the chitosan–catechol-coated hemostatic needle and the SEM image of the coating film. c) Photographic images showing the in vivo hemostatic effect of the needles after injection of saline into a rabbit marginal ear vein (top: bare needles, and bottom: 5%–oxidized chitosan–catechol-coated needles). b, c) Adapted with permission.^[212] Copyright 2016, Springer Nature. d) Images of a chitosan–catechol sponge. e) Images showing the in vivo hemostatic effect of hemostatic materials (gauze, Tachosil, Surgicel/Fibrillar, and the chitosan–catechol sponge) after application to a pig model of coagulopathic liver bleeding. d, e) Adapted with permission.^[213] Copyright 2021, American Association for the Advancement of Science. From ref. [213]. © The Authors, some rights reserved; exclusive licensee AAAS. Distributed under a CC BY-NC 4.0 license <https://creativecommons.org/licenses/by-nc/4.0/>. Reprinted with permission from AAAS. f, g) Images of a chitosan–gallol hydrogel (CS–GA)^[218] (f) and chitin nanofiber–gallol (Chitin NF–GA, right: optical image, and left: cryo-TEM image)^[217] (g). h) Wet adhesion ability of CS–GA and Chitin NF–GA with ionic complex and covalent cross-linking. f) Adapted with permission.^[218] Copyright 2019, Elsevier. g) Adapted with permission.^[217] Copyright 2015, Elsevier.

as covalent bonding, metal coordination, hydrogen bonding, cation– π interaction, and π – π stacking.^[211] The conjugation of phenolic compounds with chitosan makes the modified chitosan soluble, regardless of the pH, increasing its biomedical applications.^[209]

A chitosan–catechol thin coating on a needle surface has been reported to form a gel-like material which acts as a sealant on tissue; this needle can be used as a self-sealing hemostatic needle causing negligible blood loss (Figure 7b,c).^[212] Furthermore, a chitosan–catechol sponge has been synthesized which rapidly binds to plasma proteins (albumin, fibrinogen, and globulin) on contact with blood, forming a blood–protein barrier. It was applied for the first time in a human clinical trial of hepatectomy; it shows an excellent hemostatic effect compared to Tachosil and Surgicel/Fibrillar (Figure 7d,e).^[213] Its mucoadhesive properties have also been investigated. As chitosan–catechol forms an irreversible catechol-mediated cross-linking with mucin, the gastrointestinal-tract retention is increased, causing higher mucoadhesion compared to conventional chitosan.^[214] Dihydroxybenzoic acid-grafted-chitosan–catechol, with a high catechol content, shows strong mucoadhesive properties in mucin.^[215] The conjugation of polyphenolic compounds with chitin nanostructures improves adhesion and hemostasis fur-

ther.^[216] The adhesion of a gallol-conjugated chitin nanofiber to porcine skin is up to 10 times higher than that of a chitosan–catechol or pyrogallol polymer (Figure 7f–h).^[217] Additionally, chitosan–gallol moieties retain good hemostatic effects with high platelet attachment and blood clotting.^[218]

3.1.2. Gene and Drug Delivery

Chitosan NPs have numerous manufacturing methods, are applied in various fields, and are synthesized by emulsification, precipitation, ionic gelation, self-assembly, and so on.^[219–223] The amine groups of chitosan, due to their positive charge, easily form complexes with anionic polymers and conjugate molecules, facilitating high target specificity and immune activity. Additionally, the mucoadhesive properties of chitosan allow the uptake of chitosan NPs to target sites.^[224,225] Therefore, chitosan NPs are widely used in medicine and pharmaceuticals to deliver drugs, genes, and vaccines. The safe encapsulation of the target molecule by NPs and its transport (with protection from enzymes) and proper release at the target site is vital in a delivery process (Figure 8).^[226] Therefore, the size, stability, binding affinity, uptake capacity, and release rate of NPs should be considered

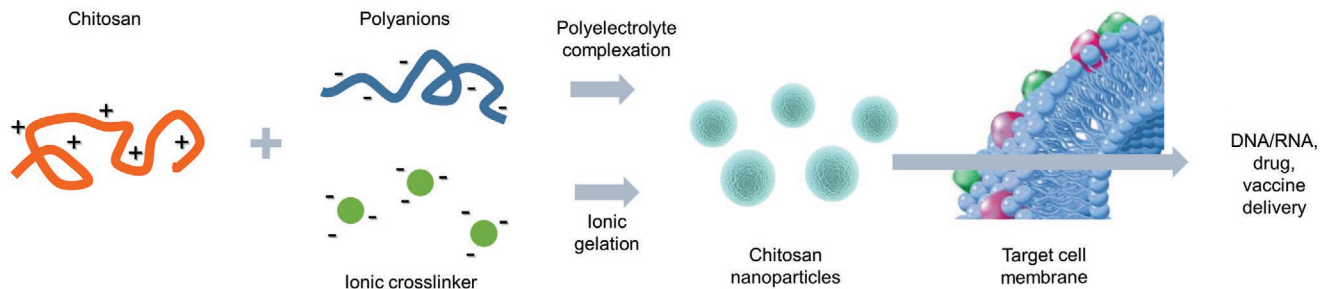


Figure 8. Chitosan nanoparticle formation mechanisms by polyelectrolyte complexation and ionic gelation. Positively charged chitosan NPs carry cargo and undergo endocytosis to uptake target cells. Subsequently, NPs transfer from endosomes to the cytoplasm and release their cargo (DNA/RNA, drugs, and vaccines) for delivery to target sites (such as the nucleus, translation machinery, and immune cells).

during synthesis. These factors are influenced by various parameters, such as MW, D_A , and amine-to-phosphate (N/P) ratios.^[227] High MW values indicate large particle size; at the oligomer range, they do not form sufficient bonds with polyanions, forming large unstable particles with 600 nm size.^[220,223,228] Particle stability and cargo protection are also improved, and the small interfering RNA (siRNA) is better protected from degrading enzymes (such as DNase) as the MW increases.^[229] Cellular uptake is affected by zeta potential and D_A (to varying degrees in different publications); the uptake reduces by 26% when the chitosan NP MW decreases from 213 to 10 kDa (however, the uptakes of 11 and 14 kDa chitosan NPs are higher than those of 53 and 100 kDa NPs, respectively).^[229,230] Chitosan NPs in the MW range of 137–620 kDa do not exhibit significant differences in transfection efficiency; in gene silencing, however, the 11 kDa chitosan NP (among NPs in the range of 11.8–110 kDa) exhibits the highest effect in LS174T cells, while the 50 kDa NP (among LMW chitosans in the range of 2–50 kDa) exhibits the highest effect in HeLa and OV-3 cells.^[228,229,231] Although LMW chitosan forms relatively unstable NPs with nucleic acid, it can effectively release intracellularly and exhibits high transfection efficiency. However, the MW range exhibiting high transfection efficiency depends on the targeted gene and cell.

Many diseases are related to gene malfunction; thus, chitosan, a nonviral vector, is used for delivering genes that can edit the disease-causing gene expression. However, since chitosan itself has insufficient transfection efficiency and target specificity, complexes incorporating peptides/molecules into chitosan are being developed to overcome these limitations. A siRNA-loaded trimethyl chitosan (TMC)–polyethylene glycol (PEG) complex that links a short peptide obtained from the rabies-virus glycoprotein, that specifically binds to the nicotinic acetylcholine receptor on neuronal cells, has been synthesized as a therapeutic target for Alzheimer's disease. These complexes exhibit high intracellular uptake, occur in Neuro2a cells, and peptidylprolyl Isomerase Like 2 (PPIL2) siRNA-loaded NPs cause efficient beta-site amyloid precursor protein cleaving enzyme 1 (BACE1) knockdown in Neuro2a cells.^[232] Galectin-1 siRNA-loaded chitosan NPs have been fabricated to reduce Galectin-1 in the tumor microenvironment of glioblastoma multiforme, a primary brain tumor. Galectin-1 siRNA delivery causes a decrease in myeloid suppressor and Tregs, and an increase in cluster of differentiation 4 (CD4⁺) and CD8⁺ T cells. During the evolution of the glioblastoma multiforme,

Galectin-1 knockdown inhibits the polarization switch of macrophages from M1 (proinflammatory) to M2 (anti-inflammatory), causing a normalization of tumor vasculature and high survival of tumor-bearing mice.^[233] For bone repair, either the expression of a bone-regeneration gene is increased, or that of a gene that interferes with bone formation is decreased. Chitosan-based NPs have been treated on collagen scaffolds to fabricate gene-activated scaffolds to facilitate mesenchymal stem cell (MSC) transfection; particle size and zeta potential are higher for MMW (160 kDa)–plasmid DNA (pDNA) NPs, while the encapsulation efficiency is higher for chitosan oligomer (7.3 kDa)–pDNA NPs. Chitosan oligomer–plasmid green fluorescent protein (pGFP) NPs exhibit 45% transfection efficiency in MSC transfection. Moreover, on loading the NPs onto collagen scaffolds, luciferase is expressed higher by chitosan oligomer NPs than MMW NPs.^[234] The transfection of chitosan oligomer NPs (7.3 kDa) carrying bone morphogenetic protein-2 (BMP-2), an osteogenic gene, and vascular endothelial growth factor (VEGF), an angiogenic gene, into MSCs causes BMP-2 and VEGF expression for more than 14 days. Implantation of the gene-activated collagen hydroxyapatite scaffold in the calvarial defect model generates high neovascularization, causing bone repair in the pBMP-2 and pVEGF scaffold.^[235]

Chitosan NPs also deliver chemical drugs via controlled release and targeted therapy in vivo. 5-Fluorouracil-loaded pH-responsive chitosan nanogels have been fabricated for melanoma by ionic gelation. Nanogel accumulates in melanoma tumor nodules, inducing the release of 5-Fluorouracil in a weakly acidic condition, causing selective drug accumulation in the melanoma sites in chemically induced melanoma animal tumor models.^[236] Doxorubicin (DOX), a solid tumor treatment drug, has been encapsulated in PEG-conjugated chitosan oligosaccharide–arachidic acid NPs to confirm the leukemia-treatment effect; the NPs (165 nm) are maintained for 72 h, with the sustained release pattern of DOX appearing at physiological pH. The DOX uptake rate is higher when human leukemia K562 cells are treated with NPs than with DOX solutions. Pharmacokinetic studies in rat indicate that the in vivo clearance of DOX in the NP group is slower than the other groups, causing a prolonged circulation period of DOX.^[237] The antitumor activity against breast cancer has been confirmed by loading Tamoxifen, a breast cancer treatment drug, on pH-responsive chitosan NPs, forming chitosan NPs (100–150 nm) that rapidly release Tamoxifen at acidic pH. These chitosan NPs

exhibit antitumor activity in human breast cancer cells (MCF-7) by increasing the cellular-uptake efficiency of Tamoxifen and inducing apoptosis in a caspase-dependent manner.^[238] The antitumor effects of the chemotherapeutic agent paclitaxel- and antiangiogenic peptide endostatin-loaded chitosan NPs on Lewis lung carcinoma have also been studied. Endostatin-loaded NPs exhibit 223.45 nm size and 71% entrapment efficiency. Paclitaxel-loaded NPs exhibit a strong antiangiogenic effect and 70% tumor-suppression rate in vivo, which is significantly higher than that of other drug groups.^[239]

3.1.3. Vaccine Adjuvants

Vaccines activate cellular immunity mediated by T cells, humoral immunity mediated by B cells that produce antibodies, and induce immunological memory. Vaccines currently in use are based on nucleic acids (DNA, mRNA), virus-like particles, viral vectors, and recombinant proteins.^[240] Innate immune recognition through PRR generates a signal necessary for adaptive immune activation; thus, adjuvants must be included in vaccine formulations for vaccines without natural PAMPs. An aluminum salt, most frequently used among the approved human vaccine adjuvants, does not adequately induce mucosal immunity and causes an inappropriate inflammatory reaction at the injection site; thus, it is vital to develop a new effective vaccine adjuvant.^[240,241] Chitin, a component of fungal cell walls, is a PAMP that is recognized by PRRs of immune cells.^[55] Chitosan, which is recognized by TLRs and C-type lectin receptors to activate immunity, can be used as an immune potentiator.

Chitosan activates the NLRP3 inflammasome and increases type I interferons (IFNs) through the cGAS–STING pathway, exhibiting strong cellular immunity through a mechanism that promotes dendritic cell (DC) maturation.^[50,70]

LMW–MMW (50–190 kDa) and HMW (310–375 kDa) chitosans induce interferon regulator pathway signaling, the activation of antigen-presenting cells, and the production of cytokine mRNA in influenza A virus protein vaccine models. LMW–MMW produces higher mRNA levels in 24 h, and HMW elevates mRNA response in 48 h. Additionally, LMW–MMW chitosan treatment increases immunoglobulin G (IgG) production, while HMW chitosan treatment increases T cell cytokine CD4 IL-4 and IL-2 production. Both chitosans act as good adjuvants by reducing influenza A virus morbidity.^[242] Administering inactivated avian infectious bronchitis virus (IBV) vaccines containing the BR-1 genotype strain encapsulated in chitosan NPs (286 nm, 19.9 mV) to chickens through the ocular–nasal route produces high levels of anti-IBV immunoglobulin A (IgA) and IgG antibodies, with a strong ability to express the IFN- γ gene, induces a mucosal immune response. Furthermore, the IBV–chitosan vaccine provides effective protection against IBV strains of the BR-1 genotype.^[243] Administering SC2 spike (S)–DNA-loaded gold–chitosan nanocarriers (core 20 nm, spike 20–30 nm, 35.8 mV) intranasally in severe acute respiratory syndrome coronavirus 2 (SARS-CoV-2) DNA vaccines increase humoral immune responses which neutralize the effects of pseudoviruses that express different spike variants of SC2. Additionally, T and B cell responses are efficiently activated in the lungs and lymph nodes, causing enhanced cell-mediated immune responses (Figure 9).^[244] Receptor-binding domains of SARS-CoV-2 spike

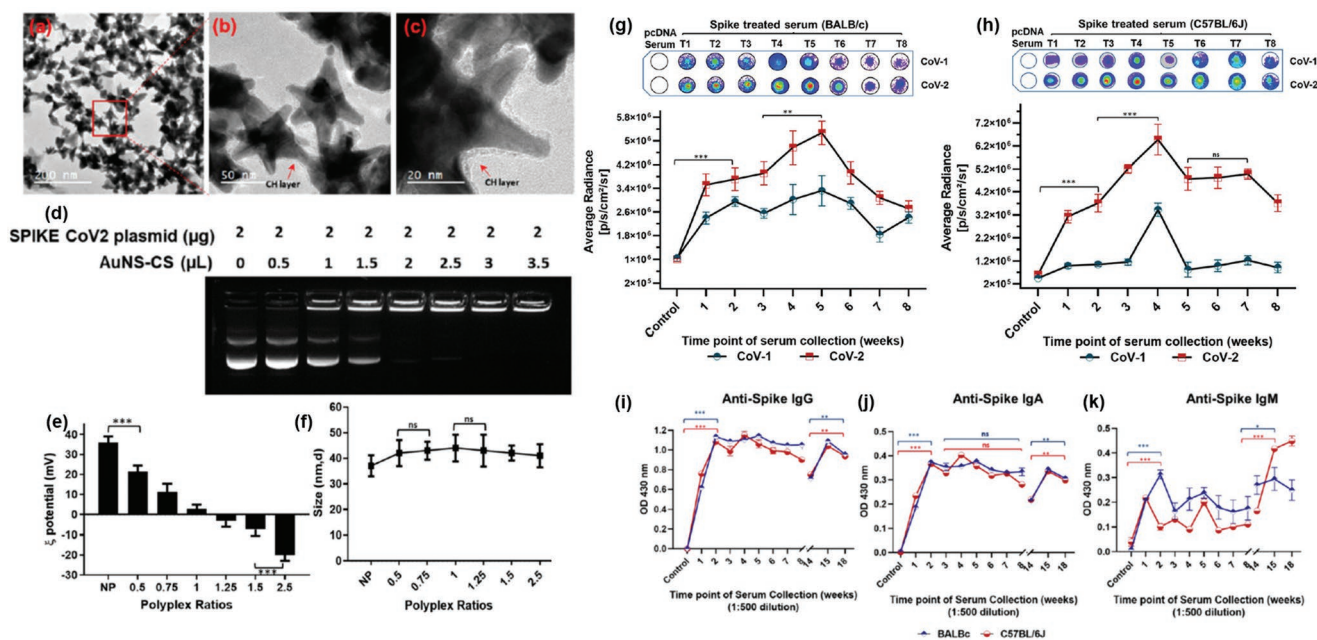


Figure 9. SARS-CoV2 (SC2) vaccines with gold nanostar (AuNS) chitosan nanocarriers. a–c) Field-emission scanning electron microscopy (FE-SEM) images of AuNS–chitosan and SC2 DNA. d) A gel retardation assay to assess AuNS–chitosan DNA loading efficiency. e, f) The zeta potentials and particle sizes of SC2-vaccine-loaded AuNS–chitosan at different ratios. g, h) Anti-SC2 antibody levels are detected in the serums of BALB/c mice (g) and C57BL/6 mice (h) immunized with AuNS chitosan loaded with CoV-1 and CoV-2. i–k) Enzyme-linked immunosorbent (ELISA) assay measured against SC2 S protein-specific IgA (i), IgG (j), and immunoglobulin M (IgM) (k) levels in serums of BALB/c and C57BL/6 mice. a–k) Adapted with permission.^[244] Copyright 2021, American Chemical Society.

glycoproteins loaded into TMC NPs (386 nm, 12.9 mV) exhibit a significantly high loading efficiency of 99% and good vaccine efficiency by intranasal delivery.^[245]

Chitosan also has been studied as an adjuvant for infectious bacteria vaccines. A comparison of the nasal-vaccine effects of lipopeptide subunit vaccine (LCP-1)-loaded and alginate/TMC-coated liposomes, and LCP-1/negatively charged polymers/TMC polyelectrolyte complexes against Group A *Streptococcus* show that the complexes (200 nm, 30 mV) induced IgG and IgA titers.^[246] *Salmonella* subunit vaccines including immunogenic outer membrane proteins, and flagellin (F)-protein-loaded and F-protein-surface-coated chitosan NPs, have been delivered orally to increase intestinal mucosal immunity to the *Salmonella* vaccine. NPs (514 nm, 40 mV) improve TLRs, and Th1 and Th2 cytokines' mRNA expression in chicken immune cells; the oral administration of NPs in avian improves specific systemic and mucosal antibody responses.^[247]

3.1.4. Biodegradable Microbeads

Microbeads are spherical solid particles with diameters ranging from 5 μm to 1 mm.^[248] They have been increasingly used as a mechanical exfoliant in personal-care and cosmetics products. However, environmental and health concerns regarding microbeads produced from petroleum-derived plastics have necessitated the development of sustainable alternatives.^[249–254] Bulk chitin and chitosan can be used to produce cost-effective microbeads with great performance and biodegradability. Chitin microbeads with homogeneous shape and narrow size distribution have been produced using ionic liquids and critical CO_2 drying.^[255] However, being expensive, this method is unsuitable for the production of cost-competitive commercial products. Emulsion diffusion, based on a “switch” in the aqueous solubility of chitin/chitosan controlled by their D_A , is a facile and cost-effective method to prepare high-performance microbeads with well-controlled sizes and smooth surfaces. Chitin microbeads have been synthesized through the acetylation of chitosan in a water-in-oil inverse emulsion system (Figure 10a). The microbeads exhibit a high cleansing efficiency due to their high mechanical and adsorption properties (Figure 10b). Furthermore, they exhibit fast degradation in activated sludge, and their presence in soils is nontoxic to model plants (Figure 10c–e).^[255]

3.2. Sustainable Materials

3.2.1. Mechanically Reinforced Biocomposites

Increasing demand for both superior mechanical properties and sustainability in construction, auto parts, electronics, and biomedical implants has driven the development of bio-sourced polymer nanocomposites (biocomposites) to replace conventional inorganic-filler-reinforced nanocomposites.^[257–260] High load-bearing natural materials (such as wood, bone, and crustacean shells) provide inspiration to fabricate biocomposites that mimic their multiscale structures

by combining natural reinforcing elements with energy-dissipating matrices.^[261,262]

1D nanochitin possesses many unique properties, such as a high longitudinal elastic modulus (theoretically more than 150 GPa^[21]), high aspect ratio, abundant polar groups capable of hydrogen bonding, and a low density (1.425 g cm^{-3}). Thus, nanochitin exhibits a higher specific modulus (modulus-to-density ratio)^[21] and larger specific surface area than ceramics and metals, and could be used to fabricate lightweight strong materials. Similar to CNC, the reinforcing ability of nanochitin is generally attributed to the formation of a hydrogen-bonded (percolated) network within the polymer matrix, and their ability to act as nucleating agents.^[105,150] Nanochitin has been used to reinforce both bio-based and petrochemical-based polymers, forming hybrid and green biocomposites, respectively.^[258] The reinforcement effectiveness of nanochitin depends on numerous factors, including nanochitin–polymer compatibility, biocomposite processing methods, and parameters relevant to nanochitin.

The hydrophilicity of nanochitin makes it compatible with hydrophilic polymers, because it enables a homogeneous dispersion of nanochitin in the polymer matrix, maximizing the filler–matrix adhesion. Nanochitin composites of hydrophilic polymers such as poly(vinyl alcohol) (PVA),^[263,264] waterborne polyurethane,^[265] and soy protein isolate^[114] exhibiting remarkable mechanical properties have been fabricated. However, most commodity and engineering plastics are hydrophobic, exhibiting low compatibility with nanochitin. Nanochitin can be chemically modified to overcome this limitation. The polymer grafting strategy has been used to fabricate ChW-g-poly(ϵ -caprolactone) (PCL) and d-ChW-g-nylon 6,6 composites with good mechanical properties.^[149,150] However, surface modification should ensure a balance between filler–matrix adhesion and filler–filler cohesion to ensure acceptable performance of the nanocomposite. For instance, hydrophobic ChNWs show unexpectedly low mechanical reinforcement of natural rubber compared with untreated nanochitin. This can be attributed to the partial destruction of the hydrogen-bonded ChNW-percolated network upon surface modification (Figure 11a1,a2).^[148,266]

Processing methods also influence the performance of a composite. Methods to prepare polymer/nanochitin composites can be broadly categorized into ex situ processing and in situ polymerization. In the ex situ approach, nanochitins are mixed with polymers using solvent/solvent systems; in the in situ approach, monomers containing predispersed nanochitin are polymerized. After mixing, nanocomposites are produced through solvent evaporation (casting–evaporation), or thermal processing after freeze-drying/precipitation.^[267] Generally, casting–evaporation generates composites with better mechanical properties than thermal processing as shown in the rubber/ChNW system^[113,266] (Figure 11b1,b2) because solvent evaporation is a slow process that provides sufficient time for the nanofiller to establish a percolated network. By contrast, shear stress in thermal processing causes nanochitin agglomeration. The solvent mixing approach can be coupled with spinning techniques to form elongated nanocomposite fibers and improve the alignment of nanochitin within the polymer matrix. PVA/ChNW and alginate/ChNW fibers of remarkable strengths have been produced using electrospinning and wet spinning from

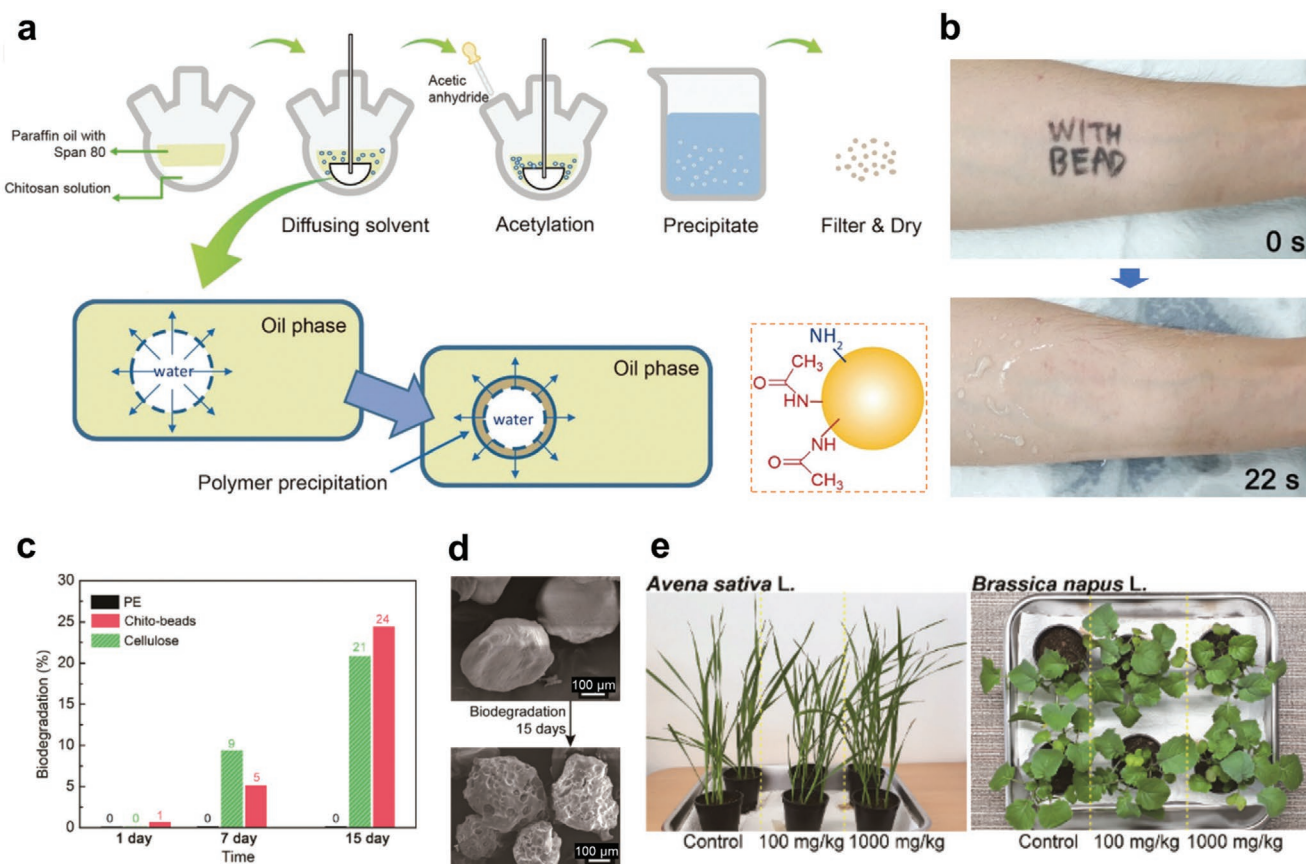


Figure 10. Sustainable chitin microbeads for cosmetic applications. a) Schematic preparation of chitosan microbeads through the acetylation of chitosan using the emulsion diffusion method; a chitin microbead is also shown. b) High ink-cleaning efficiency on human skin exhibited by a solid soap incorporating chitin microbeads. c) The biodegradation (ratio of the biochemical oxygen demand to theoretical oxygen demand of microbes, ISO 14851) of chitin microbeads (chito-beads) compared with those of polyethylene (PE) and cellulose microparticles in activated sludge. d) SEM image of chitin microbeads before and after biodegradation in activated sludge. e) Photographs of oat (*Avena sativa* L.) and rapeseed (*Brassica napus* L.) plants grown in soils mixed with chitin microbeads (100 and 1000 mg microbead kg^{-1} soil). a–e) Adapted with permission.^[256] Copyright 2021, Royal Society of Chemistry.

an aqueous medium, respectively.^[268,269] Water is the preferred medium for mixing nanochitin and polymers. Besides hydrophilic polymers, nanochitin composites of hydrophobic polymers, including poly(styrene-co-butyl acrylate),^[116] PCL,^[115] and natural rubbers,^[113,266] have been produced through casting–evaporation of their aqueous suspensions stabilized by a surfactant. Most hydrophobic polymers require nonaqueous solvents; thus, the surface of nanochitin is usually made hydrophobic to improve its dispersion in organic solvents. Examples of biocomposite films produced via this route include natural rubber/alkylated or phenylated ChNW from toluene^[148] and poly(L-lactic acid)/O-acetylated ChNF from chloroform.^[270]

Compared with the casting–evaporation, which is time-consuming and limited to the lab scale, thermal processing is a suitable alternative for the industrial-scale production of biocomposites. However, preventing nanofiller agglomeration is necessary. Because surface modification complicates the production process and reduces the economic merits of biocomposites, neat nanofillers are preferred. If the neat nanofiller is thoroughly mixed with the polymer prior to processing, nanocomposites with homogeneously dispersed nanofillers

can be formed even with thermal processing. From a thermodynamic viewpoint, in situ polymerization incorporates the nanofiller into the polymer matrix from the monomeric stage, retaining more superior dispersion than ex situ mixing. In situ polymerization has been used to engineer a wide range of hybrid and green biocomposites containing CNCs and ChNWs, such as nylon (Figure 11c), and crop-derived polycarbonates and polyesters, with remarkable reinforced mechanical properties.^[150,271–275]

Parameters related to nanochitin, including its aspect ratio, surface chemistry, and loading, greatly influence the mechanical properties of biocomposites. High-aspect-ratio ChNFs produce stiff, brittle nanocomposites, whereas low-aspect-ratio ChNWs toughen the composites (Section 2.2.4), as exemplified in studies on PVA and alginate biocomposites reinforced with nanochitin (Figure 11d).^[100,276] This is attributed to the ability of ChNFs to entangle with polymer chains, and the ability of ChNWs to facilitate stress transfer at the filler–matrix interface. The type and concentration of surface functional groups also significantly influence the reinforcement effectiveness of nanochitin. On using ChNFs as reinforcement agents in

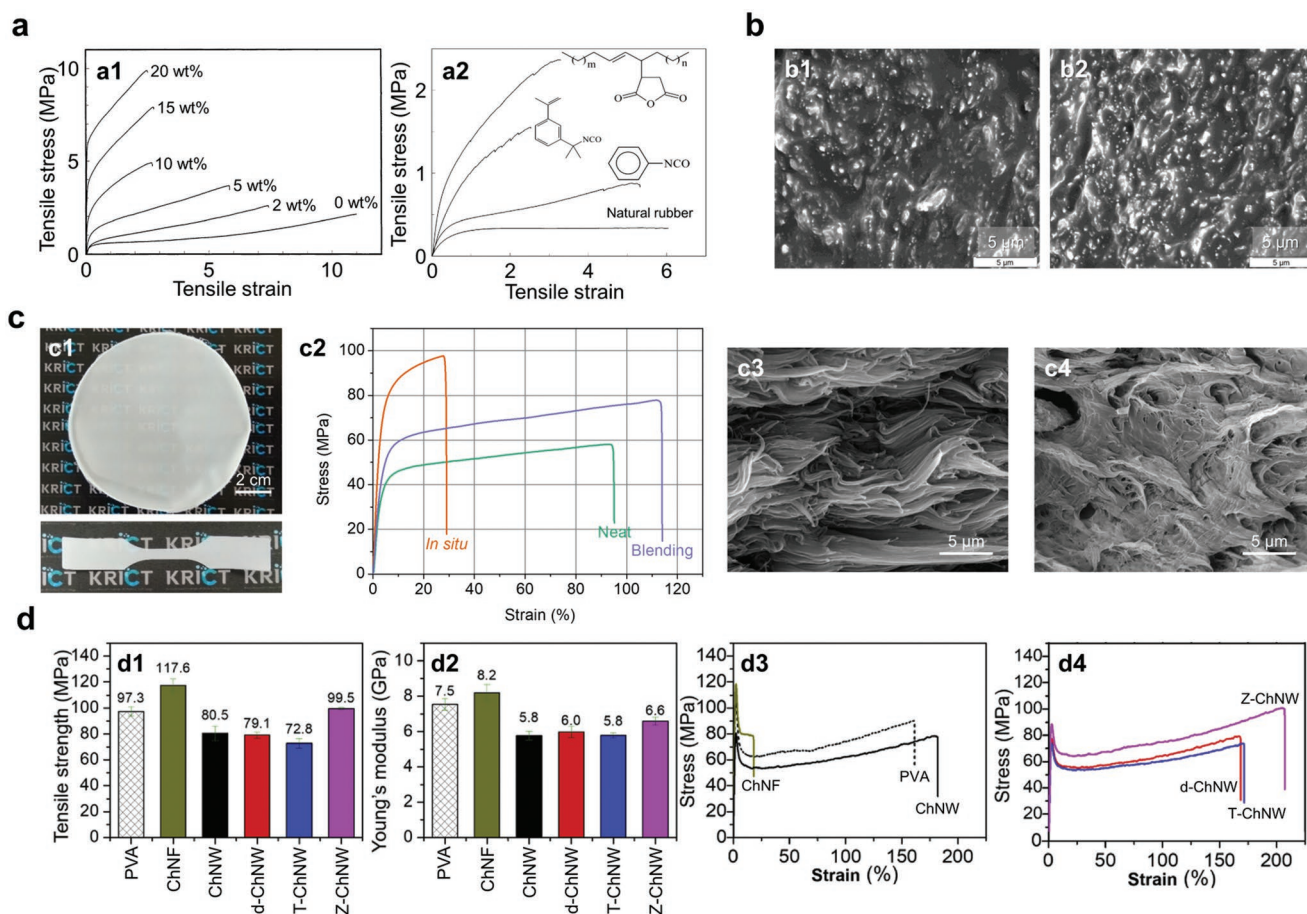


Figure 11. Nanochitin as mechanically reinforcing fillers for different polymer systems. a) Stress–strain curves of natural rubber biocomposite films with untreated ChNWs (a1) and hydrophobic ChNWs (a2), fabricated by casting–evaporation from aqueous suspensions and toluene, respectively. In (a2), the compounds shown were used for the post-surface-modification of ChNWs; the hydrophobized ChNW loading is 10 wt%. b) SEM images of cryo-fractured surfaces of natural rubber/untreated ChNW (20 wt%) composite films fabricated by b1) hot-pressing and b2) casting–evaporation. The broad smooth unfilled regions in (b1) indicate a lower whisker distribution compared with (b2). a1) Adapted with permission.^[266] Copyright 2003, American Chemical Society. a2) Reproduced with permission.^[148] Copyright 2003, American Chemical Society. b) Reproduced with permission.^[113] Copyright 2003, American Chemical Society. c) Composites of nylon 6,6/d-ChNWs (0.4 wt%): c1) (top) cast film and (bottom) dumbbell-shaped film specimens; c2) stress–strain curves of the composites prepared by in situ polymerization and ex situ blending in formic acid. SEM images of tensile-fractured surfaces of in situ polymerized (c3) and ex situ blended (c4) films, showing different modes of fracture. c) Adapted with permission.^[150] Copyright 2020, Royal Society of Chemistry. d) Composites of PVA with five different types of nanochitin, namely, chitin nanofibers (ChNFs), ChNW, deacetylated ChNW (d-ChNW), TEMPO-oxidized ChNW (T-ChNW), and zwitterionic TEMPO-oxidized deacetylated ChNW (Z-ChNW) at 10 wt%: d1) tensile strength; d2) tensile modulus; d3,d4) stress–strain curves. d) Adapted with permission.^[100] Copyright 2019, Elsevier.

carboxymethylcellulose (CMC) films, the strength of the composites is improved greatly for highly deacetylated ChNFs due to the strong interfacial adhesion of cationic ChNFs with the anionic CMC.^[277] Moreover, introducing both charges (amino and carboxylate) in zwitterionic nanochitins promotes percolation and strengthens the PVA matrix (Figure 11d).^[100] The tensile properties of biocomposites are also sensitive to nanochitin loading; there is generally an optimal percolated threshold value, which varies for different polymer matrices and nanochitin aspect ratio, at which reinforcement is the maximum. In situ polymerization requires less nanochitin loading than ex situ mixing for the same reinforcement efficiency. Beyond the threshold, nanochitin is prone to aggregation and the mechanical properties of the composite are drastically degraded.^[150,274]

In addition to isolated dispersed nanochitin, the plywood structure of nanochitin also exhibits exceptional

damage tolerance. For instance, the dactyl club of the mantis shrimp (*Odontodactylus scyllarus*) can withstand a repeat direct impact force of 1500 N without damage. Structural characterizations have shown that the dactyl club possesses multiple features that allow minimal internal damage on impact. One such feature is the ChNF plywood that dissipates impact energy by twisting the crack direction, preventing its propagation during deformation (Figure 12a–d).^[26] Few studies have attempted to fabricate high-performance biocomposites mimicking the chiral plywood structure of nanochitin. Oh et al. reproduced a hierarchical arrangement of ChNFs (originally labeled chitin nanowires) in epoxy/nanochitin biocomposites (Figure 12e). The toughness increases from 3.3 MJ m⁻³ for neat epoxy to 4.3 and 9.0 MJ m⁻³ for composites with nematic and chiral nematic structures (at 5 wt% ChNF loading), respectively (Figure 12e,f). Both the anisotropic structures exhibit higher toughening effects

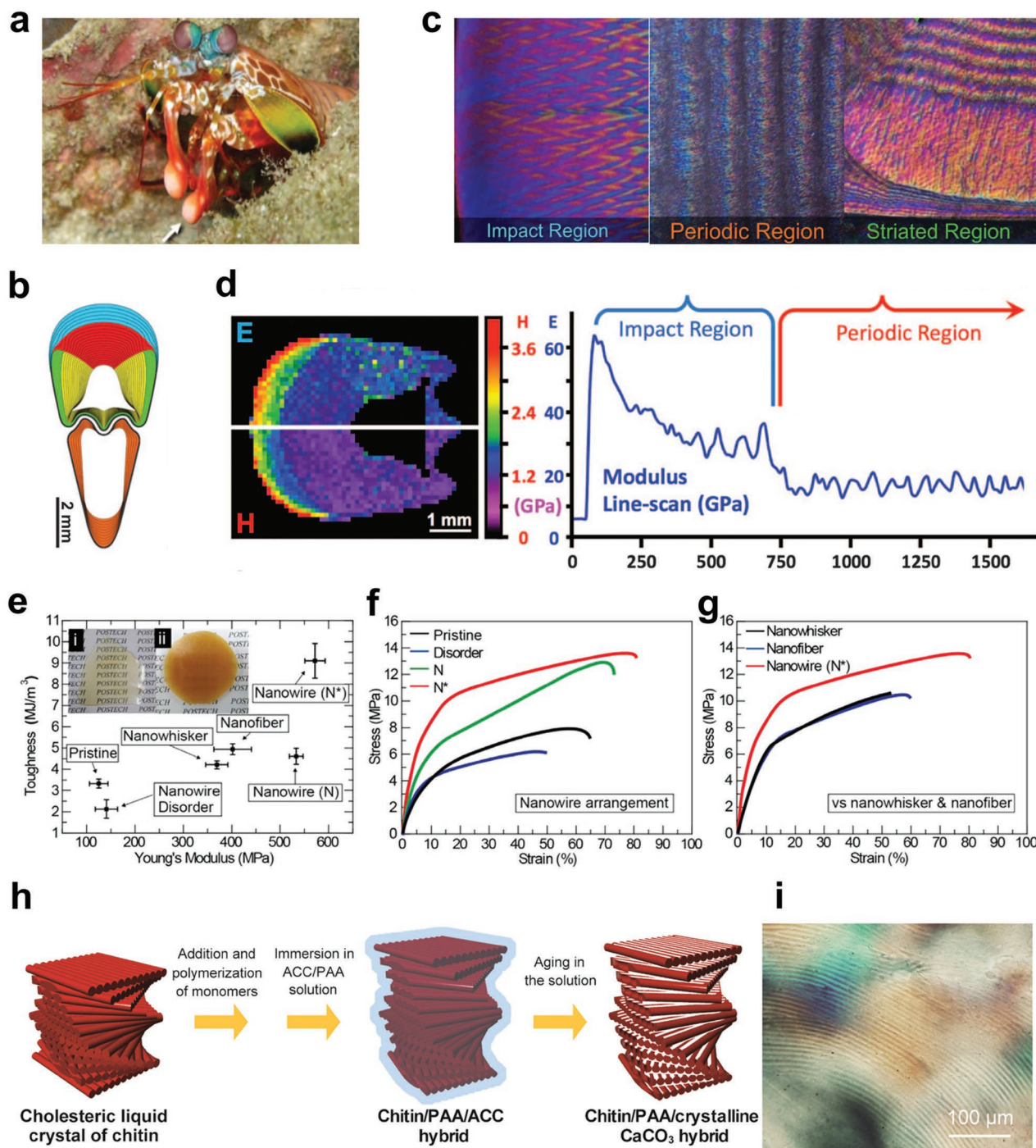


Figure 12. a) Front view of the mantis shrimp (*O. scyllarus*) showing the impact surface of the dactyl club (white arrow). b) Cross-sectional analysis of the dactyl club shows three structural domains: (blue) the impact region, the periodic region including (red) medial and (yellow) lateral zones, and (green) the striated region. c) The optical microscopy images of these regions, with the rotated-plywood structural motif of the impact region. d) (left) A nanoindentation map [elastic modulus (E) and hardness (H)] of the dactyl club, and (right) a corresponding line scan. a–d) Adapted with permission.^[26] Copyright 2012, American Association for the Advancement of Science. e) Tensile Young's modulus and toughness of pristine epoxy and nanochitin/epoxy composites. Insets: i) pristine epoxy and ii) chiral nematic nanowire/epoxy composite films. f) Tensile stress–strain curves of epoxy composites with isotropic, nematic (N), and chiral nematic (N^*) phases of nanowires (ChNFs). g) Tensile stress–strain curves of isotropic ChNW and ChNF epoxy composites are compared. The ChNF loading in (e)–(g) is 5 wt%. e–g) Reproduced under the terms of the CC-BY Creative Commons Attribution 4.0 International license (<https://creativecommons.org/licenses/by/4.0>).^[153] Copyright 2016, The Authors, published by Springer Nature. h) Development of helically ordered chitin/ CaCO_3 hybrid materials mimicking the biomineralization process. The cholesteric liquid of ChNWs is immersed in acrylic acid (AA) and amorphous calcium carbonate (ACC), polymerized, and aged to obtain the chitin/poly(acrylic acid) (PAA)/ CaCO_3 hybrid material. i) The POM image of the chiral nematic hybrid. h,i) Reproduced with permission.^[278] Copyright 2015, Wiley-VCH.

than the isotropic dispersed ChNF and ChNWs (Figure 12g).^[153] Furthermore, inspired by the biomineralization process, Matsumura et al. fabricated a chiral-nematically arranged ChNWs/CaCO₃ transparent film with high potential as an optical and mechanically superior material (Figure 12h,i).^[278] Although most studies focus on fabricating well-dispersed nanochitin biocomposites, the mantis shrimp can provide structural insights to aid the design and development of high-performance materials based on the hierarchical assembly of nanochitin.

3.2.2. Sustainable Gas Barriers for Food Packaging

Among the requirements for food packaging, barrier properties against oxygen and water vapor are the most crucial. Uncontrolled transport of these gasses across packages can reduce the quality and shorten the shelf life of food products.^[279] Traditional food packaging is made using petroleum-derived plastics (such as poly(ethylene terephthalate) (PET) and polyolefins) owing to their lightweight, strength, low cost, easy processability, and transparency,^[280,281] but they are highly permeable to oxygen.^[282] Metallized coatings and poly(vinylidene chloride) have high oxygen-barrier properties, but their usage is discouraged because they release toxins during end-of-life disposal. As food packaging is mostly single use, current studies not only investigate the performance of food-packaging materials but also highlight their sustainability.

Nanochitin is emerging as a new sustainable material for food packaging. Neat ChNF films exhibit low oxygen permeability (OP) of 1.0 mL μm m⁻² day⁻¹ kPa⁻¹ at 23 °C and 50% relative humidity (RH) because of its high crystallinity and aspect ratio, forcing gas molecules to diffuse through the films in a tortuous path.^[283] The OP of nanochitin is two orders of magnitude lower than many petroleum-based plastics.^[282,283] However, neat nanochitin films are very brittle and usually applied as additional components with polymers to produce sustainable food packaging.

The cohesion between nanochitin is stronger than nanochitin-polymer interaction; thus, continuous nanochitin layers can form anisotropic and tight networks that reduce gas permeability more remarkably compared to dispersed nanochitin fillers. This has been confirmed in a study using (2,2,6,6-tetramethylpiperidin-1-yl)oxyl radical (TEMPO)-oxidized ChNWs (T-ChNWs) to improve the barrier properties of biaxially oriented polypropylene (BOPP). Dispersed T-ChNWs in acrylic resins adhering to BOPP do not improve the oxygen barrier properties of neat BOPP, while T-ChNW layers reduce the oxygen transmission rate (OTR) from ≈400 to 203.8 mL m⁻² day⁻¹ (for an 8.3 μm thick T-ChNW coating layer) at 20 °C and 50% RH.^[284] Therefore, for a significant improvement in gas-barrier properties, nanochitin is usually coated onto the polymer film as a continuous nematic-assembled layer.

Coating of nanochitin involves the deposition of nanochitin aqueous suspensions on the polymer films through dipping, spraying, or spinning techniques followed by water evaporation.^[151,184,285] The selection of coating techniques depends on the nature of the polymer substrate (shape) and chitin suspensions (volume and viscosity), and should be evaluated for each case.^[286] Nanochitin-coated polymer films have been fabricated with dip coating and spray coating.^[226] Differences in surface

energies of nanochitin and polymers necessitate surface treatment of the polymer to improve the nanochitin-polymer adhesion. The positive charge of nanochitin provides a critical advantage; it facilitates bonding between nanochitin and the treated polymer surface via NH₃⁺-mediated electrostatic interactions with negatively charged moieties generated on treated polymer surface.^[151,184,279,285]

Nanochitin can be constructed as a single-layer coating or multilayer coating with other components. Multilayer coatings can provide multifunctionalities (such as antimicrobial properties or printability) for polymeric food packaging. Positively charged nanochitin is a perfect complementary partner to negatively charged nanocellulose for improving gas-barrier properties. Nanochitin and nanocellulose of different aspect ratios have been combined to achieve a more tightly packed network in which the nanofibers provide a rigid framework, and the nanowhiskers fill defects within the nanofiber mesh.^[285] Kim et al. have reduced the OTR of PET thin films using TEMPO-oxidized cellulose nanofibers (T-CNFs) and ChNW, confirming the synergistic interplay of ChNW and T-CNF. Bilayer-(ChNW/T-CNF)₂₀-spray-coated PET exhibits an OTR of 0.48 mL m⁻² day⁻¹ for a 2.62 μm thick coating, lower than those of single (ChNW)₄₀- and (T-CNF)₄₀-coated PET (1.91 and 1.46 mL m⁻² day⁻¹, respectively) at 23 °C and 50% RH (Figure 13a-c).^[285] Similarly, Satam et al. have also confirmed that multilayers of ChNF/CNC spray-coatings on PLA exhibit a fourfold lower OP than those coated with individual components (20 vs 80 mL μm m⁻² day⁻¹ kPa⁻¹ at 23 °C and 50% RH).^[287] More recently, Nguyen et al. assembled 20 (ChW/T-CNF) bilayers on a BOPP film through dip coating, exhibiting a 100-fold reduction in the OTR from 111751 to 13.10 mL m⁻² day⁻¹ (at 23 °C and 50% RH).^[184]

One of the challenges of using nanochitin as a barrier material is the sensitivity of the OP to RH, and its poor barrier properties against water vapor.^[151,279] The water vapor transmission rate (WVTR) of chitin is seven to eight orders of magnitude higher than hydrophobic polymers,^[288] and nanochitin exhibits a sharp rise in OP as RH increases, particularly above 50% RH.^[151] An approach to mitigate this sensitivity is thermal annealing through hot pressing, which enhances the interfibrillar hydrogen bonding and resistance to moisture by eliminating intercalating water molecules.^[151,285] Hot pressing reduces the OTR values from 0.48 to 0.35 mL m⁻² day⁻¹ in (T-CNF/ChNW)₂₀-coated PET films (23 °C, 0% RH), and the value retains as low as 0.6 mL m⁻² day⁻¹ upon exposure to water (Figure 13d-f).^[285] Another strategy is sandwiching the nanochitin layer within moisture-resistant polymer layers (laminating), but this requires a large quantity of polymeric materials and a precise control of layer deposition for acceptable film construction and performance.^[284] The slippery liquid-infused porous surfaces (SLIPS) technology has been recently used to prepare coated PET films with low barrier properties against both oxygen and water vapor, and self-cleaning properties for good recyclability (Figure 13g-j).^[151,289] A spray-assisted layer-by-layer (LbL) assembly of T-CNF and d-ChNW coated on one side of the film reduces the OTR of the film, while a porous surface of silica nanoparticles and d-ChNW impregnated with oil on the other side of the film, being superhydrophobic, exhibits a low WVTR and effectively repels contaminants. A low OTR of

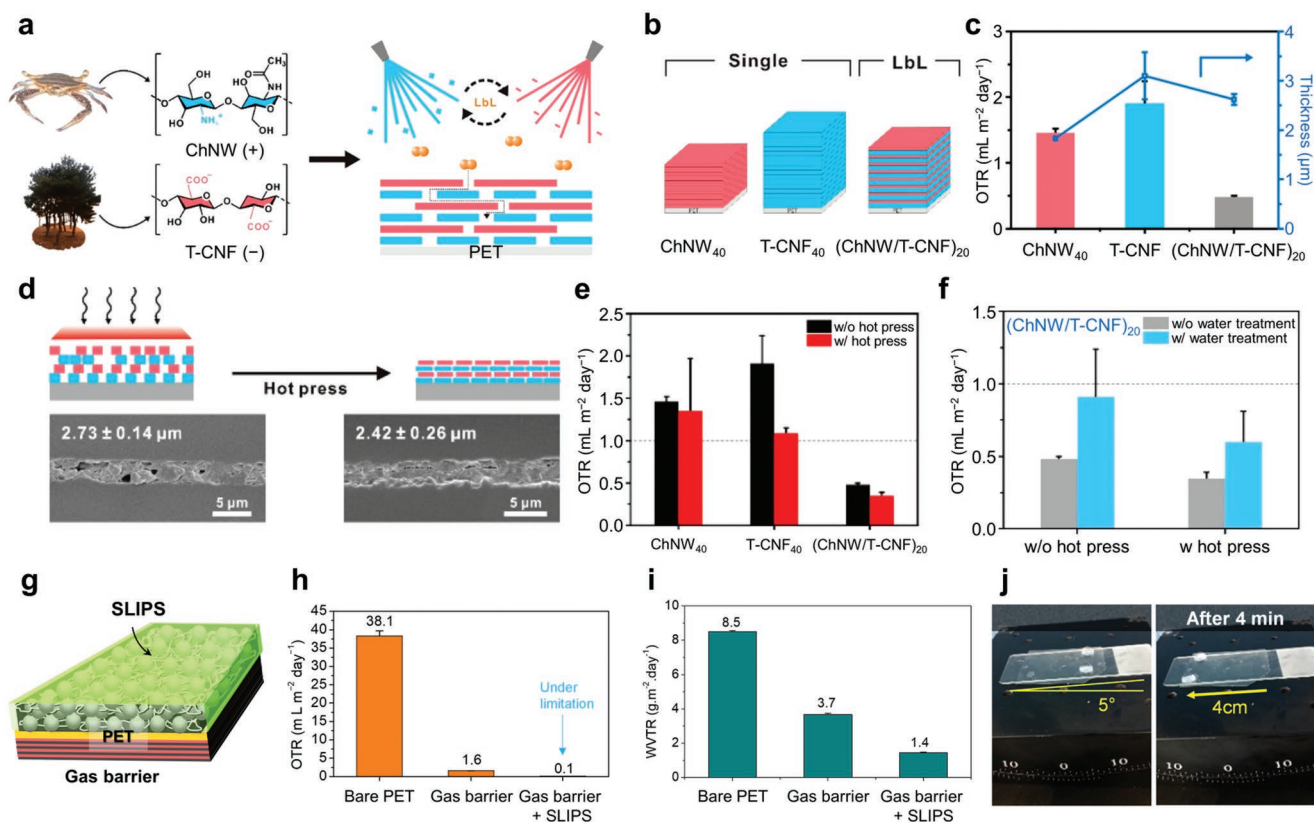


Figure 13. Nanochitin used in combination with TEMPO-oxidized cellulose nanofibers (T-CNFs) for fabricating sustainable high gas-barrier coatings on poly(ethylene terephthalate) (PET) films. a) LbL assembly of the (ChNW/T-CNF)_n bilayer coating on a PET film using spray coating; *n* denotes the number of bilayers. b) Schematic representation of single-layer and bilayer coatings on PET films, demonstrating the synergistic interplay of ChNW and T-CNF over each individual component, and c) their OTR. d) Schematic hot pressing of (ChNW/T-CNF)₂₀-coated PET films and the corresponding cross-sectional SEM images. e, f) Changes in the OTRs of T-CNF₄₀, ChNW₄₀, and (ChNW/T-CNF)₂₀-coated PET films at 0% RH, 23 °C before and after hot pressing (e), and of non-hot-pressed and hot-pressed (ChNW/T-CNF)₂₀-coated PET before and after hydration (f). a–f) Adapted with permission.^[285] Copyright 2019, American Chemical Society. g) Overcoming the moisture sensitivity of the (d-ChNW/T-ChNW)₄₀ gas-barrier coating on PET films by implementing SLIPS technology on the other side of the film. h) OTR and i) WVTR values of these films. j) Water repellence of the SLIP-coated PET sample. g–j) Adapted with permission.^[151] Copyright 2021, Royal Society of Chemistry.

<0.1 mL m⁻² day⁻¹ and WVTR of 1.4 g m⁻² day⁻¹ kPa⁻¹ has been recorded for a 7 μm thick coated layer.^[151]

In addition to mitigating the sensitivity to water, anisotropy control and surface modification of polysaccharide nanocrystals can improve their gas-barrier properties. In gas permeability studies, aligned CNC coatings on PVA films have exhibited a 900-fold reduction in O₂ transport rate on increasing the order parameter from 0.28 (isotropic) to 0.85 (anisotropic) (1 = perfect alignment).^[290] A reduction in WVTR (52%) has also been reported for highly ordered CNC-coated PVA films (order parameter of 0.78).^[291] These findings suggest the potential of aligning nanochitin to improve the barrier properties, which requires further investigation. Achieving a desirable alignment of nanochitin requires knowledge of the size-dependent rheological properties of nanochitin suspensions.

The *D_A* of ChNWs can be varied for controlling the OP of the fabricated d-ChNW films. Ji et al. reported that aggressively deacetylated ChNWs (under optimal conditions of 40 wt% NaOH, 155 °C, and 140 min) have shorter lengths and higher surface charge densities that help them align and pack more optimally with CNC, forming a bilayer coating exhibiting 99%

and 20% reductions in OP and WVTR, respectively, on cellulose acetate films.^[292]

Notably, an improvement in the barrier properties of coated polymeric films usually accompanies a reduction in their mechanical strength. Unlike the dispersed state that can upgrade the mechanical properties of the composite, continuous nanochitin is brittle and when being adhered to the ductile polymer substrate, it concentrates stress at the interface, causing premature failure of the composite during deformation. High-gas-barrier nanocellulose/nanochitin-bilayer-coated PLA,^[287] PP,^[184] and cellulose acetate^[292] exhibit 10–35% reduction in strengths compared to the neat polymers. Therefore, a balance between barrier properties and mechanical strength should be considered while developing engineering strategies for fabricating nanochitin-coated polymeric films.

3.2.3. Antimicrobial Food Packaging

Direct protection of food from pathogens and microorganisms can maintain or improve the condition and extend the shelf life

of packaged food. As mentioned in Section 2.1.6, the antimicrobial activity of chitosan can inhibit pathogenic and nonpathogenic microorganism growth, making it an attractive material for food packaging. Chitosan is modified or incorporated with various natural extracts, such as essential oils, phenolic compounds, and other fruit extracts, to improve its antimicrobial and antioxidant properties.^[293]

PEG-decorated graphene-oxide (GO)-nanohybrid-introduced PVA/chitosan (50–80 kDa) nanocomposite films exhibit significant antimicrobial properties against *S. aureus* and *E. coli*. The improved antibacterial effect of the composite film is because of the antibacterial effect of chitosan and the GO sheet, which disrupts membrane permeability and cellular respiration through strong interactions with the cell wall.^[294] The antibacterial activity of chitosan films (200 kDa) with laponite-immobilized silver NPs has been mainly evaluated with *S. aureus*, *E. coli*, *A. niger*, and *Penicillium citrinum* that cause food spoilage by invading the surface and interior of vegetables and fruits. Chitosan films with laponite-immobilized AgNPs and CS/AgNP films exhibit improved antibacterial activities compared to pure chitosan films against the microorganisms; CS/AgNP films show the best antibacterial activity due to AgNPs released from laponin immobilization. On using them for the food packaging of litchis, the film-packed litchis indicate a 2 day extension of shelf life compared to nonpacked litchis.^[295]

Chitosan films incorporating natural extracts exhibit strong antibacterial/antioxidant effects. Cinnamon-essential-oil-incorporated chitosan NPs (760 kDa) extend the shelf life of beef patties by 2–4 days; the NPs decrease the growth of yeast, mold, and lactic-acid bacteria compared to the untreated group, which slightly increases at the end of the storage period of eight days, while *S. aureus* and Enterobacteriaceae growth are continuously reduced during storage due to long-term antibacterial effects.^[296] Apple-peel polyphenol-incorporated chitosan films (400 kDa) also exhibit high antimicrobial activities in gram-positive (*B. cereus*, *S. aureus*) and gram-negative bacteria (*E. coli*, *Salmonella typhimurium*) in a concentration-dependent manner, with higher efficacy against gram-positive bacteria.^[297] Incorporation of clove-essential-oil-loaded chitosan–ZnO NPs on chitosan/pullulan nanocomposite films cause a broader antimicrobial response; the film significantly reduces the growth of *S. aureus*, *E. coli*, and *P. aeruginosa*, with the maximum inhibition of *P. aeruginosa*. The chicken shelf life on using the composite film has been confirmed by pH values. Fresh chicken exhibits a pH value of 5.8, which increases due to protein and lipid oxidation. The pH of unpackaged chicken increases on the third day of storage, whereas that of the composite film-packaged chicken increases after two more days, indicating a two day shelf-life extension.^[298] Food packaging with chitosan-based films exhibit high antimicrobial activity and extend shelf life. In general, chitosan films exhibit higher antimicrobial activity against gram-positive bacteria than gram-negative bacteria due to the difference in the cell wall structure.^[54,299]

3.2.4. Environmental-Management Applications

Biochar, a form of carbon materials, is emerging as an ideal solution for several environmental issues.^[207,300,301] The

long-term stability of biochar reduces carbon dioxide (CO₂) emissions, whereas biopolymer biodegradation releases large amounts of CO₂ into the atmosphere. Therefore, converting chitin into biochar can be a promising strategy for mitigating climate change. Biochar can also enhance the physicochemical and biological properties of soil by retaining water and nutrients in the soil, buffering the soil pH, and regulating the soil microbial community. In addition, biochar is used in water treatment because its high porosity allows an efficient adsorption and removal of contaminants from water. In many studies, chitin and chitosan have been used as co-biosorbents with carbon materials; the lone pairs of electrons on the acetamido group, amine, and hydroxy groups act as chelating sites for heavy metals and various chemicals.^[302,303] N-doped carbon materials for environmental applications have been mostly fabricated by the pyrolysis of plant biomass and manure, followed by postsynthetic treatment.^[207,304,305] Those directly obtained from chitin and chitosan are largely unexplored. To the best of our knowledge, the study of Zhang and co-workers^[306] is the only study on N-doped carbon ChNF aerogels as effective adsorbents for treatment of dyed wastewater.

3.3. Optical and Electrochemical Applications

3.3.1. Optical Materials

Color is an important feature characterizing species and enabling them to exist in nature. Many insects display bright iridescent colors which are caused by the interaction of incident light with their periodically ordered chitin structures (structural colors). For example, the color of scarab beetles (*Chrysina gloriosa*) originate from the left-handed chiral nematic structure of chitin nanocrystals that reflect circularly polarized light.^[25] Other species, such as butterflies, also display iridescent metallic blue in their wings, with the structural color originating from gyroid or Christmas-tree-like structures rather than a chiral nematic arrangement.^[25,307,308]

Fabricating an iridescent nanochitin film from aqueous suspension is still challenging (Section 2.3.1). Thus, most efforts have focused on producing optical nanochitin films from nature. Although beetles and butterflies are the most well-known for their optical properties, scientists are focusing on crustaceans to add more value to their shell waste. Pioneering work by Nguyen and MacLachlan has shown that the long-range order of nanochitin in the king crab shells become gradually less ordered from the interior to the exterior, which plausibly explains why the iridescent color of the internal part is not transferred to the external part of the shells.^[309] An intact, iridescent chitin cuticle membrane has been extracted from the crab shells, which exhibits a left-handed-chiral nematic structure like the beetle exoskeleton and solid films casted from CNC cholesteric liquid crystals (Figure 14a1,a2). Further deacetylation of the chitin membrane yields a chitosan membrane with enhanced iridescence (Figure 14a3). Both membranes exhibit responsive properties because they swell in water and change their helical pitches, causing macroscopic changes in color (Figure 14b–e). Reflected color (λ) depends on the incident angle (θ), pitch height (P), and refractive index of chitin (n),

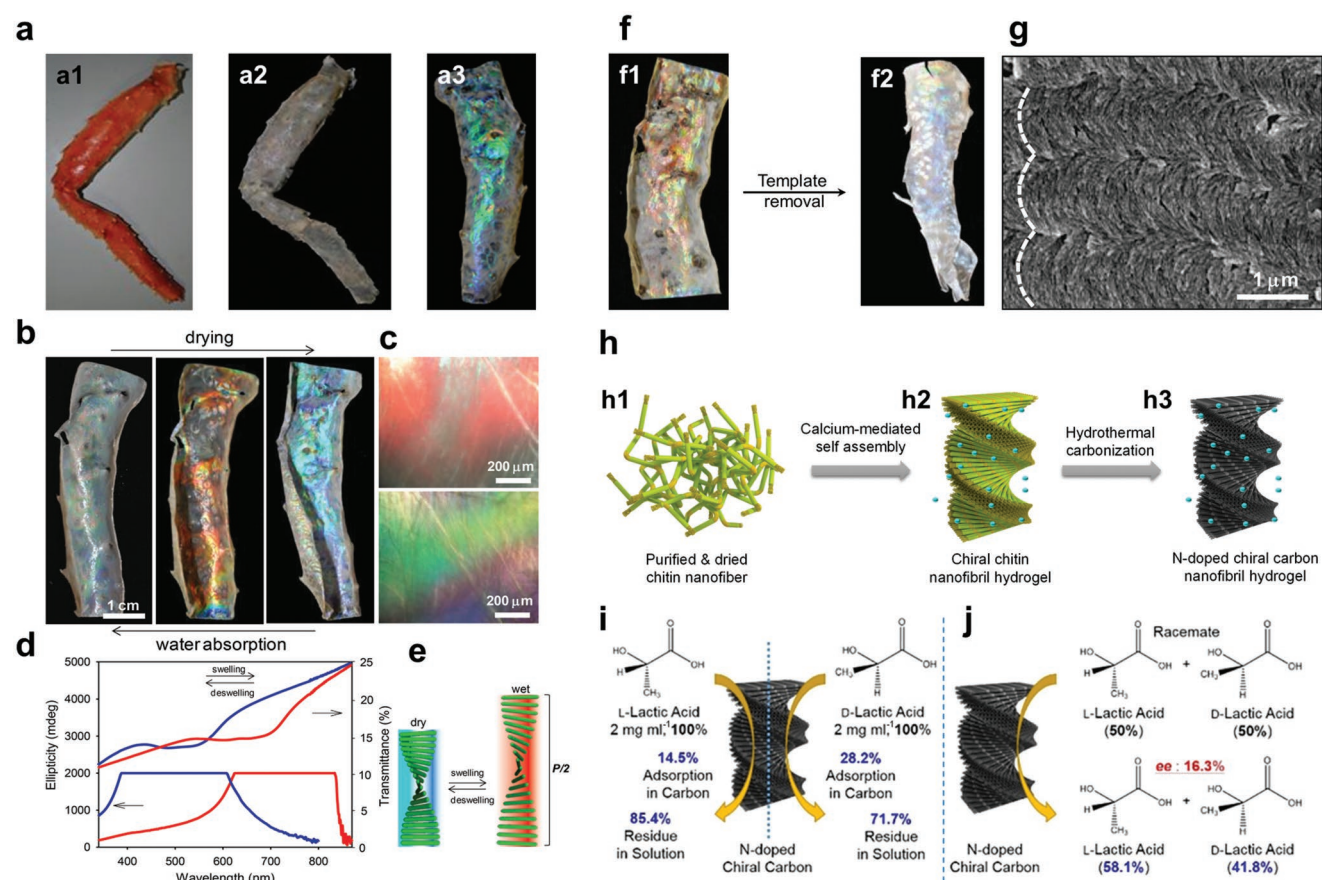


Figure 14. Optical materials derived from the chiral nematic structure of nanochitin. a) Chemical treatment and delamination of a king crab's leg (a1) produces an iridescent chitin cuticle membrane (a2). Further deacetylation of (a2) yields an iridescent chitosan membrane (a3). a) Adapted with permission.^[311] Copyright 2016, Wiley-VCH. b) Photographs of tunable iridescence of the chitosan membrane during drying and reabsorption of water. c) POM images of (top) wet and (bottom) dried chitosan membranes. d) Ultraviolet–visible (UV) and circular dichroism spectra of (red) wet and (blue) dried chitosan membranes. The UV spectrum indicates a blueshift of the reflectance peak from 720 to 540 nm upon drying. e) Tuning the helical pitch of the chitosan membranes by swelling and drying. f) Photographs of chiral nematic silica/chitin composites (f1) and mesoporous silica films (f2). g) SEM image of the silica film showing the retained helicoidal structure upon chitin removal. b–g) Reproduced with permission.^[309] Copyright 2014, Wiley-VCH. h) Methanolated calcium-mediated process converting bulk chitin (h1) to chiral nematic ChNF hydrogel (h2), which is used to obtain nitrogen (N)-doped chiral nematic carbon-sheath hydrogels using hydrothermal carbonization (h3). i) Adsorption capacity and j) enantioselective adsorption of L-lactic acid by the chiral N-doped carbon hydrogel and the resulting enantiomeric excess (ee).^[203] Copyright 2019, Wiley-VCH.

described through the equation: $\lambda = nP\sin\theta$.^[310] Chitin and chitosan membranes are tougher and more sensitive to photonic response than CNC membranes; thus, they are more suitable for extended applications.^[309]

The concept of transferring king crab shells to iridescent chitin/chitosan membranes has been extended to other species, such as shrimps,^[311] beetles,^[312,313] and butterflies,^[314–317] providing an interesting approach to utilize the optical properties of nanochitin assembly through biomimicry. These materials can be used as a sustainable and economically viable platform to produce optical functional materials. Moreover, the porosity, amino-mediated absorptivity, and high crystallinity of chitin membranes enable the templating of a secondary component to prepare chiroptical mesoporous materials. This involves introducing a second component into a chitin template and subsequently removing the chitin to obtain a replica. The templating

strategy has been used to synthesize solid materials, such as silica (Figure 14f,g),^[309] and metal or metal-oxide nanoparticles,^[314–318] which can be of great utility in catalysis and magnetophotonic devices. In addition to templating, the responsive color change and the cross-linking ability of the amino groups of chitosan membranes facilitate the fabrication of smart photonic hydrogels. They respond to external stimuli, such as pH change,^[319–323] making them potential alternatives to optical pH indicators that affect the life cycles and biocompatibility of monitored systems.

Other than chitin templates directly obtained from organisms, the *in vitro* assembly of nanochitin from liquid crystals can be used in certain applications, particularly when iridescence is not required. One such application is the separation of enantiomers, which is of significant importance in pharmaceuticals (for the separation of therapeutic enantiomers) and

polymer synthesis (for stereoregularity). Methanolated Ca^{2+} and solvent exchange with water have been used to fabricate chiral nematic ChNF hydrogels, which have been hydrothermally carbonized to generate N-doped chiral carbon-sheath hydrogels (Figure 14h). These carbonized hydrogels exhibit a chiral separation ability, preferentially adsorbing D-lactic acid over L-lactic acid at an enantiomeric excess of 16.3% (Figure 14i,j).^[203]

3.3.2. Renewable Electrodes for Electrochemical Applications

Extensive research has been carried out on high-performance electrodes for electrochemical applications (such as energy storage devices and catalysts) to address the energy demands of sustainable development. An ideal electrode can store a large amount of energy and effectively transport ions for rapid charge/discharge.^[324,325] Nitrogen-doped porous carbon materials derived from hierarchically structured chitin exhibit excellent conductivity, large surface area, abundant surface functional groups, low density, and superior electrochemical stability.^[206] The Bouligand structure of chitin of crab shells has been utilized as a template to prepare hollow carbon nanofibers, which have been used to encapsulate elements such as S and Si to fabricate efficient battery electrodes.^[206] Follow-up studies report different types of carbon electrodes for energy storage derived from different chitin sources that adapt various structural and chemical properties. Porous carbon nanosheets have been top-down exfoliated from crab shells by autoclave treatment in phytic acid and hydrogen peroxide, followed by pyrolysis under inert conditions. These sheets have been used as high-efficiency N/O-codoped anodes for sodium-ion batteries.^[326] Supercapacitor electrodes composed of N-doped carbon nanofiber aerogels, N/S-codoped biochar,^[327] carbonized microspheres,^[328,329] and N/O/P-tridoped porous carbons,^[330] have also been fabricated from crustacean shells.^[331]

N-doped carbon materials derived from chitin and chitosan have recently been used as catalysts and catalyst supports in various reactions, including oxygen reduction, and organic compound oxidation/reduction.^[202,332–335] They exhibit high catalytic activity due to their large surface area and various C–N configurations. As catalyst supports, the C–N defects provide nucleation sites and assist the uniform dispersion of the catalyst, thereby enhancing the electrocatalytic activity.^[202] Therefore, N-doped carbon materials derived from chitin and chitosan exhibit high potential as sustainable alternatives for expensive metal-based electrocatalysts.

4. Outlook

Unlike existing review articles on chitin and chitosan, here, we have focused on recent developments to understand the variations in physicochemical and biological properties of chitin and chitosan with size (from molecular- to microscale). With the aid of recent advances in molecular science and nanoscience, key outlooks have been provided on chitin nanostructures for biomedical and environmental applications.

4.1. Biomedical Applications

Unlike synthetic polymers, chitin is obtained from various natural resources, making variations in MW, D_A , and contaminants inevitable, causing inconsistent results while investigating biological properties (such as immune and antimicrobial activity). Although chitin and chitosan have good bioactivities, these discrepancies hinder their application in the biomedical field. Therefore, this review paper proposes criteria (in terms of contaminant removal and MW) to reduce ambiguity and enable the selection of chitin and chitosan for biomedical applications. Chitin nanostructures possess a high positive charge density and good adhesion properties; thus, the contaminant levels should be monitored and reduced (including the removal of negatively charged endotoxins) before applying chitin nanostructures in biomedical applications.

Reports on the immune activity of chitin and chitosan are particularly ambiguous. Many immunological experiments using chitin and chitosan in the past have been misinterpreted (without confirming/removing the content of endotoxin).^[47,57,66–69] Various parameters affect the immune activity of purified chitin and chitosan; this paper has focused on MW and summarized the MW range in which inflammation is induced and inhibited. HMW does not exhibit immune activity,^[50,56,62] while LMW shows immune-stimulation activity;^[62–64,67] chitin and chitosan with oligomer size less than 10 kDa exhibit both proinflammation and anti-inflammation properties, inducing immune modulation.^[65,68,69,75–77,79] Chitin and chitosan nanoscale materials, used as scaffolds, drug carriers, or vaccine adjuvants, should exhibit specific immune activities (nonimmunogenic, stimulating, or modulating) depending on the application. This review paper suggests the consideration of the MW range for proper selection of chitin and chitosan with the required immune activity.

The antimicrobial properties of chitin and chitosan are important in biomaterials because they can cause infection if they are contaminated by microorganisms; for instance, the COVID-19 (pandemic caused by the SARS-CoV-2 virus in 2020, and epidemics such as the SARS in 2003 and the middle east respiratory syndrome in 2012. Infectious diseases that terrify people continue to occur, making antibacterial and antiviral functional materials very relevant. Various synthetic materials for repelling microorganisms have been developed, but there is a need for antibacterial materials based on natural and renewable materials. From this point of view, chitosan is a very attractive antibacterial material, but the antibacterial activity of chitosan varies with various factors (the strain of bacteria or fungi, MW, D_A , and pH).^[86–88] In general, the electrostatic interaction between the positively charged chitosan and anionic components on the cell wall is the major mechanism of antibacterial action.^[84,85,90,94] Therefore, the MW of chitosan seems less influenced than D_A and pH. When D_A and pH are controlled, the MW should be considered because it can influence the electrostatic interactions^[38,40] and cell penetration.^[95] In particular, since the MW of good antimicrobial efficacy varies depending on the strain, when the target microorganism is specified, and the D_A and pH conditions are unified, a higher MW is better for gram-positive bacteria, while a lower MW is better for gram-negative bacteria.^[88,89,93] However, the chitosan

oligomer exhibits poor antimicrobial activity toward all microorganisms;^[93] therefore, its elimination is recommended when conducting research on antibacterial activity.

4.2. Environmental Applications

4.2.1. Merits of Chitin over Cellulose in Sustainability

Ironically, plastic bags were invented to reduce the use of paper bags that had caused an indiscriminate felling of trees. However, since nonbiodegradable plastics can generate microplastics harmful to marine life, therefore, paper straws and bags are once again in the spotlight as sustainable materials. However, the problem of indiscriminate logging to meet the demand of paper and cellulose materials is still unresolved. Also, the problem of wood-supply security is emerging, and cellulose production can interfere with other wood industries such as paper, furniture, and construction. Forests could be destroyed to construct farms that grow cotton (another cellulose source). These contribute to global warming, one of the biggest threats to humanity at present. By contrast, chitin production can refine crustacean shell wastes, contributing to the marine economy, waste management, and environment, particularly in Asian countries.^[1] Moreover, biotechnological developments can enable the utilization of fungi and insects as alternative sources for chitin and resolve issues related to the seasonal fluctuation of crustaceans.^[106] Insects comprise a promising source for chitin and chitosan in the future; protein and amino acid production by insects could be an alternative to traditional meats. Insects produce less emissions of carbon dioxide and ammonia than cattle and pigs and can significantly reduce the land and water used for cultivation. After extracting amino acids and proteins from insects, chitin and chitosan can be produced from the waste.

4.2.2. Nanochitin Production: Standardization and Reducing Its Environmental Impacts

Chitin and cellulose are equally difficult to process and very few solvents can dissolve them. The processing technology of the two materials has gradually developed, and the development can be divided into generations. Chitin of the first generation is chemically modified into soluble chitosan, similar to nitrocellulose. In the second generation, chitin is dissolved in a special solvent and then regenerated. The chitosan and regenerated chitin exhibit poor mechanical properties and a high swelling degree in wet conditions.

Nanochitin is a material fabricated without damaging the original natural-state nanofibril structure. However, the environmental impacts of nanochitin production routes have not been extensively studied. Therefore, life cycle assessments (LCAs) that evaluate all aspects of a production route, such as energy and water consumption, emissions, byproduct removal, and reagent recyclability, are necessary, particularly for the production scale-up of nanochitin. Nanocellulose is a good model for designing the LCA of nanochitin because nanocellulose is being mass-produced in Japan, Europe, and Canada.^[182,336] In

addition, it is necessary to benchmark the quality of industrially produced nanochitin against lab-synthesized chitin; rigorous testing and standardized protocols are required for each chitin biomass and production route. This can ensure the industrial production of chitin nanomaterials with small batch-to-batch variations.

Among the top-down production methods, mechanical disintegration has been used in the industrial scale by Marine Nano-Fiber Co., Ltd., (Japan) and ANPOLY Co., Ltd., (South Korea) to produce chitin nanofibers for medical and cosmetic applications. Although chitin nanowhiskers have not been industrially produced yet, acid hydrolysis exhibits the greatest potential as an industrial production route, similar to the production of CNC.^[182] Therefore, innovative methods for handling and recycling large amounts of acid, product purification, and drying for product shipping and preservation should be developed.

4.2.3. Optimizing the Performance of Chitin

Nanochitin shows great potential in preparing mechanically reinforced biocomposites and high-gas-barrier packaging films. It represents a transition from the chitin/chitosan oligosaccharide (molecular scale) to the hierarchically assembled chitin (microscale). The properties of chitin/chitosan oligosaccharides can be well established based on MW, and those of hierarchically assembled chitin are usually dependent on factors other than size. Unfortunately, the size–property relationship for nanochitin is not empirically established, but rather based on computational calculations or models for CNCs. Future studies can focus on generating nanochitin-based cohesion–size relationships and filler–matrix interactions to effectively use nanochitin as a reinforcing filler in nanocomposites. It is equally important to fully characterize chitin nanofillers, particularly their dimensions (aspect ratios), which ultimately decide their reinforcing behavior. In addition, as green and biodegradable biocomposites are gaining momentum in the sustainable Industry 4.0 era, the technique combining in situ polymerization with thermal processing, providing a green, industrially and economically viable method to produce nanochitin-reinforced green biocomposites, could be suitable in the industrial scale. In food packaging, elucidating the size-dependent phase behavior of nanochitin suspensions is helpful to well align nanochitin for achieving a high barrier performance. Furthermore, the sensitivity of nanochitin to moisture presents the greatest challenge and can be resolved by thermal annealing with nanocellulose or by using SLIPS technology. Both the methods use sustainable components.

Self-assembled nanochitin structures are used to engineer materials for optical, load-bearing, environmental-management, and electrochemical applications. Despite increasing work on the assembly of isolated nanochitin and the fabrication of biomimetic hierarchically structured materials, many challenges are to be tackled. The dimensions and morphology of nanochitin significantly vary with chitin sources and production routes (Table 3), potentially causing inconsistency in its phase-transition behavior reported in the literature. Therefore, an empirical formula describing the dimension-dependent liquid crystal transition of nanochitin should be established.

Ideally, a phase diagram of nanochitin suspensions illustrating size-, concentration-, and surface-potential-dependency should be generated.^[179] This would require more extensive experimental data combining different chitin sources and production routes. Additionally, the extraction of a natural iridescent nanochitin membrane is tedious and the optical properties are highly sensitive to impurities and additives. Therefore, elucidating the mechanism underlying the loss of perfect long-range orientation that results in noniridescent nanochitin films will be helpful in developing optical and responsive materials from isolated nanochitin.

Studies on chitin-derived N-doped porous carbon materials for electrochemical and environment-management applications are at their infancy. In electrochemical applications, further research is required to elucidate the parameters controlling the surface functionality and porosity of carbon materials during chitin carbonization. In catalytic applications, an in-depth understanding of the correlation between C–N configurations and catalytic activity can facilitate the fabrication of specific N-doped carbon materials. In energy storage, to fabricate a high-capacity electrode, balance must be maintained between small pore size (large surface area) for sufficient interfacial reactions, and large pore size for facile electrolyte diffusion. In environmental applications, chitin, after adsorbing heavy metal ions from water, is heavily contaminated and difficult to dispose of or handle. Metal ions exhibit high catalytic activities; thus, the metal-polluted chitin could be converted into a catalyst supporter to maximize the use of chitin-derived carbon materials.

5. Conclusion

This review discusses the scale-dependent (molecular, nano, micro, and bulk) physicochemical and biological properties of chitin that account for conflicting characteristics and unreproducible results across literature. At the molecular scale, the chain rigidity and solubility are changed from the oligomer MW range of chitin/chitosan, affecting adhesion and cohesion. These characteristics influence the interactions between chitin/chitosan and immune cells, and the cell walls of microorganisms, which may partially explain the cause of the mutually exclusive properties of chitin/chitosan with respect to immune responses and antibacterial activity. At the nanoscale, the mechanical properties of nanochitin are a function of its aspect ratio (length/diameter or L/D); higher-aspect-ratio nanofibers exhibit greater tensile strength, which plateaus when the fiber length exceeds 1 μm . As rod-like nanomaterials, aqueous nanochitin suspensions exhibit isotropic–chiral nematic phase transition at a critical concentration. This critical value proportionally scales with the nanochitin dimensions through the relation $(L^2D)^n$, where n remains to be determined. In addition to size, the properties of nanochitin are equally determined by their surface chemistry. Above the microscale, the properties of chitin seem to be less dependent on size, but are controlled by factors such as their alignment fashions, porosity, and nitrogen doping. Chitin and chitosan show immense application potential in various fields ranging from medical to environmental. To effectively incorporate chitin/chitosan into end products, manufacturers and end users need to carefully consider the length

scale at which they are used because each length scale determines a specific set of properties (Figure 1).

Owing to their performance and sustainable merits over cellulose, the future of chitin and chitosan is promising. The latest advances in nanoscience can facilitate future studies to fill current research gaps; the most pertinent is the complete rationalization of the size–property (mechanical and colloidal behavior) relationship of chitin at the nanoscale. This would allow more effective use of nanochitin as mechanically reinforcing fillers in biocomposites or aligning nanochitin to engineer a high gas barrier for food packaging. This review helps bridge fundamental research and practical applications, paving the way for the complete valorization of chitin, as a new-generation functional material.

Acknowledgements

S.L. and L.T.H. contributed equally to this work. This article was supported by the National Research Foundation of Korea (NRF) grant funded by the Korea government (MSIT) (Grant Nos. 2022R1A2C2007874 and 2019M3C1B7025093) and the KRICT Core Project (Grant No. SS2242-10). The authors also thank the support of the Technology Innovation Program (Grant No. 20009508, Development of biodegradation evaluation technology for building circular ecosystem related to bioplastic industry) funded by the Ministry of Trade, Industry, & Energy (MOTIE, South Korea).

Conflict of Interest

The authors declare no conflict of interest.

Keywords

biomedical applications, environmental applications, multiscale materials, nanochitin, nanochitosan

Received: April 13, 2022

Revised: May 24, 2022

Published online: September 25, 2022

- [1] N. Yan, X. Chen, *Nature* **2015**, 524, 155.
- [2] G. A. F. Roberts, *Chitin Chemistry*, The Macmillan Press, London, UK **1992**.
- [3] Y. Habibi, L. A. Lucia, O. J. Rojas, *Chem. Rev.* **2010**, 110, 3479.
- [4] R. Jayakumar, D. Menon, K. Manzoor, S. V. Nair, H. Tamura, *Carbohydr. Polym.* **2010**, 82, 227.
- [5] A. Künkel, J. Becker, L. Börger, J. Hamprecht, S. Koltzenburg, R. Loos, M. B. Schick, K. Schlegel, C. Sinkel, G. Skupin, M. Yamamoto, *Ullmann's Encyclopedia of Industrial Chemistry: Polymers, Biodegradable*, Wiley-VCH, Weinheim, Germany **2016**.
- [6] S. Nikolov, M. Petrov, L. Lymperakis, M. Friák, C. Sachs, H. O. Fabritius, D. Raabe, J. Neugebauer, *Adv. Mater.* **2010**, 22, 519.
- [7] T. Jin, T. Liu, E. Lam, A. Moores, *Nanoscale Horiz.* **2021**, 6, 505.
- [8] F. Lossada, D. Hoenders, J. Guo, D. Jiao, A. Walther, *Acc. Chem. Res.* **2020**, 53, 2622.
- [9] D. Elieh-Ali-Komi, M. R. Hamblin, *Int. J. Adv. Res.* **2016**, 4, 411.
- [10] L. Su, Y. Feng, K. Wei, X. Xu, R. Liu, G. Chen, *Chem. Rev.* **2021**, 121, 10950.

- [11] J. Wattjes, A. Niehues, S. Cord-Landwehr, J. Hoßbach, L. David, T. Delair, B. M. Moerschbacher, *J. Am. Chem. Soc.* **2019**, *141*, 3137.
- [12] X. Zhang, M. Rolandi, *J. Mater. Chem. B* **2017**, *5*, 2547.
- [13] J. Z. Knaul, M. R. Kasaai, V. T. Bui, K. A. M. Creber, *Can. J. Chem.* **1998**, *76*, 1699.
- [14] H. B. Wineinger, J. L. Shamshina, A. Kelly, C. King, R. D. Rogers, *Green Chem.* **2020**, *22*, 3734.
- [15] V. Zargar, M. Asghari, A. Dashti, *ChemBioEng Rev.* **2015**, *2*, 204.
- [16] Q. Z. Wang, X. G. Chen, N. Liu, S. X. Wang, C. S. Liu, X. H. Meng, C. G. Liu, *Carbohydr. Polym.* **2006**, *65*, 194.
- [17] J. Wattjes, S. Sreekumar, C. Richter, S. Cord-Landwehr, R. Singh, N. E. El Gueddari, B. M. Moerschbacher, *React. Funct. Polym.* **2020**, *151*, 104583.
- [18] E. Khor, *Chitin: Fulfilling a Biomaterials Promise*, Elsevier Science, Waltham, MA, USA **2014**.
- [19] M. Rinaudo, *Prog. Polym. Sci.* **2006**, *31*, 603.
- [20] W. M. F. B. W. Nawawi, M. Jones, R. J. Murphy, K. Y. Lee, E. Kontturi, A. Bismarck, *Biomacromolecules* **2020**, *21*, 30.
- [21] J. F. V. Vincent, U. G. K. Wegst, *Arthropod Struct. Dev.* **2004**, *33*, 187.
- [22] A. Miserez, T. Schnerberk, C. Sun, F. W. Zok, J. H. Waite, *Science* **2008**, *319*, 1816.
- [23] S. Nikolov, H. Fabritius, M. Petrov, M. Friák, L. Lymperakis, C. Sachs, D. Raabe, J. Neugebauer, *J. Mech. Behav. Biomed. Mater.* **2011**, *4*, 129.
- [24] N. A. R. Gow, J. P. Latge, C. A. Munro, *The Fungal Kingdom*, ASM Press, Washington, DC, USA **2017**.
- [25] J. Hou, B. E. Aydemir, A. G. Dumanli, *Philos. Trans. R. Soc., A* **2021**, *379*, 20200331.
- [26] J. C. Weaver, G. W. Milliron, A. Miserez, K. Evans-Lutterodt, S. Herrera, I. Gallana, W. J. Mershon, B. Swanson, P. Zavattieri, E. DiMasi, D. Kisailus, *Science* **2012**, *336*, 1275.
- [27] V. Sharma, M. Crne, J. O. Park, M. Srinivasarao, *Science* **2009**, *325*, 449.
- [28] A. G. Dumanli, T. Savin, *Chem. Soc. Rev.* **2016**, *45*, 6698.
- [29] D. Raabe, C. Sachs, P. Romano, *Acta Mater.* **2005**, *53*, 4281.
- [30] R. A. A. Muzzarelli, in *Chitin: Formation and Diagenesis*, (Ed: N. S. Gupta), Topics in Geobiology, Vol. 34, Springer, **2011**.
- [31] G. T. Beckham, M. F. Crowley, *J. Phys. Chem. B* **2011**, *115*, 4516.
- [32] P. Sikorski, R. Hori, M. Wada, *Biomacromolecules* **2009**, *10*, 1100.
- [33] R. Minke, J. Blackwell, *J. Mol. Biol.* **1978**, *120*, 167.
- [34] Y. Nishiyama, Y. Noishiki, M. Wada, *Macromolecules* **2011**, *44*, 950.
- [35] J. Skolnick, M. Fixman, *Macromolecules* **1977**, *10*, 944.
- [36] R. H. Pritchard, Y. Y. Huang, E. M. Terentjev, *Soft Matter* **2014**, *10*, 1864.
- [37] K. Mazeau, S. Pérez, M. Rinaudo, *J. Carbohydr. Chem.* **2000**, *19*, 1269.
- [38] D. W. Lee, C. Lim, J. N. Israelachvili, D. S. Hwang, *Langmuir* **2013**, *29*, 14222.
- [39] J. N. Israelachvili, *Intermolecular and Surface Forces*, Academic Press, Burlington, MA, USA **2011**.
- [40] C. Lim, D. W. Lee, J. N. Israelachvili, Y. Jho, D. S. Hwang, *Carbohydr. Polym.* **2015**, *117*, 887.
- [41] C. Lim, D. S. Hwang, D. W. Lee, *Carbohydr. Polym.* **2021**, *259*, 117782.
- [42] I. Aranaz, M. Mengibar, R. Harris, I. Paños, B. Miralles, N. Acosta, G. Galed, Á. Heras, *Curr. Chem. Biol.* **2009**, *3*, 203.
- [43] H. M. Mora-Montes, M. G. Netea, G. Ferwerda, M. D. Lenardon, G. D. Brown, A. R. Mistry, B. J. Kullberg, C. A. O'Callaghan, C. C. Sheth, F. C. Odds, A. J. Brown, C. A. Munro, N. A. Gow, *Infect. Immun.* **2011**, *79*, 1961.
- [44] S. Ravindranathan, B. P. Koppolu, S. G. Smith, D. A. Zaharoff, *Mar. Drugs* **2016**, *14*, 91.
- [45] J. N. Barbosa, I. F. Amaral, A. P. Aguas, M. A. Barbosa, *J. Biomed. Mater. Res.* **2010**, *93A*, 20.
- [46] C. A. Da Silva, C. Chalouni, A. Williams, D. Hartl, C. G. Lee, J. A. Elias, *J. Immunol.* **2009**, *182*, 3573.
- [47] T. A. Reese, H. E. Liang, A. M. Tager, A. D. Luster, N. Van Rooijen, D. Voehringer, R. M. Locksley, *Nature* **2007**, *447*, 92.
- [48] C. Gorzelanny, B. Poppelmann, K. Pappelbaum, B. M. Moerschbacher, S. W. Schneider, *Biomaterials* **2010**, *31*, 8556.
- [49] K. Fuchs, Y. Cardona Gloria, O. O. Wolz, F. Herster, L. Sharma, C. A. Dillen, C. Taumer, S. Dickhofer, Z. Bittner, T. M. Dang, C. A. Singh, D. Haischer, M. A. Schloffel, K. J. Koymans, T. Sanmuganatham, M. Krach, T. Roger, D. Le Roy, N. A. Schilling, F. Frauhammer, L. S. Miller, T. Nurnberger, S. LeibundGut-Landmann, A. A. Gust, B. Macek, M. Frank, C. Gouttefangeas, C. S. Dela Cruz, D. Hartl, A. N. Weber, *EMBO Rep.* **2018**, *19*, e46065.
- [50] C. L. Bueter, C. K. Lee, V. A. Rathinam, G. J. Healy, C. H. Taron, C. A. Specht, S. M. Levitz, *J. Biol. Chem.* **2011**, *286*, 35447.
- [51] M. S. Lee, Y. J. Kim, *Annu. Rev. Biochem.* **2007**, *76*, 447.
- [52] M. S. Jin, J. O. Lee, *Immunity* **2008**, *29*, 182.
- [53] S. E. Hardison, G. D. Brown, *Nat. Immunol.* **2012**, *13*, 817.
- [54] L. Brown, J. M. Wolf, R. Prados-Rosales, A. Casadevall, *Nat. Rev. Microbiol.* **2015**, *13*, 620.
- [55] K. Vega, M. Kalkum, *Int. J. Microbiol.* **2012**, *2012*, 920459.
- [56] C. A. Da Silva, D. Hartl, W. Liu, C. G. Lee, J. A. Elias, *J. Immunol.* **2008**, *181*, 4279.
- [57] P. Zhang, W. Liu, Y. Peng, B. Han, Y. Yang, *Int. Immunopharmacol.* **2014**, *23*, 254.
- [58] Y. Han, L. Zhao, Z. Yu, J. Feng, Q. Yu, *Int. Immunopharmacol.* **2005**, *5*, 1533.
- [59] H. P. Dulal, Y. Adachi, N. Ohno, Y. Yamaguchi, *Glycobiology* **2018**, *28*, 612.
- [60] S. Hanashima, A. Ikeda, H. Tanaka, Y. Adachi, N. Ohno, T. Takahashi, Y. Yamaguchi, *Glycoconjugate J.* **2014**, *31*, 199.
- [61] S. Lee, S. Byun, C. Lee, S. H. Park, D. Rudra, Y. Iwakura, Y. J. Lee, S.-H. Lim, D. S. Hwang, *Adv. Healthcare Mater.* **2022**, <https://doi.org/10.1002/adhm.202102667>.
- [62] S. H. Chang, Y. Y. Lin, G. J. Wu, C. H. Huang, G. J. Tsai, *Int. J. Biol. Macromol.* **2019**, *131*, 167.
- [63] N. Wu, Z. S. Wen, X. W. Xiang, Y. N. Huang, Y. Gao, Y. L. Qu, *Mar. Drugs* **2015**, *13*, 6210.
- [64] B. Zheng, Z. S. Wen, Y. J. Huang, M. S. Xia, X. W. Xiang, Y. L. Qu, *Mar. Drugs* **2016**, *14*, 169.
- [65] Y. Yang, R. Xing, S. Liu, Y. Qin, K. Li, H. Yu, P. Li, *Mar. Drugs* **2019**, *17*, 36.
- [66] Z. Abedian, A. A. Moghadamnia, E. Zabihi, R. Pourbagher, M. Ghasemi, H. R. Nouri, H. Tashakorian, N. Jenabian, *Caspian J. Intern. Med.* **2019**, *10*, 439.
- [67] C. Qin, Y. Dua, L. Xiao, Z. Li, X. Gao, *Int. J. Biol. Macromol.* **2002**, *31*, 111.
- [68] B. Jing, G. Cheng, J. Li, Z. A. Wang, Y. Du, *Mar. Drugs* **2019**, *17*, 415.
- [69] J. Feng, L. Zhao, Q. Yu, *Biochem. Biophys. Res. Commun.* **2004**, *317*, 414.
- [70] E. C. Carroll, L. Jin, A. Mori, N. Munoz-Wolf, E. Oleszycka, H. B. T. Moran, S. Mansouri, C. P. McEntee, E. Lambe, E. M. Agger, P. Andersen, C. Cunningham, P. Hertzog, K. A. Fitzgerald, A. G. Bowie, E. C. Lavelle, *Immunity* **2016**, *44*, 597.
- [71] L. Shi, B. Fang, Y. Yong, X. Li, D. Gong, J. Li, T. Yu, R. Gooneratne, Z. Gao, S. Li, X. Ju, *Carbohydr. Polym.* **2019**, *219*, 269.
- [72] H. J. Yoon, M. E. Moon, H. S. Park, S. Y. Im, Y. H. Kim, *Biochem. Biophys. Res. Commun.* **2007**, *358*, 954.
- [73] S. H. Lee, M. Senevirathne, C. B. Ahn, S. K. Kim, J. Y. Je, *Bioorg. Med. Chem. Lett.* **2009**, *19*, 6655.
- [74] E. J. Yang, J. G. Kim, J. Y. Kim, S. Kim, N. Lee, C. G. Hyun, *Open Life Sci.* **2010**, *5*, 95.

- [75] P. Jitprasertwong, M. Khamphio, P. Petsrichuang, V. G. H. Eijsink, W. Poolsri, C. Muanprasat, K. Rangnoi, M. Yamabhai, *PLoS One* **2021**, *16*, e0246381.
- [76] H. T. Liu, W. M. Li, X. Y. Li, Q. S. Xu, Q. S. Liu, X. F. Bai, C. Yu, Y. G. Du, *Basic Clin. Pharmacol. Toxicol.* **2009**, *106*, 362.
- [77] H. T. Liu, P. Huang, P. Ma, Q. S. Liu, C. Yu, Y. G. Du, *Acta Pharmacol. Sin.* **2011**, *32*, 478.
- [78] S. T. Holgate, S. Wenzel, D. S. Postma, S. T. Weiss, H. Renz, P. D. Sly, *Nat. Rev. Dis. Primers* **2015**, *1*, 15025.
- [79] T. S. Vo, C. S. Kong, S. K. Kim, *Carbohydr. Polym.* **2011**, *84*, 649.
- [80] M. J. Chung, J. K. Park, Y. I. Park, *Int. Immunopharmacol.* **2012**, *12*, 453.
- [81] K. Azuma, T. Osaki, S. Kurozumi, M. Kiyose, T. Tsuka, Y. Murahata, T. Imagawa, N. Itoh, S. Minami, K. Sato, Y. Okamoto, *Carbohydr. Polym.* **2015**, *115*, 448.
- [82] M. Yousef, R. Pichyangkura, S. Soodvilai, V. Chatsudthipong, C. Muanprasat, *Pharmacol. Res.* **2012**, *66*, 66.
- [83] W. Kunanusornchai, B. Witoonpanich, T. Tawonsawatruk, R. Pichyangkura, V. Chatsudthipong, C. Muanprasat, *Pharmacol. Res.* **2016**, *113*, 458.
- [84] Y. C. Chung, C. Y. Chen, *Bioresour. Technol.* **2008**, *99*, 2806.
- [85] I. Galván Márquez, J. Akuaku, I. Cruz, J. Cheetham, A. Golshani, M. L. Smith, *Int. J. Food Microbiol.* **2013**, *164*, 108.
- [86] J. Li, S. Zhuang, *Eur. Polym. J.* **2020**, *138*, 109984.
- [87] J. Li, Y. Wu, L. Zhao, *Carbohydr. Polym.* **2016**, *148*, 200.
- [88] S. H. Chang, H. T. Lin, G. J. Wu, G. J. Tsai, *Carbohydr. Polym.* **2015**, *134*, 74.
- [89] I. Younes, S. Sellimi, M. Rinaudo, K. Jellouli, M. Nasri, *Int. J. Food Microbiol.* **2014**, *185*, 57.
- [90] D. Raafat, K. von Bargaen, A. Haas, H. G. Sahl, *Appl. Environ. Microbiol.* **2008**, *74*, 3764.
- [91] J. L. Chen, Y. Zhao, *J. Food Sci.* **2012**, *77*, E127.
- [92] J. Kingkaew, S. Kirdponpattara, N. Sanchavanakit, P. Pavasant, M. Phisalaphong, *Biotechnol. Bioprocess Eng.* **2014**, *19*, 534.
- [93] J. Simunek, V. Brandysova, I. Koppova, J. Simunek, Jr., *Folia Microbiol.* **2012**, *57*, 341.
- [94] H. Liu, Y. Du, X. Wang, L. Sun, *Int. J. Food Microbiol.* **2004**, *95*, 147.
- [95] S.-C. Park, J.-W. Nah, Y. Park, *Macromol. Res.* **2011**, *19*, 853.
- [96] C. L. Ke, Y. T. Liao, C. H. Lin, *Virulence* **2021**, *12*, 281.
- [97] L. G. S. Garcia, G. M. M. Guedes, M. L. Q. da Silva, D. Castelo-Branco, J. J. C. Sidrim, R. A. Cordeiro, M. F. G. Rocha, R. S. Vieira, R. S. N. Brilhante, *Carbohydr. Polym.* **2018**, *195*, 662.
- [98] S. N. Kulikov, S. A. Lisovskaya, P. V. Zelenikhin, E. A. Bezrodnykh, D. R. Shakirova, I. V. Blagodatskikh, V. E. Tikhonov, *Eur. J. Med. Chem.* **2014**, *74*, 169.
- [99] S. Ifuku, *Molecules* **2014**, *19*, 18367.
- [100] T. H. Tran, H. L. Nguyen, D. S. Hwang, J. Y. Lee, H. G. Cha, J. M. Koo, S. Y. Hwang, J. Park, D. X. Oh, *Carbohydr. Polym.* **2019**, *205*, 392.
- [101] K. Ohkawa, D. Cha, H. Kim, A. Nishida, H. Yamamoto, *Macromol. Rapid Commun.* **2004**, *25*, 1600.
- [102] J. D. Schiffman, C. L. Schauer, *Biomacromolecules* **2007**, *8*, 594.
- [103] K. Ohkawa, K. I. Minato, G. Kumagai, S. Hayashi, H. Yamamoto, *Biomacromolecules* **2006**, *7*, 3291.
- [104] H. Homayoni, S. A. H. Ravandi, M. Valizadeh, *Carbohydr. Polym.* **2009**, *77*, 656.
- [105] J.-B. Zeng, Y.-S. He, S.-L. Li, Y.-Z. Wang, *Biomacromolecules* **2012**, *13*, 1.
- [106] T. Hahn, E. Tafi, A. Paul, R. Salvia, P. Falabella, S. Zibek, *J. Chem. Technol. Biotechnol.* **2020**, *95*, 2775.
- [107] X. Yang, J. Liu, Y. Pei, X. Zheng, K. Tang, *Energy Environ. Mater.* **2020**, *3*, 492.
- [108] J. Jin, P. Hassanzadeh, G. Perotto, W. Sun, M. A. Brenckle, D. Kaplan, F. G. Omenetto, M. Rolandi, *Adv. Mater.* **2013**, *25*, 4482.
- [109] K. T. Smitha, A. Anitha, T. Furuike, H. Tamura, S. V. Nair, R. Jayakumar, *Colloids Surf., B* **2013**, *104*, 245.
- [110] K. S. Huang, Y. R. Sheu, I. C. Chao, *Polym.-Plast. Technol. Eng.* **2009**, *48*, 1239.
- [111] J. F. Revol, R. H. Marchessault, *Int. J. Biol. Macromol.* **1993**, *15*, 329.
- [112] J. Li, J. F. Revol, E. Naranjo, R. H. Marchessault, *Int. J. Biol. Macromol.* **1996**, *18*, 177.
- [113] K. Gopalan Nair, A. Dufresne, *Biomacromolecules* **2003**, *4*, 657.
- [114] Y. Lu, L. Weng, L. Zhang, *Biomacromolecules* **2004**, *5*, 1046.
- [115] A. Morin, A. Dufresne, *Macromolecules* **2002**, *35*, 2190.
- [116] M. Paillet, A. Dufresne, *Macromolecules* **2001**, *34*, 6527.
- [117] A. K. Dutta, H. Izawa, M. Morimoto, H. Saimoto, S. Ifuku, *J. Chitin Chitosan Sci.* **2014**, *2*, 179.
- [118] L. Liu, F. T. Setta, X. An, J. Yang, W. Zhang, H. Dai, H. Cao, Q. Xu, H. Liu, *Cellulose* **2020**, *27*, 9853.
- [119] H. Ma, L. Liu, J. Yu, Y. Fan, *Biomacromolecules* **2021**, *22*, 4373.
- [120] Y. Fan, T. Saito, A. Isogai, *Biomacromolecules* **2008**, *9*, 192.
- [121] Y. Fan, T. Saito, A. Isogai, *Carbohydr. Polym.* **2009**, *77*, 832.
- [122] K. Pang, B. Ding, X. Liu, H. Wu, Y. Duan, J. Zhang, *Green Chem.* **2017**, *19*, 3665.
- [123] J. Jiang, J. Yu, L. Liu, Z. Wang, Y. Fan, T. Satio, A. Isogai, *J. Agric. Food Chem.* **2018**, *66*, 11372.
- [124] J. Jiang, W. Ye, J. Yu, Y. Fan, Y. Ono, T. Saito, A. Isogai, *Carbohydr. Polym.* **2018**, *189*, 178.
- [125] A. A. Oun, J. W. Rhim, *Carbohydr. Polym.* **2018**, *197*, 349.
- [126] A. A. Oun, J. W. Rhim, *Carbohydr. Polym.* **2017**, *175*, 712.
- [127] P. Liu, H. Liu, T. Schäfer, T. Gutmann, H. Gibhardt, H. Qi, L. Tian, X. C. Zhang, G. Buntkowsky, K. Zhang, *Green Chem.* **2021**, *23*, 745.
- [128] Y. Yuan, S. Hong, H. Lian, K. Zhang, H. Liimatainen, *Carbohydr. Polym.* **2020**, *236*, 116095.
- [129] S.-L. Cao, W.-M. Gu, W.-D. Ou-Yang, D.-C. Chen, B.-Y. Yang, L.-H. Lai, Y.-D. Wu, Y.-J. Liu, J. Zhu, W.-J. Chen, Z.-Q. Gai, X.-D. Hou, Y.-Z. Ma, Y.-X. An, *Carbohydr. Polym.* **2019**, *213*, 304.
- [130] S. Hong, Y. Yuan, Q. Yang, L. Chen, J. Deng, W. Chen, H. Lian, J. D. Mota-Morales, H. Liimatainen, *Carbohydr. Polym.* **2019**, *220*, 211.
- [131] Y. Fan, T. Saito, A. Isogai, *Carbohydr. Polym.* **2010**, *79*, 1046.
- [132] S. Ifuku, M. Nogi, K. Abe, M. Yoshioka, M. Morimoto, H. Saimoto, H. Yano, *Biomacromolecules* **2009**, *10*, 1584.
- [133] S. Ifuku, M. Nogi, M. Yoshioka, M. Morimoto, H. Yano, H. Saimoto, *Carbohydr. Polym.* **2010**, *81*, 134.
- [134] S. Ifuku, M. Nogi, K. Abe, M. Yoshioka, M. Morimoto, H. Saimoto, H. Yano, *Carbohydr. Polym.* **2011**, *84*, 762.
- [135] H. P. Zhao, X. Q. Feng, H. Gao, *Appl. Phys. Lett.* **2007**, *90*, 2006.
- [136] Y. Fan, T. Saito, A. Isogai, *Biomacromolecules* **2008**, *9*, 1919.
- [137] A. M. Salaberria, S. C. M. Fernandes, R. H. Diaz, J. Labidi, *Carbohydr. Polym.* **2015**, *116*, 286.
- [138] A. M. Salaberria, R. H. Diaz, J. Labidi, S. C. M. Fernandes, *Food Hydrocolloids* **2015**, *46*, 93.
- [139] F. Riehle, D. Hoenders, J. Guo, A. Eckert, S. Ifuku, A. Walther, *Biomacromolecules* **2019**, *20*, 1098.
- [140] C. Chen, Y. Wang, Y. Yang, M. Pan, T. Ye, D. Li, *Carbohydr. Polym.* **2018**, *195*, 387.
- [141] Y. F. Aklog, T. Nagae, H. Izawa, M. Morimoto, H. Saimoto, S. Ifuku, *J. Nanosci. Nanotechnol.* **2017**, *17*, 5037.
- [142] G. L. Clark, A. F. Smith, *J. Phys. Chem.* **1936**, *40*, 863.
- [143] H. Wang, C. Qian, M. Roman, *Biomacromolecules* **2011**, *12*, 3708.
- [144] I. Colijn, R. Fokkink, K. Schroën, *Sci. Rep.* **2021**, *11*, 17217.
- [145] Y. Okita, T. Saito, A. Isogai, *Biomacromolecules* **2010**, *11*, 1696.
- [146] J. Araki, M. Kurihara, *Biomacromolecules* **2015**, *16*, 379.

- [147] Y. Huang, M. He, A. Lu, W. Zhou, S. D. Stoyanov, E. G. Pelan, L. Zhang, *Langmuir* **2015**, *31*, 1641.
- [148] K. G. Nair, A. Dufresne, A. Gandini, M. N. Belgacem, *Biomacromolecules* **2003**, *4*, 1835.
- [149] L. Feng, Z. Zhou, A. Dufresne, J. Huang, M. Wei, L. An, *J. Appl. Polym. Sci.* **2009**, *112*, 2830.
- [150] L. T. Hao, Y. Eom, T. H. Tran, J. M. Koo, J. Jegal, S. Y. Hwang, D. X. Oh, J. Park, *Nanoscale* **2020**, *12*, 2393.
- [151] V. T. T. Thuy, L. T. Hao, H. Jeon, J. M. Koo, J. Park, E. S. Lee, S. Y. Hwang, S. Choi, J. Park, D. X. Oh, *Green Chem.* **2021**, *23*, 2658.
- [152] L. Yan, P. Li, W. Zhou, Z. Wang, X. Fan, M. Chen, Y. Fang, H. Liu, *ACS Sustainable Chem. Eng.* **2019**, *7*, 2064.
- [153] D. X. Oh, Y. J. Cha, H. L. Nguyen, H. H. Je, Y. S. Jho, D. S. Hwang, D. K. Yoon, *Sci. Rep.* **2016**, *6*, 23245.
- [154] T. Jin, D. Kurdyla, S. Hrapovic, A. C. W. Leung, S. Régnier, Y. Liu, A. Moores, E. Lam, *Biomacromolecules* **2020**, *21*, 2236.
- [155] J. Li, J. F. Revol, R. H. Marchessault, *J. Colloid Interface Sci.* **1997**, *192*, 447.
- [156] A. K. Dutta, M. Egusa, H. Kaminaka, H. Izawa, M. Morimoto, H. Saimoto, S. Ifuku, *Carbohydr. Polym.* **2015**, *115*, 342.
- [157] S. Ifuku, N. Suzuki, H. Izawa, M. Morimoto, H. Saimoto, *RSC Adv.* **2014**, *4*, 19246.
- [158] S. Ifuku, N. Suzuki, H. Izawa, M. Morimoto, H. Saimoto, *React. Funct. Polym.* **2014**, *85*, 121.
- [159] J. Zhou, N. Butchosa, H. S. N. Jayawardena, Q. Zhou, M. Yan, O. Ramström, *Bioconjugate Chem.* **2014**, *25*, 640.
- [160] L. T. Hao, S. Park, S. Choy, Y. Kim, S. Lee, Y. S. Ok, J. M. Koo, S. Y. Hwang, D. S. Hwang, J. Park, D. X. Oh, *JACS Au* **2021**, *1*, 1399.
- [161] J. Zhang, F. Luan, Q. Li, G. Gu, F. Dong, Z. Guo, *Mar. Drugs* **2018**, *16*, 380.
- [162] H. Zhu, S. Zhu, Z. Jia, S. Parvinian, Y. Li, O. Vaaland, L. Hu, T. Li, *Proc. Natl. Acad. Sci. USA* **2015**, *112*, 8971.
- [163] J. G. Torres-Rendon, F. H. Schacher, S. Ifuku, A. Walther, *Biomacromolecules* **2014**, *15*, 2709.
- [164] J. L. Shamshina, O. Zavgorodnya, P. Berton, P. K. Chhotaray, H. Choudhary, R. D. Rogers, *ACS Sustainable Chem. Eng.* **2018**, *6*, 10241.
- [165] Y. Qin, Xingmei Lu, N. Sun, R. D. Roger, *Green Chem.* **2010**, *12*, 968.
- [166] Y. Bamba, Y. Ogawa, T. Saito, L. A. Berglund, A. Isogai, *Biomacromolecules* **2017**, *18*, 4405.
- [167] Q. Wu, N. E. Mushi, L. A. Berglund, *Biomacromolecules* **2020**, *21*, 604.
- [168] T. Naghdi, H. Golmohammadi, H. Yousefi, M. Hosseinifard, U. Kostiv, D. Horák, A. Merkoçi, *ACS Appl. Mater. Interfaces* **2020**, *12*, 15538.
- [169] N. E. Mushi, T. Nishino, L. A. Berglund, Q. Zhou, *ACS Sustainable Chem. Eng.* **2019**, *7*, 1692.
- [170] Y. Fan, H. Fukuzumi, T. Saito, A. Isogai, *Int. J. Biol. Macromol.* **2012**, *50*, 69.
- [171] A. Wei, J. Fu, F. Guo, *J. Mater. Sci.* **2021**, *56*, 12048.
- [172] Q. Wu, E. Jungstedt, M. Šoltéssová, N. E. Mushi, L. A. Berglund, *Nanoscale* **2019**, *11*, 11001.
- [173] S. Ifuku, A. Ikuta, M. Egusa, H. Kaminaka, H. Izawa, M. Morimoto, H. Saimoto, *Carbohydr. Polym.* **2013**, *98*, 1198.
- [174] D. Montroni, S. Fermani, K. Morellato, G. Torri, A. Naggi, L. Cristofolini, G. Falini, *Carbohydr. Polym.* **2019**, *207*, 26.
- [175] J. Cui, Z. Yu, D. Lau, *Int. J. Mol. Sci.* **2016**, *17*, 61.
- [176] A. Dufresne, *Molecules* **2010**, *15*, 4111.
- [177] M. I. Shams, S. Ifuku, M. Nogi, T. Oku, H. Yano, *Appl. Phys. A: Mater. Sci. Process.* **2011**, *102*, 325.
- [178] F. Larbi, A. García, L. J. del Valle, A. Hamou, J. Puiggalí, N. Belgacem, J. Bras, *Carbohydr. Polym.* **2018**, *196*, 385.
- [179] Y. Xu, A. Atrens, J. R. Stokes, *Adv. Colloid Interface Sci.* **2020**, *275*, 102076.
- [180] L. Onsager, *Ann. N. Y. Acad. Sci.* **1949**, *51*, 627.
- [181] J. Araki, *Soft Matter* **2013**, *9*, 4125.
- [182] O. M. Vanderfleet, E. D. Cranston, *Nat. Rev. Mater.* **2021**, *6*, 124.
- [183] J. Li, J. F. Revol, R. H. Marchessault, *J. Colloid Interface Sci.* **1996**, *183*, 365.
- [184] H. L. Nguyen, T. H. Tran, L. T. Hao, H. Jeon, J. M. Koo, G. Shin, D. S. Hwang, S. Y. Hwang, J. Park, D. X. Oh, *Carbohydr. Polym.* **2021**, *271*, 118421.
- [185] S. Bhattacharjee, *J. Controlled Release* **2016**, *235*, 337.
- [186] E. Belamie, P. Davidson, M. M. Giraud-Guille, *J. Phys. Chem. B* **2004**, *108*, 14991.
- [187] A. Narkevicius, L. M. Steiner, R. M. Parker, Y. Ogawa, B. Frka-Petescic, S. Vignolini, *Biomacromolecules* **2019**, *20*, 2830.
- [188] L. Bai, T. Kämäräinen, W. Xiang, J. Majoinen, J. Seitsonen, R. Grande, S. Huan, L. Liu, Y. Fan, O. J. Rojas, *ACS Nano* **2020**, *14*, 6921.
- [189] J. Araki, S. Kuga, *Langmuir* **2001**, *17*, 4493.
- [190] W. J. Orts, L. Godbout, R. H. Marchessault, J. F. Revol, *Macromolecules* **1998**, *31*, 5717.
- [191] A. Hirai, O. Inui, F. Horii, M. Tsuji, *Langmuir* **2009**, *25*, 495.
- [192] Y. Zhang, Q. Cheng, C. Chang, L. Zhang, *J. Appl. Polym. Sci.* **2018**, *135*, 45702.
- [193] S. B. Murray, A. C. Neville, *Int. J. Biol. Macromol.* **1998**, *22*, 137.
- [194] M. Yokoi, R. Tanaka, T. Saito, A. Isogai, *Biomacromolecules* **2017**, *18*, 2564.
- [195] W. Liu, K. Liu, L. Zhu, W. Li, K. Liu, W. Wen, M. Liu, H. Li, C. Zhou, B. Luo, *Int. J. Biol. Macromol.* **2020**, *157*, 24.
- [196] H. Liu, Y. Feng, X. Cao, B. Luo, M. Liu, *ACS Appl. Mater. Interfaces* **2021**, *13*, 11356.
- [197] B. Alonso, E. Belamie, *Angew. Chem., Int. Ed.* **2010**, *49*, 8201.
- [198] M. Y. Boltoeva, I. Dozov, P. Davidson, K. Antonova, L. Cardoso, B. Alonso, E. Belamie, *Langmuir* **2013**, *29*, 8208.
- [199] M. M. Titirici, R. J. White, N. Brun, V. L. Budarin, D. S. Su, F. del Monte, J. H. Clark, M. J. MacLachlan, *Chem. Soc. Rev.* **2015**, *44*, 250.
- [200] W. Shen, W. Fan, *J. Mater. Chem. A* **2013**, *1*, 999.
- [201] J. P. Paraknowitsch, A. Thomas, *Energy Environ. Sci.* **2013**, *6*, 2839.
- [202] A. Khan, M. Goepel, J. C. Colmenares, R. Gläser, *ACS Sustainable Chem. Eng.* **2020**, *8*, 4708.
- [203] H. Nguyen, S. Ju, L. T. Hao, T. H. Tran, H. G. Cha, Y. J. Cha, J. Park, S. Y. Hwang, D. K. Yoon, D. S. Hwang, D. X. Oh, *ChemSusChem* **2019**, *12*, 3236.
- [204] R. J. White, M. Antonietti, M. M. Titirici, *J. Mater. Chem.* **2009**, *19*, 8645.
- [205] L. Gao, D. Ying, T. Shen, Y. Zheng, J. Cai, D. Wang, L. Zhang, *ACS Sustainable Chem. Eng.* **2020**, *29*, 10881.
- [206] H. Yao, G. Zheng, W. Li, M. T. McDowell, Z. Seh, N. Liu, Z. Lu, Y. Cui, *Nano Lett.* **2013**, *13*, 3385.
- [207] W. J. Liu, H. Jiang, H. Q. Yu, *Chem. Rev.* **2015**, *115*, 12251.
- [208] M. Abdelmoula, H. Ben Hlima, F. Michalet, G. Bourduche, J. Y. Chavant, A. Gravier, C. Delattre, M. Grédiac, J. D. Mathias, S. Abdelkafi, *Polysaccharides* **2021**, *2*, 110.
- [209] J. H. Ryu, Y. Lee, W. H. Kong, T. G. Kim, T. G. Park, H. Lee, *Biomacromolecules* **2011**, *12*, 2653.
- [210] Y. Hino, H. Ejima, *J. Photopolym. Sci. Technol.* **2020**, *33*, 123.
- [211] J. Saiz-Poseu, J. Mancebo-Aracil, F. Nador, F. Busqu, D. Ruiz-Molina, *Angew. Chem., Int. Ed.* **2019**, *58*, 696.
- [212] M. Shin, S. G. Park, B. C. Oh, K. Kim, S. Jo, M. S. Lee, S. S. Oh, S. H. Hong, E. C. Shin, K. S. Kim, S. W. Kang, H. Lee, *Nat. Mater.* **2017**, *16*, 147.
- [213] K. Kim, J. H. Ryu, M. Y. Koh, S. P. Yun, S. Kim, J. P. Park, C. W. Jung, M. S. Lee, H. I. Seo, J. H. Kim, H. Lee, *Sci. Adv.* **2021**, *7*, eabc9992.

- [214] K. Kim, K. Kim, J. H. Ryu, H. Lee, *Biomaterials* **2015**, *52*, 161.
- [215] C. Guyot, A. Adoungotchodo, W. Taillades, M. Cerrutic, S. Lerouge, *J. Mater. Chem. B* **2021**, *9*, 8406.
- [216] X. He, R. Liu, H. Liu, R. Wang, Z. Xi, Y. Lin, J. Wang, *Polymers* **2021**, *13*, 4322.
- [217] D. X. Oh, S. Kim, D. Lee, D. S. Hwang, *Acta Biomater.* **2015**, *20*, 104.
- [218] N. D. Sanandiyaa, S. Lee, S. Rho, H. Lee, I. S. Kim, D. S. Hwang, *Carbohydr. Polym.* **2019**, *208*, 77.
- [219] B. R. Riegger, B. Bauer, A. Mirzayeva, G. E. M. Tovar, M. Bach, *Carbohydr. Polym.* **2018**, *180*, 46.
- [220] F. Brunel, L. Veron, C. Ladaviere, L. David, A. Domard, T. Delair, *Langmuir* **2009**, *25*, 8935.
- [221] A. G. Luque-Alcaraz, J. Lizardi-Mendoza, F. M. Goycoolea, I. Higuera-Ciagara, W. Argüelles-Monal, *RSC Adv.* **2016**, *6*, 59250.
- [222] W. Fan, W. Yan, Z. Xu, H. Ni, *Colloids Surf., B* **2012**, *90*, 21.
- [223] H. V. Sæther, H. K. Holme, G. Maurstad, O. Smidsrød, B. T. Stokke, *Carbohydr. Polym.* **2008**, *74*, 813.
- [224] T. M. M. Ways, W. M. Lau, V. V. Khutoryanskiy, *Polymers* **2018**, *10*, 267.
- [225] A. Malik, M. Gupta, V. Gupta, H. Gogoi, R. Bhatnagar, *Int. J. Nanomed.* **2018**, *13*, 7959.
- [226] Y. Cao, Y. F. Tan, Y. S. Wong, M. W. J. Liew, S. Venkatraman, *Mar. Drugs* **2019**, *17*, 381.
- [227] S. Sreekumar, F. M. Goycoolea, B. M. Moerschbacher, G. R. Rivera-Rodriguez, *Sci. Rep.* **2018**, *8*, 4695.
- [228] J. C. Fernandes, X. Qiu, F. M. Winnik, M. Benderdour, X. Zhang, K. Dai, Q. Shi, *Int. J. Nanomed.* **2012**, *7*, 5833.
- [229] M. Alameh, D. Dejesus, M. Jean, V. Darras, M. Thibault, M. Lavertu, M. D. Buschmann, A. Merzouki, *Int. J. Nanomed.* **2012**, *7*, 1399.
- [230] M. Huang, E. Khor, L. Y. Lim, *Pharm. Res.* **2004**, *21*, 344.
- [231] A. Bozkir, O. M. Saka, *Drug Delivery* **2004**, *11*, 107.
- [232] Y. Gao, Z. Y. Wang, J. Zhang, Y. Zhang, H. Huo, T. Wang, T. Jiang, S. Wang, *Biomacromolecules* **2014**, *15*, 1010.
- [233] M. Van Woensel, T. Mathivet, N. Wauthoz, R. Rosiere, A. D. Garg, P. Agostinis, V. Mathieu, R. Kiss, F. Lefranc, L. Boon, J. Belmans, S. W. Van Gool, H. Gerhardt, K. Amighi, S. De Vleeschouwer, *Sci. Rep.* **2017**, *7*, 1217.
- [234] R. M. Raftery, E. G. Tierney, C. M. Curtin, S. A. Cryan, F. J. O'Brien, *J. Controlled Release* **2015**, *210*, 84.
- [235] R. M. Raftery, I. Mencia Castano, G. Chen, B. Cavanagh, B. Quinn, C. M. Curtin, S. A. Cryan, F. J. O'Brien, *Biomaterials* **2017**, *149*, 116.
- [236] P. Sahu, S. K. Kashwah, S. Sau, V. Kushwah, S. Jain, R. K. Agrawal, A. K. Iyer, *Colloids Surf., B* **2019**, *174*, 232.
- [237] U. Termsarasab, I. S. Yoon, J. H. Park, H. T. Moon, H. J. Cho, D. D. Kim, *Int. J. Pharm.* **2014**, *464*, 127.
- [238] R. Vivek, V. Nipun Babu, R. Thangam, K. S. Subramanian, S. Kannan, *Colloids Surf., B* **2013**, *111*, 117.
- [239] F. Xie, R. L. Ding, W. F. He, Z. J. Liu, S. Z. Fu, J. B. Wu, L. L. Yang, S. Lin, Q. L. Wen, *Drug Delivery* **2017**, *24*, 1410.
- [240] A. Iwasaki, S. B. Omer, *Cell* **2020**, *183*, 290.
- [241] I. Dmour, N. Islam, *Int. J. Biol. Macromol.* **2022**, *200*, 498.
- [242] A. T. Lampe, E. J. Farris, D. M. Brown, A. K. Pannier, *Biotechnol. Bioeng.* **2021**, *118*, 1224.
- [243] P. D. Lopes, C. H. Okino, F. S. Fernando, C. Pavani, V. M. Casagrande, R. F. V. Lopez, M. F. S. Montassier, H. J. Montassier, *Vaccine* **2018**, *36*, 2630.
- [244] U. S. Kumar, R. Afjei, K. Ferrara, T. F. Massoud, R. Paulmurugan, *ACS Nano* **2021**, *15*, 17582.
- [245] T. Jeeranaiwitayakul, M. Seesen, R. Chawengkirttikul, P. Limthongkul, S. Apichirapokey, S. Sapsutthipas, S. Phumiamorn, P. Sunintaboon, S. Ubol, *Vaccines* **2021**, *9*, 768.
- [246] L. Zhao, W. Jin, J. G. Cruz, N. Marasini, Z. G. Khalil, R. J. Capon, W. M. Hussein, M. Skwarczynski, I. Toth, *Nanomaterials* **2020**, *10*, 823.
- [247] S. Renu, Y. Han, S. Dhakal, Y. S. Lakshmanappa, S. Ghimire, N. Feliciano-Ruiz, S. Senapati, B. Narasimhan, R. Selvaraj, G. J. Renukaradhya, *Carbohydr. Polym.* **2020**, *243*, 116434.
- [248] C. M. Rochman, S. M. Kross, J. B. Armstrong, M. T. Bogan, E. S. Darling, S. J. Green, A. R. Smyth, D. Verissimo, *Environ. Sci. Technol.* **2015**, *49*, 10759.
- [249] J. A. Ivar Do Sul, M. F. Costa, *Environ. Pollut.* **2014**, *185*, 352.
- [250] Z. Zhang, Y. Chen, *Chem. Eng. J.* **2020**, *382*, 122955.
- [251] M. A. Browne, P. Crump, S. J. Niven, E. Teuten, A. Tonkin, T. Galloway, R. Thompson, *Environ. Sci. Technol.* **2011**, *45*, 9175.
- [252] K. L. Law, R. C. Thompson, *Science* **2014**, *345*, 144.
- [253] J. Barrett, Z. Chase, J. Zhang, M. M. B. Holl, K. Willis, A. Williams, B. D. Hardesty, C. Wilcox, *Front. Mar. Sci.* **2020**, *7*, 576170.
- [254] L. G. A. Barboza, A. Dick Vethaak, B. R. B. O. Lavorante, A. K. Lundebye, L. Guilhermino, *Mar. Pollut. Bull.* **2018**, *133*, 336.
- [255] C. A. King, J. L. Shamshina, O. Zavgorodnya, T. Cutfield, L. E. Block, R. D. Rogers, *ACS Sustainable Chem. Eng.* **2017**, *5*, 11660.
- [256] S. Ju, G. Shin, M. Lee, J. M. Koo, H. Jeon, Y. S. Ok, D. S. Hwang, S. Y. Hwang, D. X. Oh, J. Park, *Green Chem.* **2021**, *23*, 6953.
- [257] M. Faustini, L. Nicole, E. Ruiz-Hitzky, C. Sanchez, *Adv. Funct. Mater.* **2018**, *28*, 1704158.
- [258] A. K. Mohanty, S. Vivekanandhan, J. M. Pin, M. Misra, *Science* **2018**, *362*, 536.
- [259] A. Nel, T. Xia, L. Mädler, N. Li, *Science* **2006**, *311*, 622.
- [260] C. R. Estrellan, F. Iino, *Chemosphere* **2010**, *80*, 193.
- [261] P. Fratzl, R. Weinkamer, *Prog. Mater. Sci.* **2007**, *52*, 1263.
- [262] F. J. Martin-Martinez, K. Jin, D. López Barreiro, M. J. Buehler, *ACS Nano* **2018**, *12*, 7425.
- [263] J. Sriupayao, P. Supaphol, J. Blackwell, R. Rujiravanit, *Polymer* **2005**, *46*, 5637.
- [264] J. Junkasem, R. Rujiravanit, B. P. Grady, P. Supaphol, *Polym. Int.* **2010**, *59*, 85.
- [265] J. Huang, J. W. Zou, P. R. Chang, J. H. Yu, A. Dufresne, *eXPRESS Polym. Lett.* **2011**, *5*, 362.
- [266] K. Gopalan Nair, A. Dufresne, *Biomacromolecules* **2003**, *4*, 666.
- [267] J. Huang, P. R. Chang, N. Lin, A. Dufresne, *Polysaccharide-Based Nanocrystals: Chemistry and Application*, Wiley-VCH, Weinheim, Germany **2015**.
- [268] J. Junkasem, R. Rujiravanit, P. Supaphol, *Nanotechnology* **2006**, *17*, 4519.
- [269] A. Watthanaphanit, P. Supaphol, H. Tamura, S. Tokura, R. Rujiravanit, *J. Appl. Polym. Sci.* **2008**, *110*, 890.
- [270] T. H. Tran, H. L. Nguyen, L. T. Hao, H. Kong, J. M. Park, S. H. Jung, H. G. Cha, J. Y. Lee, H. Kim, S. Y. Hwang, J. Park, D. X. Oh, *Int. J. Biol. Macromol.* **2019**, *125*, 660.
- [271] T. Kim, H. Jeon, J. Jegal, J. H. Kim, H. Yang, J. Park, D. X. Oh, S. Y. Hwang, *RSC Adv.* **2018**, *8*, 15389.
- [272] J. M. Koo, J. Kang, S. H. Shin, J. Jegal, H. G. Cha, S. Choy, M. Hakkarainen, J. Park, D. X. Oh, S. Y. Hwang, *Compos. Sci. Technol.* **2020**, *185*, 107885.
- [273] S. A. Park, Y. Eom, H. Jeon, J. M. Koo, E. S. Lee, J. Jegal, S. Y. Hwang, D. X. Oh, J. Park, *Green Chem.* **2019**, *21*, 5212.
- [274] H. Kim, M. S. Shin, H. Jeon, J. M. Koo, Y. Eom, S. Choi, G. Shin, D. X. Oh, S. Y. Hwang, J. Park, *Int. J. Biol. Macromol.* **2021**, *173*, 128.
- [275] H. Kim, H. Jeon, G. Shin, M. Lee, J. Jegal, S. Y. Hwang, D. X. Oh, J. M. Koo, Y. Eom, J. Park, *Green Chem.* **2021**, *23*, 2293.
- [276] R. Grande, L. Bai, L. Wang, W. Xiang, O. Ikkala, A. J. F. Carvalho, O. J. Rojas, *ACS Sustainable Chem. Eng.* **2020**, *8*, 1137.
- [277] M. C. Li, Q. Wu, K. Song, H. N. Cheng, S. Suzuki, T. Lei, *ACS Sustainable Chem. Eng.* **2016**, *4*, 4385.
- [278] S. Matsumura, S. Kajiyama, T. Nishimura, T. Kato, *Small* **2015**, *11*, 5127.

- [279] J. Wang, D. J. Gardner, N. M. Stark, D. W. Bousfield, M. Tajvidi, Z. Cai, *ACS Sustainable Chem. Eng.* **2018**, *6*, 49.
- [280] M. Rabnawaz, I. Wyman, R. Auras, S. Cheng, *Green Chem.* **2017**, *19*, 4737.
- [281] O. Horodytska, F. J. Valdés, A. Fullana, *Waste Manage.* **2018**, *77*, 413.
- [282] J. Lange, Y. Wyser, *Packag. Technol. Sci.* **2003**, *16*, 149.
- [283] C. C. Satam, C. W. Irvin, C. J. Coffey, R. K. Geran, R. Ibarra-Rivera, M. L. Shofner, J. C. Meredith, *Biomacromolecules* **2020**, *21*, 545.
- [284] T. Zhong, M. P. Wolcott, H. Liu, J. Wang, *Carbohydr. Polym.* **2019**, *226*, 115276.
- [285] T. Kim, T. H. Tran, S. Y. Hwang, J. Park, D. X. Oh, B. S. Kim, *ACS Nano* **2019**, *13*, 3796.
- [286] G. Barroso, Q. Li, R. K. Bordia, G. Motz, *J. Mater. Chem. A* **2019**, *7*, 1936.
- [287] C. C. Satam, C. W. Irvin, A. W. Lang, J. C. R. Jallorina, M. L. Shofner, J. R. Reynolds, J. C. Meredith, *ACS Sustainable Chem. Eng.* **2018**, *6*, 10637.
- [288] Z. Yu, Y. Ji, V. Bourg, M. Bilgen, J. C. Meredith, *Emergent Mater.* **2020**, *3*, 919.
- [289] T. S. Wong, S. H. Kang, S. K. Y. Tang, E. J. Smythe, B. D. Hatton, A. Grinthal, J. Aizenberg, *Nature* **2011**, *477*, 443.
- [290] R. A. Chowdhury, M. Nuruddin, C. Clarkson, F. Montes, J. Howarter, J. P. Youngblood, *ACS Appl. Mater. Interfaces* **2019**, *11*, 1376.
- [291] R. A. Chowdhury, C. Clarkson, V. A. Apalangya, S. M. N. Islam, J. P. Youngblood, *Cellulose* **2018**, *25*, 6547.
- [292] Y. Ji, S. Waters, E. Lim, A. W. Lang, P. N. Ciesielski, M. L. Shofner, J. R. Reynolds, J. C. Meredith, *ACS Sustainable Chem. Eng.* **2022**, *10*, 124.
- [293] M. Flórez, E. Guerra-Rodríguez, P. Cazón, M. Vázquez, *Food Hydrocolloids* **2022**, *124*, 107328.
- [294] S. Mohammadi, A. Babaei, *Int. J. Biol. Macromol.* **2022**, *201*, 528.
- [295] Z. Wu, X. Huang, Y. C. Li, H. Xiao, X. Wang, *Carbohydr. Polym.* **2018**, *199*, 210.
- [296] M. Ghaderi-Ghahfarokhi, M. Barzegar, M. A. Sahari, H. Ahmadi Gavlighi, F. Gardini, *Int. J. Biol. Macromol.* **2017**, *102*, 19.
- [297] A. Riaz, S. Lei, H. M. S. Akhtar, P. Wan, D. Chen, S. Jabbar, M. Abid, M. M. Hashim, X. Zeng, *Int. J. Biol. Macromol.* **2018**, *114*, 547.
- [298] T. Gasti, S. Dixit, V. D. Hiremani, R. B. Chougale, S. P. Masti, S. K. Vootla, B. S. Mudigoudra, *Carbohydr. Polym.* **2022**, *277*, 118866.
- [299] O. Akhavan, E. Ghaderi, *ACS Nano* **2010**, *4*, 5731.
- [300] M. Ahmad, A. U. Rajapaksha, J. E. Lim, M. Zhang, N. Bolan, D. Mohan, M. Vithanage, S. S. Lee, Y. S. Ok, *Chemosphere* **2014**, *99*, 19.
- [301] L. Wang, D. O'Connor, J. Rinklebe, Y. S. Ok, D. C. W. Tsang, Z. Shen, D. Hou, *Environ. Sci. Technol.* **2020**, *54*, 14797.
- [302] M. J. Ahmed, B. H. Hameed, E. H. Hummadi, *Carbohydr. Polym.* **2020**, *247*, 116690.
- [303] Y. Zhou, B. Gao, A. R. Zimmerman, J. Fang, Y. Sun, X. Cao, *Chem. Eng. J.* **2013**, *231*, 512.
- [304] P. Zhang, W. Duan, H. Peng, B. Pan, B. Xing, *ACS Environ. Au* **2022**, *2*, 115.
- [305] C. Deng, M. Zhu, *Energy Fuels* **2020**, *34*, 9320.
- [306] B. Ding, S. Huang, K. Pang, Y. Duan, J. Zhang, *ACS Sustainable Chem. Eng.* **2018**, *6*, 177.
- [307] S. Kinoshita, S. Yoshioka, K. Kawagoe, *Proc. R. Soc. B* **2002**, *269*, 1417.
- [308] W. Zhang, J. Gu, Q. Liu, H. Su, T. Fan, D. Zhang, *Phys. Chem. Chem. Phys.* **2014**, *16*, 19767.
- [309] T. D. Nguyen, M. J. MacLachlan, *Adv. Opt. Mater.* **2014**, *2*, 1031.
- [310] C. D. Edgar, D. G. Gray, *Cellulose* **2001**, *8*, 5.
- [311] T. D. Nguyen, B. U. Peres, R. M. Carvalho, M. J. MacLachlan, *Adv. Funct. Mater.* **2016**, *26*, 2875.
- [312] R. A. Guerrero, E. B. Aranas, *Mater. Sci. Eng., C* **2010**, *30*, 1170.
- [313] J. W. Galusha, L. R. Richey, M. R. Jorgensen, J. S. Gardner, M. H. Bartl, *J. Mater. Chem.* **2010**, *20*, 1277.
- [314] X. Liu, S. Zhu, D. Zhang, Z. Chen, *Mater. Lett.* **2010**, *64*, 2745.
- [315] W. Zhang, D. Zhang, T. Fan, J. Ding, J. Gu, Q. Guo, H. Ogawa, *Bioinspir. Biomim.* **2006**, *1*, 89.
- [316] W. Peng, S. Zhu, W. Wang, W. Zhang, J. Gu, X. Hu, D. Zhang, Z. Chen, *Adv. Funct. Mater.* **2012**, *22*, 2072.
- [317] R. Boruah, P. Nath, D. Mohanta, G. A. Ahmed, A. Choudhury, *Nanosci. Nanotechnol. Lett.* **2011**, *3*, 458.
- [318] T. Nguyen, W. Y. Hamad, M. J. MacLachlan, *Chem. Mater.* **2016**, *28*, 2581.
- [319] X. Zang, Y. Tan, Z. Lv, J. Gu, D. Zhang, *Sens. Actuators, B* **2012**, *166–167*, 824.
- [320] Q. Yang, S. Zhu, W. Peng, C. Yin, W. Wang, J. Gu, W. Zhang, J. Ma, T. Deng, C. Feng, D. Zhang, *ACS Nano* **2013**, *7*, 4911.
- [321] C. T.- Turo, I. Carmagnola, A. Chiappone, Z. Feng, G. Ciardelli, M. Hakkarainen, M. Sangermano, *Bioprinting* **2020**, *18*, e00082.
- [322] Z. Feng, M. Hakkarainen, H. Grützmacher, A. Chiappone, M. Sangermano, *Macromol. Chem. Phys.* **2019**, *220*, 1900174.
- [323] Z. Feng, K. Odelius, M. Hakkarainen, *Carbohydr. Polym.* **2018**, *196*, 135.
- [324] H. Sun, J. Zhu, D. Baumann, L. Peng, Y. Xu, I. Shaker, Y. Huang, X. Duan, *Nat. Rev. Mater.* **2019**, *4*, 45.
- [325] L. Wu, Y. Li, Z. Fu, B. L. Su, *Natl. Sci. Rev.* **2020**, *7*, 1667.
- [326] L. Gao, J. Ma, S. Li, D. Liu, D. Xu, J. Cai, L. Chen, J. Xie, L. Zhang, *Nanoscale* **2019**, *11*, 12626.
- [327] S. Huang, Y. Ding, Y. Li, X. Han, B. Xing, S. Wang, *Energy Fuels* **2021**, *35*, 1557.
- [328] B. Duan, X. Gao, X. Yao, Y. Fang, L. Huang, J. Zhou, L. Zhang, *Nano Energy* **2016**, *27*, 482.
- [329] L. Gao, L. Xiong, D. Xu, J. Cai, L. Huang, J. Zhou, L. Zhang, *ACS Appl. Mater. Interfaces* **2018**, *10*, 28918.
- [330] J. Qu, C. Geng, S. Lv, G. Shao, S. Ma, M. Wu, *Electrochim. Acta* **2015**, *176*, 982.
- [331] R. Vinodh, Y. Sasikumar, H. J. Kim, R. Atchudan, M. Yi, *J. Ind. Eng. Chem.* **2021**, *104*, 155.
- [332] Q. Liu, Y. Duan, Q. Zhao, F. Pan, B. Zhang, J. Zhang, *Langmuir* **2014**, *30*, 8238.
- [333] D. W. Lee, M. H. Jin, D. Oh, S. W. Lee, J. S. Park, *ACS Sustainable Chem. Eng.* **2017**, *5*, 9935.
- [334] H. Yuan, L. Deng, X. Cai, S. Zhou, Y. Chen, Y. Yuan, *RSC Adv.* **2015**, *5*, 56121.
- [335] C. Zhao, Z. Zhang, Y. Liu, N. Shang, H. J. Wang, C. Wang, Y. Gao, *ACS Sustainable Chem. Eng.* **2020**, *8*, 12304.
- [336] K. Heise, E. Kontturi, Y. Allahverdiyeva, T. Tammelin, M. B. Linder, Nonappa, O. Ikkala, *Adv. Mater.* **2021**, *33*, 2004349.



Suyoung Lee obtained her Ph.D. in integrative biosciences and biotechnology at the Pohang University of Science and Technology (POSTECH). She is currently a postdoctoral scholar in Prof. Dong Soo Hwang's Lab at the POSTECH. Her research interests focus on the characterization and modification of polysaccharides and recombinant proteins for the application of biomaterials.



Lam Tan Hao obtained his Bachelor of Science degree in Biotechnology from the Can Tho University (Vietnam) in 2016. He is currently pursuing a Ph.D. degree in chemical engineering and advanced materials under the supervision of Dr. Dongyeop X. Oh and Dr. Jeyoung Park at the Korea Research Institute of Chemical Technology (KRICT), supported by a scholarship from University of Science and Technology (UST, South Korea). His research interests cover sustainable materials and technology, biopolymer-based nanomaterials, and surface chemistry.



Jeyoung Park is a Principal Researcher in the Research Center for Bio-Based Chemistry at the KRICT (South Korea). He also serves as an Associate Professor in the Department of Advanced Materials and Chemical Engineering at the UST, and an Affiliate Faculty Member in the Division of Environmental Science & Engineering at the POSTECH. After his Ph.D. in 2012 in the Department of Chemistry at the Korea Advanced Institute of Science and Technology (KAIST), he worked for two years at SK Innovation Co. as a R&D researcher. His research interests include biorenewable polymers and sustainable plastics used in industrial applications.



Dongyeop X. Oh is a Principal Researcher in the Research Center for Bio-Based Chemistry at the KRICT, South Korea. He also serves as an Associate Professor in the Department of Advanced Materials and Chemical Engineering at the UST. In 2011, he received B.S. and M.S. degrees in polymer engineering from Hanyang University. He then earned a Ph.D. in environmental engineering at POSTECH in 2016 with Prof. Dong Soo Hwang. In his research, a particular emphasis is placed on the development of natural-nanofiber-based polymer composites to replace petrochemical high-performance plastics.



Dong Soo Hwang is a Professor at the POSTECH and leads the Biological, Biomimetic, and Eco-Friendly Materials Laboratory. After his Ph.D. in 2006 in chemical engineering at POSTECH, he received additional training as a postdoctoral researcher for 4 years in the biological and biomimetic materials at the University of California, Santa Barbara, thereafter returning to the POSTECH. His research interest is understanding and translating biological materials, and he is one of the cofounders of ANPOLY, Ltd. (Pohang, South Korea) that manufactures biopolymers—nanocellulose and nanochitin from natural resources.